12-2022

Re-engineering cardio-oncology testing using biomimetic heart slice cultures.

Jessica Miller
University of Louisville

RE-ENGINEERING CARDIO-ONCOLOGY TESTING USING BIOMIMETIC

HEART SLICE CULTURES

By

Jessica Miller

B.S., University of Alabama at Birmingham, 2019

A Dissertation

Submitted to the Graduate School

at the University of Louisville,

In Partial Fulfillment of the Requirements

For the Degree of

Doctor of Philosophy in Interdisciplinary Studies,

Specialization in Translational Bioengineering

Interdisciplinary Studies

University of Louisville

Louisville, KY

December 2022

RE-ENGINEERING CARDIO-ONCOLOGY TESTING USING BIOMIMETIC

HEART SLICE CULTURES

By

Jessica Marie Miller

B.S. University of Alabama at Birmingham

A Dissertation Approved on

11/14/2022

By the following Dissertation Committee:

_____

Dr. Guruprasad Giridharan, Dissertation Chair

_____

Dr. Tamer Mohamed, Dissertation Co-Chair

_____

Dr. Thomas Roussel, Committee member

_____

Dr. Stuart Williams, Committee member

_____

Dr. Ayman El-Baz, Committee member

DEDICATION

This dissertation is dedicated to my family,

my friends,

and, of course, my cats

who have provided me with

continuous love and support.

ACKNOWLEDGMENTS

ABSTRACT

RE-ENGINEERING CARDIO-ONCOLOGY TESTING USING BIOMIMETIC

HEART SLICE CULTURES

Jessica M. Miller

November 14, 2022

Recently, the rapid pace of cancer therapeutic development has led to numerous unforeseen consequences on heart function. Additionally, recent articles suggest that cardiovascular disease (CVD) diagnosis following primary cancer treatment has been associated with cancer progression. To address these adverse cardiac effects, two emerging research fields have started to be established termed cardio-oncology and reverse cardio-oncology. While *in vivo* animal models and *in vitro* cell culture models (i.e., human induced pluripotent stem cell derived cardiomyocytes (hiPSC-CM)) have been of paramount importance for the discovery and detection of many cardiotoxic effects, they lack the ability to accurately model the intact human myocardium. Recently, our group developed a 300 μm thin cardiac tissue slice culture system which has several advantages such as emulating the organotypic structure of the heart and allows for the reliable replication of normal cardiac functionality.

Therefore, we hypothesize that cardiac tissue slices can emulate the complexity of the human heart and can be a potential platform for reliable drug testing and various ex-vivo cardio-oncology studies.

In this dissertation, three studies were performed to evaluate cardiac tissue slices as a potential platform to study cardio-oncology and reverse cardio-oncology related research questions.

Firstly, to test whether cardiac tissue slices can be used in cardiotoxicity screening, tissue slices and hiPSC-CMs were treated with doxorubicin, trastuzumab, and sunitinib for 48 hours. hiPSC-CMs did not detect the cardiotoxic effects of sunitinib at nanomolar concentrations, while heart slices did. Secondly, to validate that cardiac tissue slices can more accurately detect cardiotoxicities compared to hiPSC-CMs, 12 clinically established cardiotoxic therapeutics were tested. Only 2 out of the 12 compounds showed cardiotoxic effects at the clinically relevant dosage in hiPSC-CMs. However, on cardiac tissue slices, all 12 compounds demonstrated cardiotoxic phenotype(s) at the clinically relevant dosage. Lastly, to investigate the potential crosstalk between CVD and tumorigenesis a co-culture bioreactor system was designed. By positioning a hexagon shaped baffle within the center of the tissue slice culture chamber, a uniform exchange of solution across all 6 tissue slices was established.

This dissertation outlines how cardiac tissue slices are an effective platform for cardiotoxicity screening and can more accurately detect clinically known cardiotoxic effects compared to hiPSC-CMs. Additionally, a novel CVD-tumor bioreactor was designed providing a platform to investigate the crosstalk between tumor cells and cardiac tissue.

TABLE OF CONTENTS

LIST OF TABLES

LIST OF FIGURES

CHAPTER 1: INTRODUCTION

1.1. Cardio-oncology

Unforeseen disruption of cardiomyocyte electrical conduction and contractility has been a major cause of drug withdrawal from the market, accounting for 28% of drug withdrawals. [67, 95, 122, 128] Many of these drugs are used for cancer therapies and have often led to severe damage to the heart. [115] Some examples are anthracyclines, radiation (traditional treatment), and trastuzumab (targeted), which have resulted in cardiovascular complications in a small subset of patients. [105, Moslehi, 2016 #40] While the mechanisms of these therapies are well known, newer classes of drugs, such as PI3K or CDK4/6 inhibitors, remain elusive. [193, Knudsen, 2017 #36] Due to both the known and the predicted cardiotoxic side effects of anti-cancer therapeutics, an emerging field between cardiologists and oncologists (cardio-oncology) has started to form. This new field aims to reduce cardiotoxic side effects in accordance with the International Council for Harmonization of Technical Requirements for Pharmaceuticals for Human Use (ICH) guidelines. [144]

In more recent years, cancer drug development has occurred at a rapid pace, leading to numerous unforeseen consequences. Many patients are exposed to a complex regimen of medications that may have some unknown side effects. Additionally, due to

many confounding factors such as age, genetics, food consumption or nutritional supplements, adverse drug effects can sometimes be difficult to predict with new therapies. Therefore, it is essential to obtain insight into the mechanism of potential adverse drug effects to reduce the risk of detrimental effects in patients.

Alterations in cardiac rhythm can occur due to both direct and indirect effects of anticancer drugs on the intracellular regulation of myocyte action potentials. [10, Alexandre, 2018 #46] While various types of arrhythmias can occur as an adverse consequence of cancer treatment, the prolongation of the QT interval is the most common. [10] A prolongation of the QT interval increases the risk factor of patients for developing Torsades de Pointes (TdP), a condition in which the ventricles become tachycardic and can lead to sudden death. [6, Peter Westervelt, 2001 #44]

Table 1 shows cancer therapeutics that have been associated with prolonged QT intervals and the development of TdPs. Arsenic trioxide has the highest risk of these events occurring, with doxorubicin and several TKIs (nilotinib, sunitinib, and lapatinib) following close behind. Additionally, the combination of multiple medications induces an additive effect on QT interval prolongation and a further increased risk to the patients. [10]

Patients that are treated with cancer therapies can develop cancer therapy-related cardiac dysfunction (CTRCD). [10] Classification of a patient as having CTRCD occurs when LVEF is between 10 to 53%. [111, 142] Individuals who receive anthracyclines, such as doxorubicin (Dox), have a higher risk of developing CTRCD with systolic dysfunction and HF. [169] Patients administered with a combination of an anthracycline and another chemotherapeutic, such as trastuzumab (Tras), cyclophosphamide, or taxanes, have a further increased risk of cardiotoxicity. [72] For example, treatment of Tras alone has a 2-3% risk of patients developing HF, while a combination treatment of Tras and Dox can lead to a >7-fold increased risk of HF. [21]

Anticancer agenets	increased QTc	TdP
Nontrageted agents		
Arsenic trioxide	+++	++
Doxorubicin	+++	Possible
Histone deacetylase inhibitors		
Pabinostat	++	Possible
Vorinostat	++	Possible
Selective estrogen receptor modulators		
Toremifene	++	-
TKIs		
Ceritinib	+	-
Crizotinib	++	-
Lapatinib	+++	-
Nilotinib	++	+
Pazopanib	++	+
Ribociclib	++	-
Sorafenib	-	-
Sunitinib	++	+
Vandetanib	+++	+
Vemurafenib	++	-

Table 1: Cancer therapeutics associated with altered QT and risk of Torsades de Pointes. [10] List of anticancer agents that cause increased QT intervals and Torsades de Pointes (TdP). +++ indicates a high risk, ++ indicates a moderate risk, + indicates a risk, and – indicated no risk of development.

Hypertension is the most common cardiovascular comorbidity in cancer patients. It is also considered the most modifiable risk factor for cardiovascular complications in cancer survivors and patients still being treated for cancer. [33] VEGF inhibitors are the common cancer therapeutic that is linked to hypertension. [186] The reported cases of first-time VEGF inhibitor treated patients have a 21 to 40% risk of developing hypertension. [186] Typically, VEGF inhibitors cause vascular regression, renal parenchyma, and vasoconstriction by a decrease in endothelial nitric oxide production. [90]

1.2. Chemotherapeutic cardiotoxins

Many chemotherapeutic treatments have adverse side effects, such as hypertension, thromboembolism, cardiotoxicity, and cardiac contractile dysfunction (prolonged QT interval). [21, 42, 90, 92, 134][105, 145, 195] The most detrimental of these adverse side effects is cardiotoxicity. There are many mechanisms in which to induce cardiotoxicity but the most common forms that appear with chemotherapeutics are cardiotoxicities induced through mitochondrial or energetic damage, a disruption in contractile function, a disruption in the electro-physiology, and a direct distribution to the myofilaments (contractile machinery of the cell discussed in more detail below).

Table 2 summarizes common chemotherapeutic drug classifications, the type of cardiotoxicity induced, and the clinical dosage. Lenneman et al [105] summarizes drug cardiotoxicity modes of action (Figure 1).

Compound name	Classification	CAS #	Energetics/ mitochondrial toxicant	Electro-Physiological disturbance	Contractility	Structural/ myofilament	Clinical dosage range
Doxorubicin	anthracyclines	25316-40-9	X				60-75 mg/m² [24]
Vinorelbine	vinca alkaloids	125317-39-7				X	25-30 mg/m2 [39]
Erlotinib	kinase inhibitors	183321-74-6	X				100-150 mg [94]
Sunitinib	tyrosine kinase inhibitors	557795-19-4	X				12.5-50 mg [34]
Endothelin-1	vasoconstrictor	117399-94-7				X	62.5-125 mg [10]
Pentamidine	cytotoxic	100-33-4		X			3-4 mg/kg [1]
Arsenic Trioxide	cytotoxic	1327-53-3		X			10 mg [88]
BMS-986094	anti-viral	1234490-83-5			X		100-200 mg [5]
Vincristine	vinca alkaloids	2068-78-2				X	1.4-2 mg/m² [60]
Milrinone	antimetabolite	78415-72-2			X		9-18 µg/m² [22]
Nilotinib	kinase inhibitors	641571-10-0			X		400-800 mg [47]
Vinblastine	vinca alkaloids	143-67-9				X	3.7-18 mg/m² [95]
Trastuzumab	HER2-targeted monoclonal antibody	180288-69-1			X		100-250 mg [12]
Acetaminophen	analgesics and antipyretics	103-90-2					325-500 mg [7]

Table 2: Classification of cancer therapeutics and associated cardiotoxicity. Known cardiotoxic cancer therapeutics with corresponding drug classification, CAS # (compound ID number), clinically associated cardiotoxicity, and clinical dosage range.
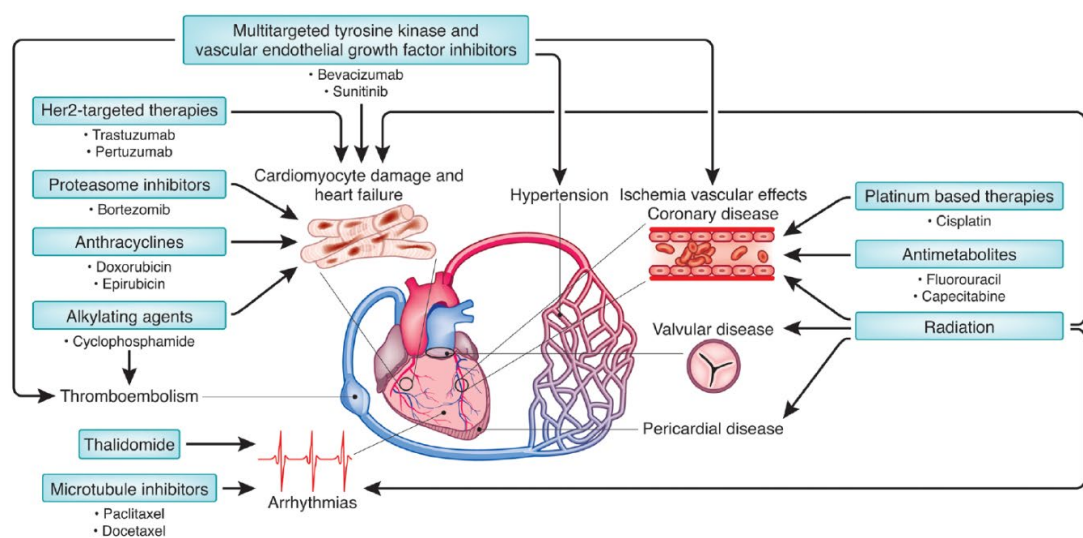
Figure 1: **Cardiotoxicity mechanism of cancer therapeutics.** [58] Mechanisms of cardiotoxicity caused by common cancer therapeutics.

1.3.1. Anthracyclines – Doxorubicin

Anthracyclines such as doxorubicin (Dox), idarubicin, daunorubicin, and epirubicin, induce energetic/mitochondria damage. [105] Anthracyclines are a class of antibiotics that are used to treat various types of cancer (breast, leukemia, lymphoma) and are the most effective cancer therapy. [52, 184] This classification of drug inhibits topoisomerase II (inhibiting ligase repair of DNA breaks), intercalates DNA base pairs, creates iron-mediated free radicals (inducing more DNA damage), and reduces histones (further reducing DNA repair). [52, 135, 201] While anthracyclines are highly effective in treating cancer, they cause cardiotoxicity. [27, 51, 103, 105, 158] 5-23% of patients develop HF and LV dysfunction in both short- and long-term exposure to these compounds. [27, 103] The exact cardiotoxic mechanism of this class of therapeutics remains elusive but it is believed to be caused by the accumulation of free radicals (inducing a stress response and DNA damage) and inhibition of DNA repair. [77, 201]

1.3.2. Alkylating agents – Vinorelbine, vincristine, and vinblastine

Another cardiotoxic classification is alkylating agents, such as vinorelbine, vincristine, and vinblastine. [49, 62, 107] Vinca-alkaloids are considered spindle toxins that interfere with beta-tubulin subunit of the alpha/beta-tubulin heterodimer thus inhibiting tubulin polymerization, which is a key protein in microtubule assembly. [62] In cardiomyocytes, there are three distinct populations of microtubules: cortical, interfibrillar, and perinuclear. [25] The cortical microtubules span across the cardiomyocyte perpendicular to myofibrils. [164, 165] They are responsible for mechanotransduction of external cues and regulate ion channels as well as transmembrane proteins. [164, 165] Interfibrillar microtubules are responsible for

positioning organelles within the cell, maintaining intercalated disc, and T-tubule and SR membrane regulation. [26, 116, 147, 151, 176, 199, 202] Lastly, perinuclear microtubules surround the nucleus. This type of microtubule is responsible for organizing perinuclear organelles and interacting with the LINC complex that mechanically couples the nucleoskeleton to the microtubule cytoskeleton. [35, 133, 168] A disruption in these microtubules can cause major cellular dysregulation. [49, 62, 107] This category of therapeutics has been linked to cardiac dysfunction and pulmonary hypertension caused by a disruption in myofilaments. [49, 62, 107]

1.3.3. Tyrosine kinase and VEGF inhibitors – Erlotinib, sunitinib, and nilotinib

Tyrosine kinase (TKI) and vascular endothelial growth factor (VEGF) inhibitors also induce cardiotoxicity. [105] Some common tyrosine kinase and VEGF inhibitors are erlotinib, sunitinib, and nilotinib. [105] Sunitinib binds to the phosphorylation site of the VEGFR receptors, inhibiting the VEGF signaling pathway. [134] In normal VEGF signaling activation one of two pathways can be activated. The first is the PI3K/AKT pathway which increases intracellular calcium, resulting in the activation endothelial nitric oxide (eNOS) synthase which, in turn, increases nitric oxide (NO) production. [20, 137] The other pathway is the mitogen-activated protein kinase (MAPK) pathway which increases intracellular prostacyclin (PGI_2) concentrations. [190] High concentrations of NO or PGI_2 will induce vasorelaxation, increase vascular permeability, and improve endothelial survival and angiogenesis. [134] With the treatment of sunitinib these pathways are inhibited, resulting in low intracellular concentrations of NO and PGI_2 thus inducing vasoconstriction, decreasing vascular permeability, and reducing angiogenesis. [134] Interestingly, in patients treated with sunitinib, there is an increase in endothlian-1

(ET-1) within the circulation, which further increases vasoconstriction. [89, 90] With VEGF having so many influences there are many adverse cardiovascular events of VEGF inhibits. Patients who receive this form of treatment are reported to have hypertension, thromboembolism, and cardiac contractile dysfunction (prolonged QT interval). [105, 145, 195] Nilotinib inhibits the tyrosine kinases BCR-ABL, cKit, and PDG-FR. [130] The only reported cardiovascular effect of this compound is the prolongation of the QT interval. [88] It should be noted that while sunitinib and nilotinib both induce cardiovascular complications, erlotinib is very well handled in patients and cases of cardiotoxicity are very rare (4 cases reported to date). [42, 102, 125, 140]

1.3.4. Antimetabolites – Milrinone

Antimetabolites, such as cytarabine and milrinone, inhibit DNA and RNA growth by substituting normal building blocks of the RNA/DNA, thus inhibiting the cells during the S phase of mitosis. [132][66] Milrinone is a phosphodiesterase inhibitor that slows the degradation of cyclic AMP. [120] This induces an accumulation of cytosolic cAMP which will activate PKA, L-type calcium channels, and the ryanodine receptor, thus increasing intracellular calcium. [198] Activation of PKA causes the phosphorylation of troponin I, which in turn allows for faster force relaxation and contraction. [12, 198] The commonly reported cardiac effects are ECG changes (ST-segment and T-wave irregularities), chest pain, and myocardial ischemia. [105, 132] [51, 66]

1.3.5. HER2/neu receptor inhibitors - Trastuzumab

Her2-targeted therapies consist of trastuzumab (Tras) and pertuzumab. [105] Tras is a humanized monoclonal antibody used to treat HER2-positive breast cancer patients. [105] The inhibition of HER/neu receptor disrupts the intracellular transduction pathway

that is a critical regulator of normal myocyte growth, homeostasis, and survival. [105, 139, 167] This HER/neu signaling also controls the sympathetic output and vasomotor tone of the heart. [105] Clinically, HER2-targeted therapies result in asymptomatic cardiac dysfunction, but in a subset of patients it can cause heart failure. [129] Recent studies utilizing hiPSC-CMs, revealed that Tras directly causes cardiomyocyte damage, resulting in a decline in cardiac expression and contractile function. [92, 100]

1.3.6. Antiprotozoal – Pentamidine

Pentamidine is an antiprotozoal agent that is used to treat pneumocystis jiroveci pneumonia in patients with immunodeficiency virus infection. [16, 56, 60, 80, 82, 183] While this treatment is an effective alternative to the primary treatment, it does have a large number of adverse consequences. [60] Immediately after treatment patients are reported to experience hallucinations, nausea, vomiting, and hypotension. [60] With just 1 week of treatment, pentamidine induces nephrotoxicity, pancreatitis, and cardiotoxicity. [60, 183] The cardiotoxic events that occur include the prolongation of the QT-interval, torsade de points, sinus bradycardia, and ventricular tachycardia. [16, 56, 60, 80, 82, 183] This is due to the cardiotoxic mechanism of action of pentamidine. Pentamidine inhibits the transcription of the human ether-a-go-go-related gene (hERG), thus reducing the number of potassium channels on the cell surface. [34, 101, 183] This subsequently blocks the I_{K1} current, inducing QT prolongation and TdP. [34, 101, 183]

1.3.7. Cytotoxin – Arsenic trioxide

Arsenic trioxide, a natural toxin, has been used for centuries to treat various diseases, such as myelodysplastic syndrome, leukemia, and many types of cancers. [43, 157, 205] Due to the non-specificity of arsenic trioxide, there is a dosage limit to reduce

the damage to other cells. [29, 76] In the heart, this toxin causes a prolongation of the QT-interval inducing ventricular arrhythmias. [45] This is hypothesized to be due to arsenic reducing cardiac phosphorylation, thus decreasing intracellular ATP concentrations inhibiting the activation of potassium-ATP ion channel. [45]

1.3.8. Other – Endothelin-1

Endothelin-1 (ET-1) is a peptide that has been linked to tumor survival, proliferation, immune modulation, metastasis, and angiogenesis [154] Over the past 3 decades, ET-1 therapies have been developed to interfere with ET-1 receptor activation. [7, 153] This has proven to be an effective method in treating various types of cancers but there are adverse events associated with ET-1 therapies. [7] In the cell, a balance between NO concentrations and ET-1 binding to its receptor controls contraction and relaxation. [19] NO contractions directly regulate cGAMP synthesis resulting in the relaxation of the cell. When there is a higher amount of ET-1 binding to the receptors there will be increased contraction. [19] Endothelin-1 receptors are expressed throughout the body leading to both direct and indirect cardiovascular complications. [7] Clinically, these complications can range from hypertension to ischemic heart failure. [36, 66, 68, 112, 172, 174, 175]

1.3.9. Other – BMS-986094

BMS-986094 (BMS) is an anti-hepatitis C virus therapy that was stopped during phase II clinical trials due to unforeseen cardiotoxic events. [3, 178, 185] With long-term treatment, BMS was found to induce a decrease in left ventricular ejection fraction.[3, 185] Through *in vivo* and *in vitro* studies, it was discovered that BMS directly altered CM contractility through the disruption of calcium transients. [161] Additionally, BMS has

been reported to induce mitochondrial toxicity with long term exposure in cell cultures, however, this effect has not been reproduced in animals. [9, 46, 53, 117, 161]

1.3. Reverse Cardio-oncology

Cardiovascular disease (CVD) and cancer are the two leading causes of death, sharing many common risk factors. [18] Whether the relationship between CVD and cancer is due to causality or to the shared risk factors is still under debate. [37] Recent articles, however, suggest that CVD diagnosis subsequent to primary cancer diagnosis has been associated with cancer progression. [97] Due to these studies, an interest has been invoked to understand the bi-directional relationship between these two diseases. [39]

The field of cardio-oncology has advanced in the recent years from simply observing increased risk of CVD following cancer treatment to linking a decline in lifestyle activity (indirect) or direct cardiotoxic influences of immunotherapies on heart function. [83] With the continued growth of cardio-oncology classifications, an additional field of study addressing the possibility of CVD progressing cancer pathogenesis has emerged. This new subfield has been termed as 'reverse cardio-oncology.' [2]

Clinical evidence has demonstrated that higher cancer prognosis has been associated with CVD. [96] Cancer prognosis is either due to tumorigenesis or the acceleration and growth of preexisting occult tumors. [96] It has been observed in a cohort study that myocardial infarction patients who developed heart failure (HF) one month after treatment were more likely to develop cancer when compared to participants without HF. [74, 110] NT-ProBNP, a standard HF detection biomarker, has also been associated with increased new cancer incidence. [113] This study also reported that pro-

inflammatory cytokines (C-reactive protein, pro-endothelin, and pro-adrenomedullin) have been linked to incident cancer.

Acute coronary syndrome (ACS) patients have been reported to be at a higher risk of malignancy development post ACS diagnosis. [13] Additionally, venous thromboembolism, atrial fibrillation, and aortic stenosis have been linked to the development of cancer. It should be noted, however, that these patients are possibly exposed to detection bias, due to the more frequent lab testing, chest X-rays, CT, MRI, and PET scans that could reveal previously undetected malignancies. [38] Nevertheless, the risk of CVD patients of developing tumors needs to be investigated.

Current *in vitro* research has revealed that CVD-induced cancer pathogenesis has been linked with specific CVDs inducing tissue specific tumor development. Koelwyn et al [96] demonstrated that an MI after primary cancer leads to an upregulation of LY6C^{hi} monocytes, promoting breast cancer tumor growth. Meijers et al [113] demonstrated that MI-induced heart failure leads to an increase of circulating SerpinA3, which directly promotes colon cancer pathogenesis. Avraham et al [5] demonstrated that TAC induced mice models displayed larger primary tumors with increased proliferation rates and more metastasis in both lung and breast cancer due to increased periostin release.

1.4. Functionality and cellular composition of the heart [1]

1.4.1. Cardiac anatomy

Oxygenated, nutrient-rich blood is pumped by the heart to support various tissues throughout the body. Figure 2A depicts the structure of the heart. The heart is composed

---

[1] Part of the work in this chapter has been published in [114] M. H. Meki, J. M. Miller, and T. M. A. Mohamed, "Heart Slices to Model Cardiac Physiology," (in English), Frontiers in Pharmacology, Mini Review vol. 12, no. 23, 2021-February-04 2021, doi: 10.3389/fphar.2021.617922.

of four chambers: the left and right atrium and the left and right ventricles. Deoxygenated blood returns to the right atrium of the heart from the venous circulation via the inferior and superior vena cava. The blood flows through the tricuspid valve into the right ventricle where it is pumped into the pulmonary artery to be transported to the lungs to be oxygenated. The oxygenated blood flows back to the heart into the left atrium. The mitral valve will open and allow the blood to flow into the left ventricle where it is pumped out of the aorta to the rest of the body. Due to the vascular resistance, pulmonary circulation pressures are significantly lower than the systemic circulation. This difference results in smaller cardiomyocyte size (the contractile cells that compose the myocardium) with the right ventricular myocardium compared to left. [70]
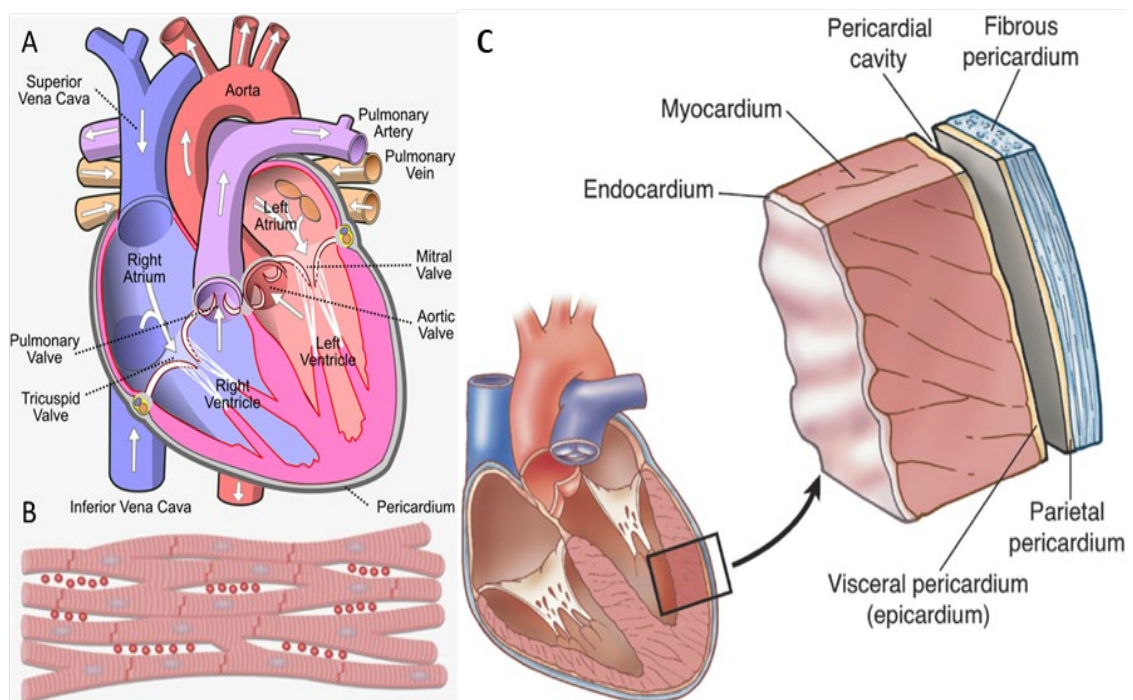
Figure 2: **Anatomy of the heart.** [70] (A) Cross-section view of chambers of the heart, valves, and veins and arteries. (B) Diagram of the composition of the myocardium with intercalated disks (dark red lines) connecting the cardiomyocytes. (C) Composition of the ventricular wall: endocardium, myocardium, and pericardium.

1.4.2. Cellular composition of the heart

The cardiomyocytes within the myocardium are similar to skeletal muscles in that they are striated and their contractile machinery consists of actin and myosin filaments. [61] These two filaments actively slide over one another when electrically stimulated. Cardiomyocytes differ from skeletal muscle in that they are connected to other cardiomyocytes via intercalated disks (Figure 2B). [61, 70] These intercalated disks enable an exchange of ions from one cell to the next allowing for the action potential to propagate along the cardiac tissue for a synchronized contraction.

The ventricular wall contains three layers: the endocardium, myocardium, and pericardium (Figure 2C). The endocardium is composed of epithelium and connective tissue while the epicardium contains fatty and connective tissue. [70] The myocardium is composed of many cell types, such as endothelial, fibroblasts, and cardiomyocytes (CMs), with CMs being the most abundant and responsible for the heart's contractile function. [70]

1.5. Models of the heart

Currently there is a lack of a reliable cardiac testing platform that can accurately replicate the human myocardial environment. Such a system would incorporate physiological inotropic, chronotropic, and dromotropic effects. The most common cardiac screening platform used are animal models. Animal models can be relatively expensive at the early stage of drug development due to the large volume of compounds needed to generate pharmacokinetic profiles. Additionally, animal models are limited in their reliability of reproducing the same effects of the drugs as seen in human hearts. [65, 108, 156] The ideal cardiac testing platform is one that has high specificity and

sensitivity to a wide range of pharmacological interventions and therapeutics while at the same time accurately replicating physiological and pathophysiology conditions of the human heart. [187]

The controlled culture environment of *in vitro* systems has the unique advantage of characterizing drug-related changes on the cellular level at a lower cost compared to animal models. 28% of drugs are withdrawn from the market due to unanticipated cardiotoxic effects of therapeutic compounds demonstrating the unsuitability of the current cardiac models in detecting toxic effects. [67] To address this issue, there are many groups working to develop a reliable preclinical model of the human myocardium. The success of *in vitro* systems increases with its ability to accurately detect calcium homeostasis, electrophysiology, contractile measurements, protein expression (e.g., contractile and gap junction proteins), and transcriptional profile. Guth et al. [65] outlines the essential features for *in vivo* drug testing platforms. While many of the models shown in Figure 3 have their own advantages, most lack the ability to model the physiology and pathophysiology of an adult human heart. This limitation is due to the complexity of the myocardium, which is composed of a multi-cellular environment maintained by chronic neurohormonal stimulation.
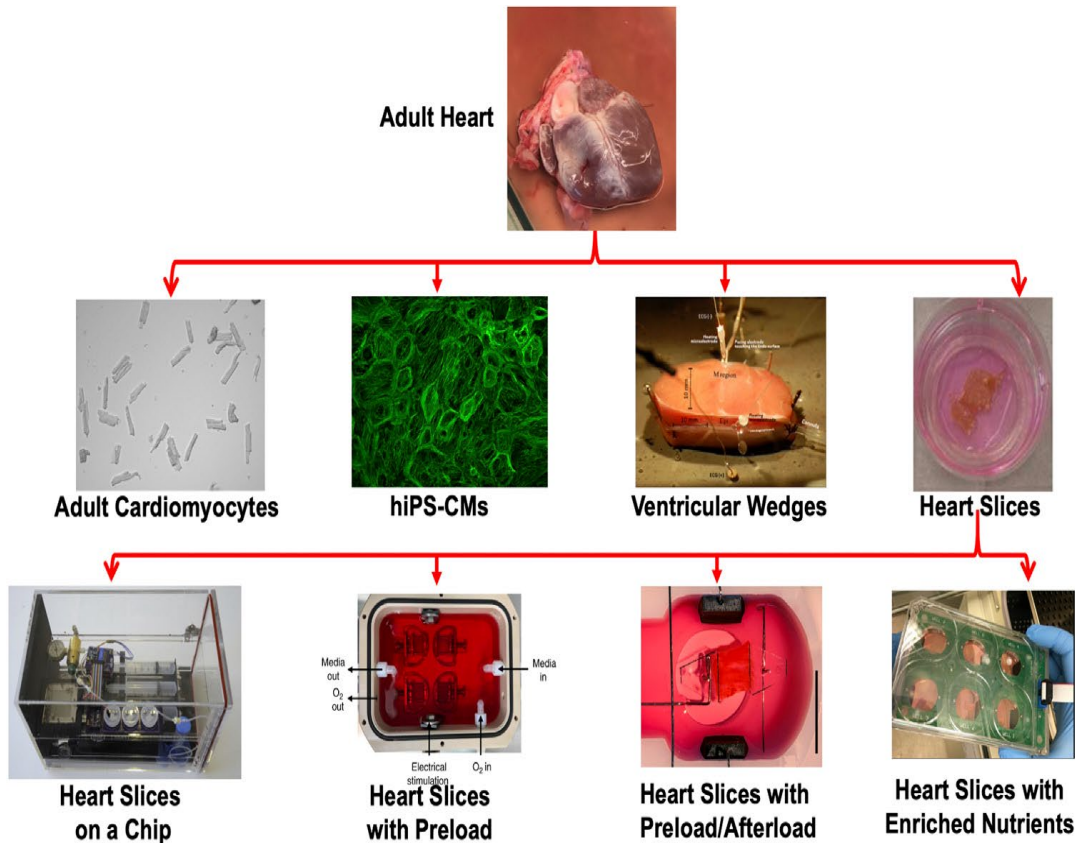
Figure 3: **Models of the heart in culture.** [114] (top row) Isolated heart. (middle row) Models of the cardiac physiology in culture ranging from adult cardiomyocytes, hiPSC-CMs, ventricular wedges, and heart slices. (bottom row) Recent advancements of the use of cardiac tissue slices in culture.

1.5.1. *in vitro* models – Isolated adult cardiomyocytes

The first successful isolation and culture of adult cardiomyocytes was performed in 1976 by Powell and Twist. [146] Since this study, this technique has been used to study the response to sepsis [28], calcium dynamics [15], cardiac electrophysiology [14, 91], gene transfer [84], and contractile function [123, 138]. These studies demonstrate that a simplified unicellular culture can provide insightful data while avoiding confounding factors seen in more complex models such as tissue preparations. [54]

Another unique characteristic of adult cardiomyocyte culture is that by culturing the cells on a coated plastic surface, the cardiac phenotype of rod-shaped morphology, t-tubule organization, and cell-cell coupling can be maintained. [121]

While this platform has been a key element in cellular level research, it is limited in its ability to accurately predict macrolevel responses and cardiotoxicities of drugs and therapies. Additionally, isolated cardiomyocytes are restricted by their culture life. These cells will rapidly dedifferentiate and lose normal cardiac functionality within 48 hours. [17] Another limitation is the low number of cells and high amount of cellular damage during isolation using the current enzymatic isolation protocols. [44, 177] In order to improve the cell yield and reduce cellular damage, some groups are focusing on optimizing these isolation protocols. [64] Callaghan et al. [24] demonstrates that by using Geltrex and blebbistatin, adult mouse cardiomyocytes have improved viability and maintained cellular function. The major limitation of this method is the use of blebbistatin, which inhibits cardiomyocyte contraction, which may limit contractile assessment.

1.5.2. *in vitro* models – Human-induced pluripotent stem cell-derived cardiomyocytes (hiPSC-CMs)

Due to the simplicity of hiPSC-CM generation and culture process [40, 170], this cell type has been extensively used for drug cardiotoxicity testing, arrhythmogenicity [143, 159, 162], and cardiac disease modeling [85, 194]. However, due to hiPSC-CM's fetal-like properties of under-developed sarcoplasmic reticulum, lack of T-tubules, and lack of cell-cell coupling, they are structurally and functionally incompetent. [40]

Many groups, discussed in detail by Ahmed et al. [4], are working towards methods that promote the maturation of these cells. These studies incorporate certain factors found in the native myocardial environment such as the extracellular matrix [150], electrical stimulation [126, 173], 3-D structure [200, 203], and electro-mechanical stimulation [81, 152, 155]. Kroll et al [99] demonstrates that by applying a force stretch system with synchronized electro-mechanical stimulation to hiPSC-CMs cultured on a flexible PDMS membrane, the cells will express enhanced stress fiber formation, N-cadherin signaling, sarcomere shortening, and contractile protein expression. These improvements to hiPSC-CM cultures allow for these cells to be the most widely used drug screening platform due to their extended culture life and physiological resemblance to the human heart.

1.5.3. *in vitro* models – Left ventricular wedge preparations

Ventricular wedge preparations prepared from canine and other animal hearts (including human) have been extensively used for investigating arrhythmias, conduction velocity, and the heart's electrophysiology. [30, 58, 109, 127, 191, 192] These models allow for a 3-dimensional macrolevel snapshot of the cardiac physiology and pathophysiology. Ventricular wedges, however, have a low throughput due to the complexity of the preparation and a low sample yield per heart. [148] Additionally, these preparations only have a few hours of culture life before rapid dedifferentiation, thus restricting their use in chronic drug studies.

1.5.4. *in vitro* models – Heart slices

Thin (<400 μm) heart slices were first proposed as a potential cardiac model in 1992 with relatively precise and reproducible slice thickness. [1] In Parrish et al.'s [1]

study, ventricular heart slices were prepared from rat hearts and cultured for 24 hours with maintained viability and metabolic function. The key element of this study was the use of continuous oxygenation of the culture media, which was achieved by rotating the preparations within a cylinder. A decade later, Brandenburger et al. [22] simplified tissue slice cultures by using a transwell membrane that allowed for a liquid-air interface.

Since Brandenburger's simplified culture system, 300 μm thin heart slices have demonstrated maintained conduction velocity and calcium handling, viability, and organotypic structure for 24 hours in culture. [86, 189] Additionally, since heart slices retain a 3-dimensional structure composed of multiple cell types and the presence of an extracellular matrix, a mature myocardial phenotype can be maintained. [171, 197] These slices can be prepared at a medium to high throughput enabling them for use in acute drug discovery.

Detailed protocols for the preparation of heart slices from different animals as well as human hearts have been described by many groups. [22, 131, 188, 189] Brandenburger et al's study demonstrated that cardiac slices could maintain β-adrenergic response, viability, and electrophysiological properties for 28 days. This prolonged culture, however, resulted in a loss in the tissue's functional (90% decline in contractility) and structural integrity after only 24 hours in culture. The decline in structural integrity and a downregulation of MLC2 and α-actin on the transcriptional level indicate that the slices were undergoing dedifferentiation. [22] Other groups that used this culture system demonstrated the same effects. [86, 189]

Neurohormonal factors and hemodynamics are the two main elements of the native myocardium that regulate the functional integrity of the heart and changes in either

will result in adaptive remodeling. [8] This illustrates the importance of biomimetic factors for maintaining the cardiac phenotype. Due to complexity of the cardiovascular system, it is difficult to identify all the myocardial environmental factors that are essential for properly maintaining this balance. In more recent years, groups have been investigating relevant factors such as electrical pacing, mechanical, and continuous oxygenation and nutrient support. [47, 131, 148, 188]

The synchronization of action potential propagation and cardiac contraction are regulated through gap junctions. [196] Arrhythmias can occur if there is a disruption in connexin 43, a gap junction protein, expression or localization. hiPSC-CM cultures have demonstrated that with continuous electrical stimulation, connexin 43 expression and organization can be improved. [75]

Mechanical cues on the other hand are essential in regulating physiological and pathological remodeling such as in dilated or hypertrophic cardiomyopathy. [8] The absence of electrical and mechanical stimulation in traditional transwell tissue slice culture may be the cause for the loss of contractile and contractile protein expression after 24 hours in culture. [22]

Additionally, while both electrical and mechanical stimulation are essential, there may be other elements to consider such as nutrients, oxygenation, or humoral stimulation. The myocardium has a high metabolic demand that basic culture medium cannot sustain. Qiao et al. [148], developed a heart-on-a-chip culture system that incorporates heart slices into a culture system with continuous oxygen and carbon dioxide injection, an orbital shaker, and continuous circulation of the culture media. This system, however, does not include the other two essential factors of mechanical or electrical stimulation. This

system allowed for the tissue slices to be maintained in culture for 4 days with anisotropic conduction, average transverse conduction velocity, and uniform repolarization.

Watson et al. [188], developed a culture system that applied electrical stimulation and preload to rabbit and failing human heart tissue. This system utilized a continuous stretch apparatus to apply a constant sarcomeric length to the tissue slices. They found that slices cultured for 24 hours with a sarcomeric length of 2.2 μm, maintained conduction velocity, contractile function, calcium handling, electrophysiology, and action potential similar to fresh samples. The tissue slices showed no deterioration in contractile function for at least 5 days in culture. Interestingly, this model had an upregulation of hypertrophic genes and an increase in calcium transient amplitude within 24 hours of culture while maintaining normal cardiomyocyte cell size.

Fischer et al. [47], developed a similar culture system. Heart slices from failing human hearts were stretched between two posts with electrical stimulation. One end was connected to a spring cantilever, which applied a linear mechanical afterload. A magnet was placed on the free end post of the tissue slice and using a magnetic field sensor the contractile force of the slice was recorded in real-time. With the application of a low stimulation pace (0.2 Hz), tissue slices could be maintained for 4 months with conserved contractility, connexin 43 localization, α-actinin expression, and preserved tissue elasticity. There was, however, a significant downregulation of cardiac gene expression at 8 days in culture. This system, unlike Watson et al.'s [188], allowed for active tissue shortening and contraction. Regardless, as mentioned by Pitoulis et al. [141] this method

of contraction is far from physiological where normal relaxation and contraction are separated by a time of isomeric relaxation and contraction.

Ou et al. [131] demonstrated that using optimized culture media, frequent oxygenation, and electrical stimulation of tissue slices cultured in a 6-well transwell culture plate, samples can be maintained with preserved viability, structural integrity, and functionally for 6 days in culture (Figure 4). By 10 days in culture, however, the samples show evident dedifferentiation through a differential expression of more than 500 genes,
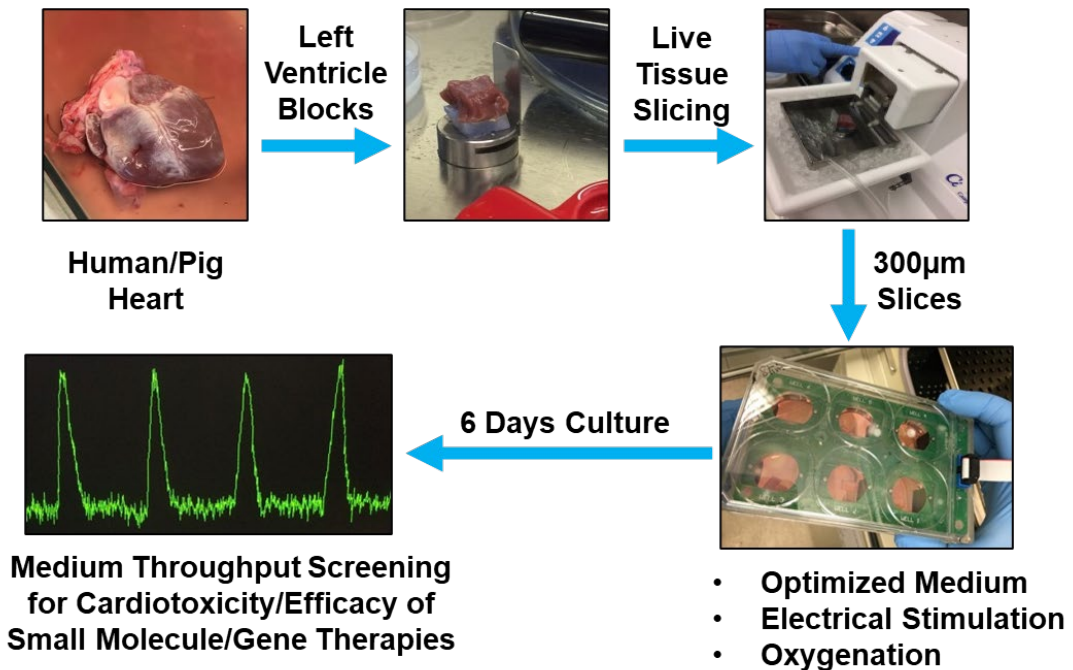
Figure 4: **Optimization of pig heart slice biomimetic culture conditions.** Once a full pig heart is obtained, the left ventricle is dissected into 1–2 cm^3 cubes and placed on a holder. Setup for slicing 300 µm thick heart slices in ice-cold bath using a vibrating microtome. Heart slice trimmed and glued to light polyurethane supports and submerged in the medium in a 6-well plate, which is covered by the C-Dish cover containing graphite electrodes and connected to the C-Pace electron microscopy (EM) stimulator.

a disruption in connexin 43 localization, and loss of contractile function. While this culture system did not incorporate mechanical cues, it does demonstrate that with proper nutrients, oxygenation, and electrical stimulation, cardiac expression can be maintained in a simplified culture system.

Lastly, Miller et al. [118] developed a cardiac tissue culture model (CTCM) that incorporated electro-mechanical stimulation to heart slice cultures allowing for the application of physiological stretches emulating systole and diastole (Figure 5). The tissue culture system used a programmable pneumatic driver to cyclically distend a flexible silicone membrane inducing a stretch of the heart slices in the chambers above. Using this method, they were able to partially improve the viability of the hears slices but not the structural integrity after 12 days in culture. To address this, Miller et al incorporated the small molecules tri-iodothyronine and dexamethasone into their optimized culture media enabling the preservation of the microscopic structure of the slices. The combination of humoral stimulation and electromechanical stimulation allowed for maintained transcriptional profile, metabolic activity, structural integrity, and tissue viability for 12 days. Additionally, this group demonstrated the versatility of their system by emulating stretch-induced hypertrophy. This study illustrates a unique culture system that has the ability to model cardiac physiology and pathophysiology for extended culture, thus providing a potentially reliable drug screening platform.
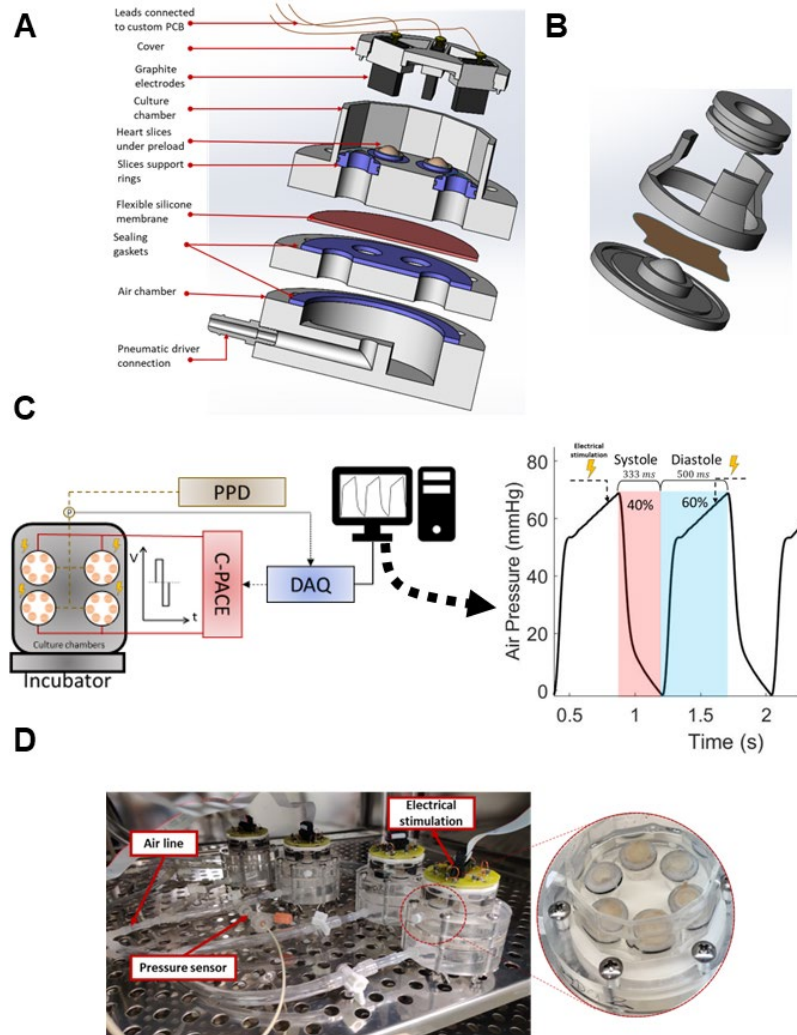
***Figure 5*: Illustration of the cardiac tissue culture model (CTCM).** (A) Exploded CAD schematic of CTCM. (B) Schematic illustration of tissue oversizing apparatus, ring guide, and support ring. (C) A diagram depicting the timing of the electrical stimulation in relation to the pressure within the air chamber controlled by the programmable pneumatic driver (PPD). A data acquisition device was used to synchronize electrical stimulation using a pressure probe sensor. (D) Image of four CTCM devices set up on a shelf of an incubator.

1.5.5. Heart slices in cardiotoxicity screening

Currently, the ideal human cardiac testing platform does not exist. While bioengineered 3-dimensional hiPSC-CMs tissue cultures present as a promising platform with a relatively mature, heterogenous cardiac construct that can be applied to a wide range of applications (e.g., basic science studies, personalized assays, and regenerative medicine), they still fall short of accurately detecting cardiotoxic events seen in the adult human myocardium. [4, 59, 104] The recent improvements to biomimetic heart slice cultures discussed above demonstrate that the technology could be a promising platform for medium to high throughout drug testing.

In 1994, tissue slices were proposed as a platform for 'detecting unfriendly cardiac compounds.' [5, 70] In this study, tissue slices were cultured using a rotating cylinder method Parrish et al [2] proposed in 1992. Tissue slices were exposed to doxorubicin and allylamine and demonstrated a concentration and time dependent toxicity. A major disadvantage of Parrish et al.'s culture system is the rapid loss of contractile function in tissue slices.

CHAPTER 2: EVALUATION OF CARDIAC TISSUE SLICES AS A PLATFORM FOR CARDIOTOXICITY TESTING [2]

2.1. Introduction

Unforeseen cardiotoxic side effects are a major cause of drug withdrawal from the market. [70, 72] This is especially true for new cancer therapies, which have been introduced at a rapid pace. [10] [11, 88] Both targeted (e.g., trastuzumab) and traditional (e.g., anthracyclines and radiation) breast cancer treatments result in adverse cardiovascular complications. [105, 124] The effects of newer therapeutics such as PI3K inhibitors and CDK4/6 inhibitors remain unclear. [94, 193] While cancer patient survival rates have been increasing recently, there is also an increase in morbidity and mortality in these individuals due to cardiotoxic side effects of anti-cancer therapeutics. [71] A close collaboration between oncologists and cardiologists aims to reduce these complications to ensure that patients are treated as effectively and safely as possible. [144] Thus, there is an urgent need for a more reliable preclinical screening platform for evaluating the potential cardiotoxicity of emerging therapies. [160]

The use of *in vivo* and *in vitro* platforms is needed to detect the cardiotoxic effects of drug candidates before clinical trials. [79] Animal models, such as mice and pigs, can be expensive, do not replicate many biochemical properties, do not accurately mimic the hemodynamics of the human heart and circulation, [32, 78] and can fail to detect cardiotoxic effects of drugs. [181, 182]

While *in vitro* models, such as hiPSC-CMs, are a partial solution for this need, they cannot capture the diverse multi-cellular influence of the native myocardium. [84] Additionally, these cells express fetal-like properties of under-developed sarcoplasmic reticulum, lack of T-tubules and cell-cell coupling. [27] More recent work to induce a more mature phenotype in these cells has started to be developed by incorporating hiPSC-CMs into microtissues. [55, 136] While these microtissues exhibit some cell-to-cell coupling and gap junction protein expression, they do not function in a synchronized manner as seen in an intact heart. [152] A less commonly used single cell culture method is isolated primary human cardiomyocytes. These cells can be used as a high throughput testing platform and are functionally mature, however, they readily dedifferentiate in culture limiting their ability to be used in subacute and chronic cardiotoxicity studies. [17]

The adult myocardium is composed of a complex heterogenous mixture of multiple cell types (e.g., cardiomyocytes, smooth muscle cells, various types of stromal fibroblasts, and endothelial cell) all linked together by extracellular matrix proteins. [17] This mixture of non-cardiomyocyte cell population is the major roadblock in developing a model for the adult myocardium using single cell types. [48, 87, 98] An alternative method to using single cell cultures are ventricular wedges and thin cardiac tissue slices.

Ventricular wedge preparations are typically used in electrophysiology studies, are large in size, have a low throughput, and are only viable for a few hours, thus limiting their ability to be used in drug screening. [57, 109]

Thin (< 300 μm) tissue slices can be prepared from both animal and human hearts. They have several advantages such as emulating an organotypic structure and can reliably replicate cardiomyocyte structural, functional, and transcriptional expression. [65, 68, 74, 83] In our 2019 culture system [131], we introduced periodically oxygenated culture media containing additional nutrients (FBS, FGF, and VEGF) to keep up with the energetic demand of the tissue slices. Additionally, this culture system introduced electrical stimulation of 10 V paced at 1.2 Hz to tissue slices attached to PLA supports cultured in a standard 6-well culture plate. The combination of optimized culture media and electrical stimulation allowed the culture life of a basic transwell culture of tissue slices to be extended from 24 hours to 6 days with maintained viability, functionally, structural integrity, and transcriptional expression.

Utilizing this tissue slice culture system, we tested three known cardiotoxins (doxorubicin, sunitinib, and trastuzumab) that induce cardiotoxic effects through different signaling pathways to assess the capability of heart slices to detect clinically relevant cardiotoxicities. Doxorubicin induces cardiotoxicity through the accumulation of ROS within the mitochondria of cells. This is highly detrimental to CMs due through their high energy demand. Sunitinib causes cardiotoxicity through inhibiting the tyrosine kinase, VEGF, causing a disruption in the intracellular signaling pathways responsible for nitric oxidate and PGI_2 production thus reducing contractility. Lastly, trastuzumab inhibits the

HER2/neu pathway which is responsible for normal myocyte growth, homeostasis, and survival.

2.2. Study hypothesis

In order to improve cardiotoxicity detection screening, we hypothesize that cardiac tissue slices can capture the complexity of the human myocardium and reliably detect cardiotoxic effects. Here we use our previously optimized heart tissue slice culturing method [65, 74] and exposed slices to three cancer therapeutics (sunitinib, trastuzumab, and doxorubicin) that induce cardiotoxicity through 3 different mechanisms. Each drug was tested at 3 concentrations for 48 hours and the structural, functional, transcriptional expression, and viability were evaluated. The drug concentrations were determined by the compounds C_{max} and 10X increase in concentrations were used. To determine the effectiveness of cardiac tissue slices in detecting cardiotoxicity, the results obtained from the slices were compared to hiPSC-CM data.

2.3. Experimental design

For this project, all animal procedures were performed in accordance with the institutional guidelines and approved by the University of Louisville Institutional Animal Care and Use Committee. The protocol for harvesting pig hearts were performed as described in [131, 149].

Tissue slices were treated with doxorubicin (Dox; 100 nM, 1 μM, and 10 μM), trastuzumab (Tras; 1 μg/mL, 10 μg/mL, and 100 μg/mL) and sunitinib (Sun; 100 nM, 1 μM, and 10 μM) for 48 hours. Control tissue slices were treated with DMSO at the same dilution factor as the drug-treated slices. The culture media was changed 3 times per day with fresh compound added each time. The viability, structural integrity, transcriptional

expression, and functionality were assessed after 48 hours of exposure. All comparisons were to same day control tissue slices.

To test viability, MTT assay was performed. The optical density (OD) measurements were normalized to the tissue slice weight and assessed as a percentage of the control tissue. The structural integrity was determined by connexin 43, a gap junction protein, and cardiac specific troponin T expression. A decline in structural integrity was determined by visual assessment of immunolabeled sections. The defining characteristics of cardiac structure are z-disc alignment (organization of connexin 43 along the edges of the cardiomyocytes and at junctions between CMs) and uniform troponin T expression.

RNA sequencing was performed to determine the differentially expressed genes. Volcano plots of the up- and down-regulated genes compared to control tissue were generated. Additionally, the gene ontology (GO) terms were investigated for each condition and heatmaps for the top up- and down-regulated GO terms were generated.

Lastly, to determine the functionality of the tissue slices, calcium-transient assessment was used. For the calcium-transient assessment, tissue slices were loaded with Fluoro-4am labeled calcium from a calcium direct kit following the manufacturer's protocol. The calcium amplitude was quantified and scored as a percentage of the control tissue slices.

Two-tailed, one-way ANOVA was performed to assess the statistical difference of each dosage compared to control tissue slices. A significance level of $p < 0.05$ was considered statistically significant.

2.4. Results

2.4.1. At clinically relevant nanomolar concentrations, hiPSC-CMs detect cardiotoxic effects of doxorubicin but not sunitinib

In cancer therapies, direct cardiomyocyte death and detrimental effects to non-cardiomyocyte cells within the heart can lead to the development of cardiomyopathy. [31, 106, 179, 204] In the literature it has been previously reported that hiPSC-CMs detect the cardiotoxic phenotype of doxorubicin in nanomolar concentrations, however, they cannot detect the cardiotoxic effects of sunitinib at these low concentrations. [204] To reproduce these findings, we tested the effects of various concentrations of sunitinib and doxorubicin on hiPSC-CMs on cell viability using caspase3/7 apoptosis assay over a course of 48 hours. As negative controls for this study, aspirin and erlotinib (non-cardiotoxic TKI) were included (Figure 6). Figure 6D demonstrates that sunitinib had no toxic effect on hiPSC-CMs at 500 nM or 1 μM concentrations, which is consistent with the literature. [204] At high concentrations (60 μM) of sunitinib treatment, an acute apoptotic response is observed within 1 hour of exposure (Figure 6E and F). This resulted in a stable fluorescence detected over the experiment for this concentration (Figure 6D). At the lowest concentration (500 nM) of doxorubicin treatment the known toxic effect of this compound is observed (Figure 6B). Lastly, the negative controls showed no apoptosis over the course of the experiment even at the 60 μM concentration (Figure 6A and C).
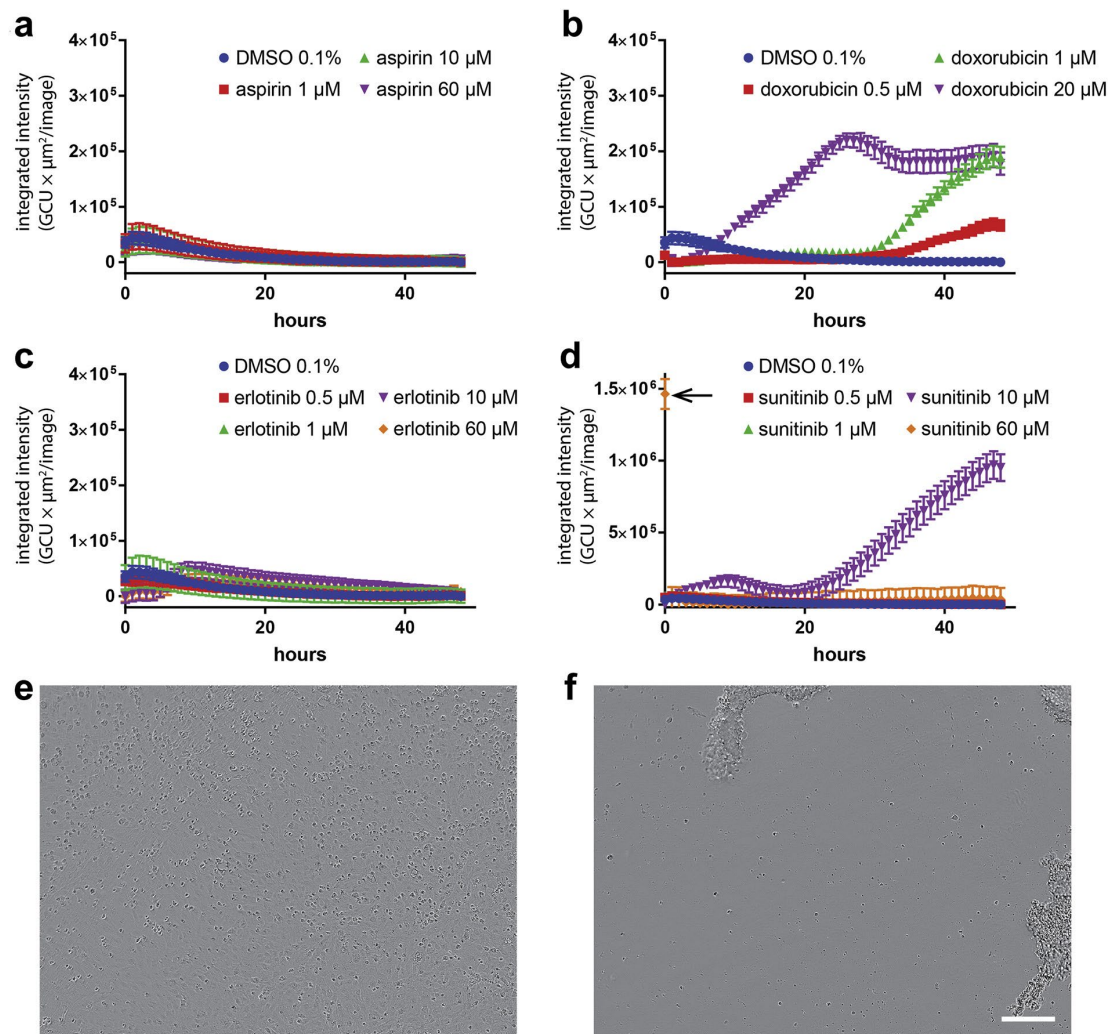
Figure 6: [92] Kinetics of caspase-3/7 activation, an indicator for apoptosis, in hiPSC-CMs treated with a range of concentrations of (a) aspirin, (b) doxorubicin, (c) erlotinib, and (d) sunitinib. A concentration of 0.1% of DMSO was added to the medium for control cells. Phase contrast images of cells before (e) and after (f) 1 hour exposure to 60 μM sunitinib (Scale bar, 200 μm).

2.4.2. Heart slices detect known cardiotoxic effects of doxorubicin

Dox, an anthracycline, disrupts RNA and DNA synthesis, impairs DNA repair, and induces an accumulation of ROS. [52, 135] The exact mechanisms of Dox are poorly

understood but it has been reported that there are multiple forms of direct cardiomyocyte damage due to the accumulation of free radicals. [77] The direct damage to the cardiac tissue slices with all concentrations of Dox are shown by a decline in MTT viability (Figure 7A), a disruption in connexin 43 and troponin T expression (Figure 7B), and a lack of calcium transients (Figure 8A). For the transcriptional gene expression of Dox treated tissue slices, a global downregulation of cardiac developmental, mitochondria viability, and oxidative phosphorylation was observed (Figure 9B). This is due to the direct cardiac damage caused by the production and accumulation of ROS within the mitochondria of the CMs. Additionally, Dox treatment resulted in an upregulation in oxidative and reductive responses due to the predicted oxidative stress caused by the accumulation of ROS (Figure 9C).

2.4.3. Heart slices detect downregulation in homeostasis and CM growth related genes with trastuzumab treatment

Tras, a humanized monoclonal antibody targeting HER2/neu receptors, inhibits the activation of the HER2/neu transduction pathway. [41] This leads to an inactivation of tyrosine kinases, a key regulator of the cell cycle. [41] In patients, Tras very rarely induces symptomatic HF. [129] For the cases of Tras-induced cardiotoxicity, it is believed to occur by disrupting normal CM growth, homeostasis, and survival. [167] Consistent with this knowledge, Figures 7 and 8 demonstrated that Tras induced a disruption in connexin 43 and troponin T expression as well as a decline in calcium transients. Transcriptionally, heart slices exposed to Tras resulted in a downregulation in homeostasis and CM growth related genes (Figure 10B).

2.4.4. Heart slices exposed to sunitinib detected a disruption in calcium transients and downregulation of angiogenesis related genes

Sun, a TKI, inhibits vascular endothelial growth factor receptor (VEGFR) resulting in declined angiogenesis. In patients, Sun can induce vascular disease, hypertension, and cardiomyopathy. [145] In 10-15% of patients treated with sorafenib, another TKI, and Sun experienced a disruption in coronary microvascular pericytes, causing CM hypoxia and cardiomyopathies. [31, 124] While the Dox and Tras therapeutic effects on CM could be reproduced in hiPSC-CMs, Sun's effect on CMs could not. This is possibly due to the indirect CM influence of Sun. [201, 204] Figure 7 demonstrates that none of the concentrations of Sun resulted in a significant change in cardiomyocyte structure but there was a functional disruption in calcium transients (Figure 8). Figure 11B indicates that transcriptionally Sun induced a significant downregulation in genes related to angiogenesis.
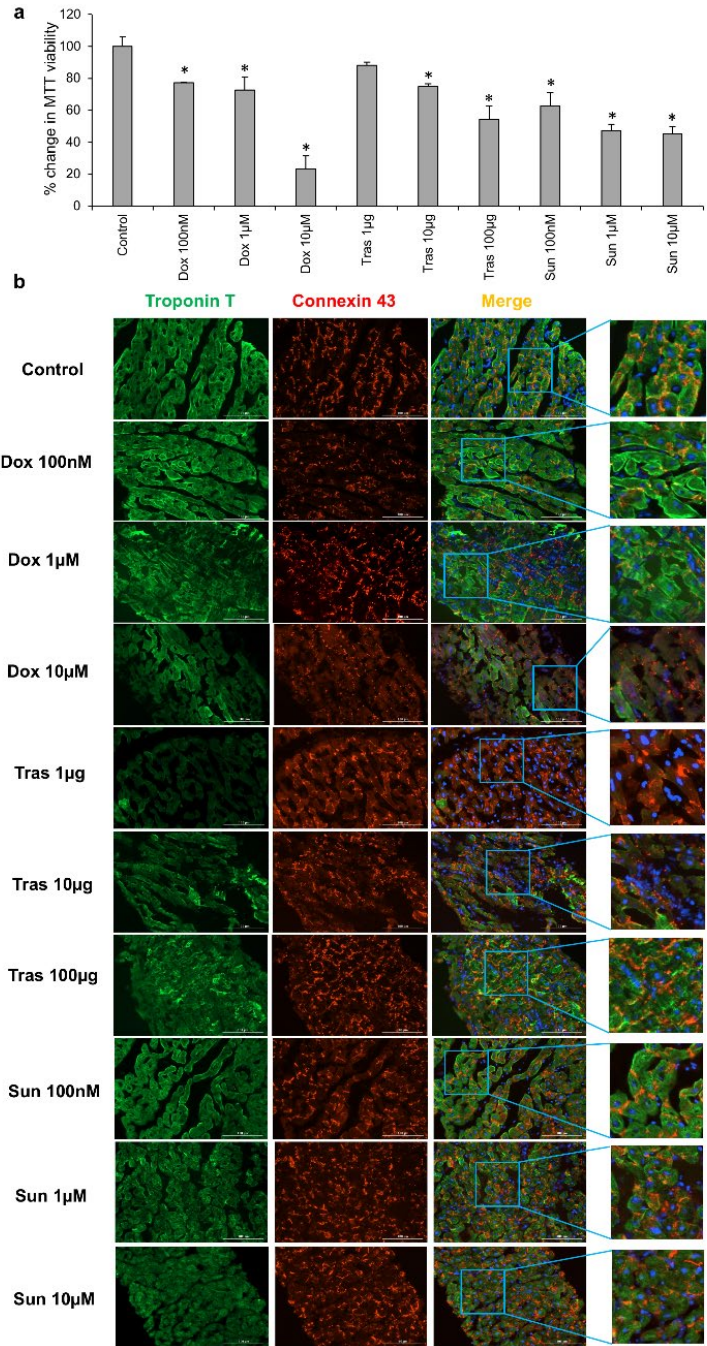
***Figure 7*: [100] The viability and structural effects of cardiotoxins on cardiac tissue slices.** (a) Graphic representation of heart slice viability after 48-hour exposure to corresponding cardiotoxin (n = 2 in 4 replicates). (b) Representative troponin T (green), connexin 43 (red), and DAPI (blue) immunolabeled tissue slices treated for 48 hours with respective cardiotoxin concentrations (Scale bar, 100 μm).
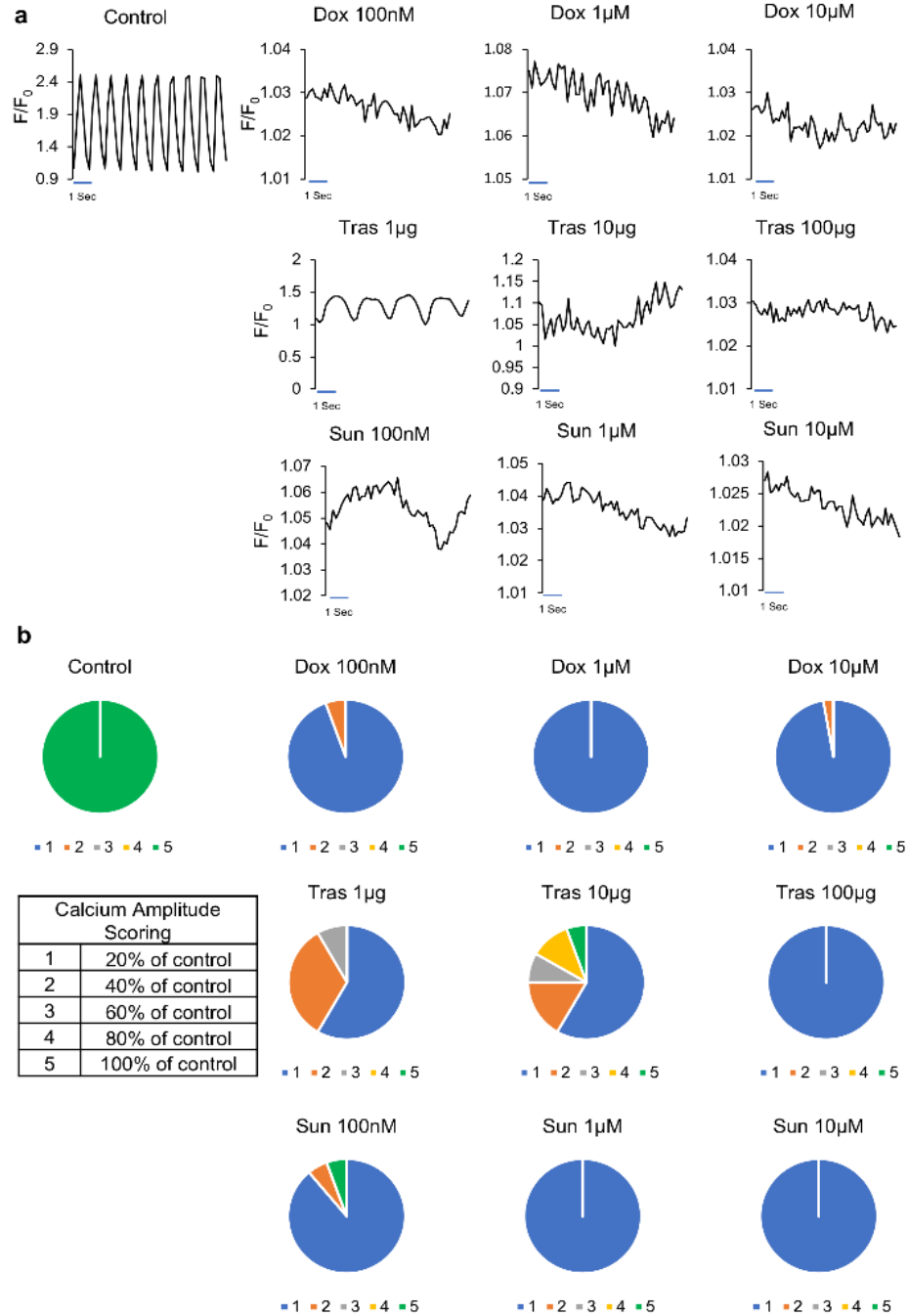
***Figure 8*: [100] Calcium transient assessment of cardiac tissue slices treated with corresponding concentrations of cardiotoxins.** (a) Representative calcium traces of heart slices exposed for 48-hours with respective concentrations of each cardiotoxin. (b) Calcium transient amplitude scoring indicating cardiomyocyte functionality as a percentage of control tissue slices (n = 36 cells).
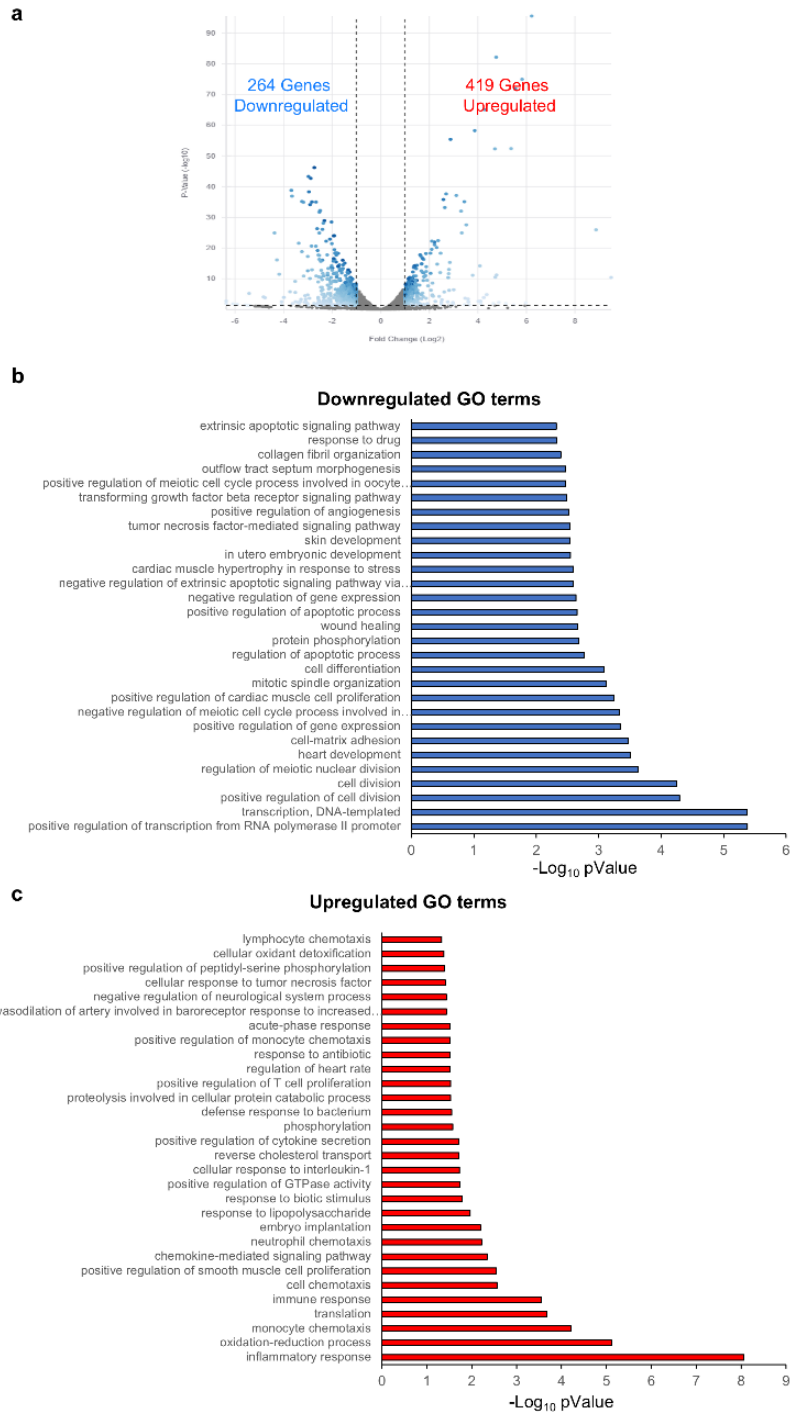
Figure 9: **[100] Differential gene expression of cardiac tissue slice treated with 100 nM Dox compared to control slices.** (a) Volcano plot demonstrating significantly changed gene expression. Representative bar graphs of significantly downregulated (b) or upregulated (c) gene ontology (GO) terms (n = 2).
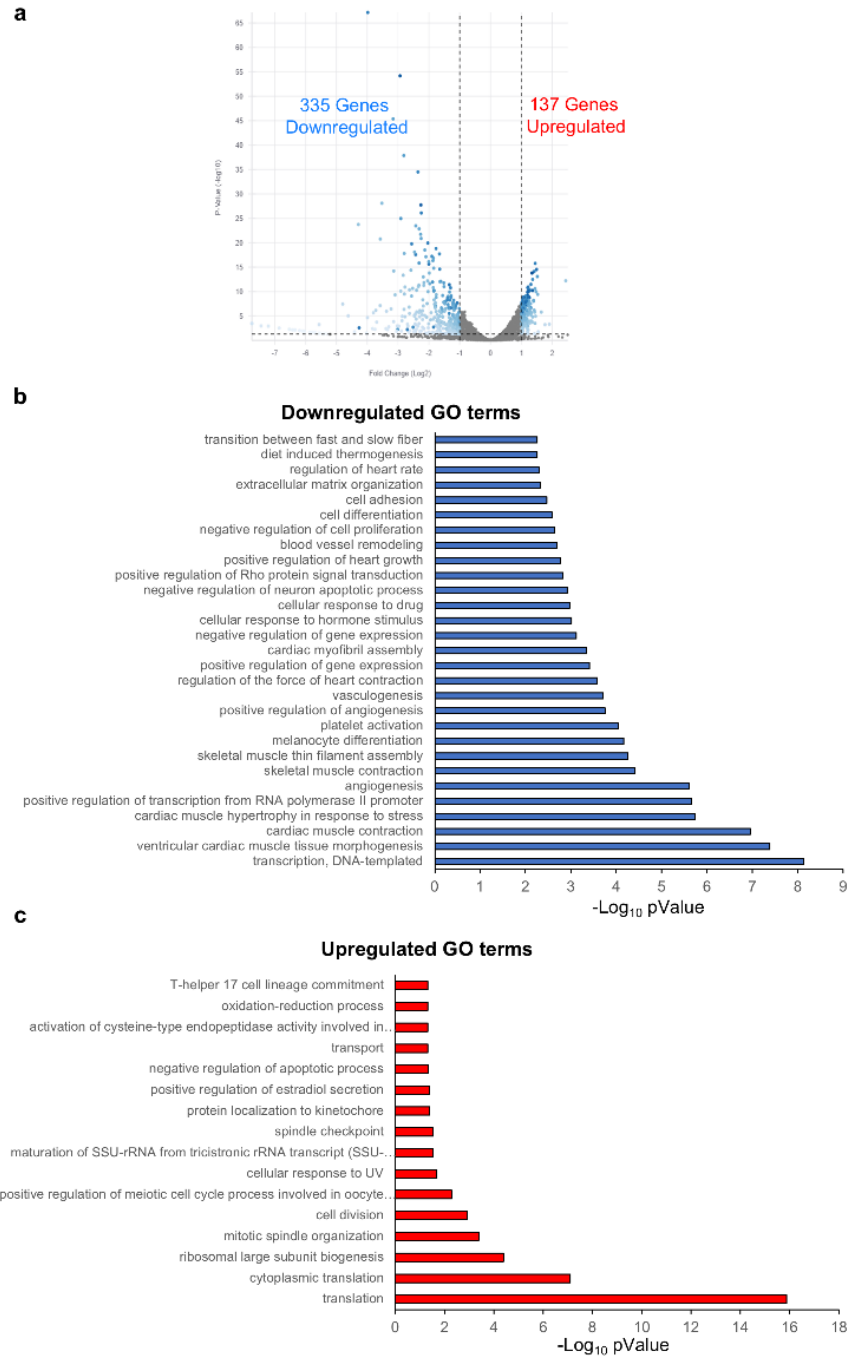
Figure 10: **[100] Differential gene expression of cardiac tissue slice with 1 µg/mL Tras compared to control slices.** (a) Volcano plot demonstrating significantly changed gene expression. Representative bar graphs of significantly downregulated (b) or upregulated (c) GO terms (n = 2).
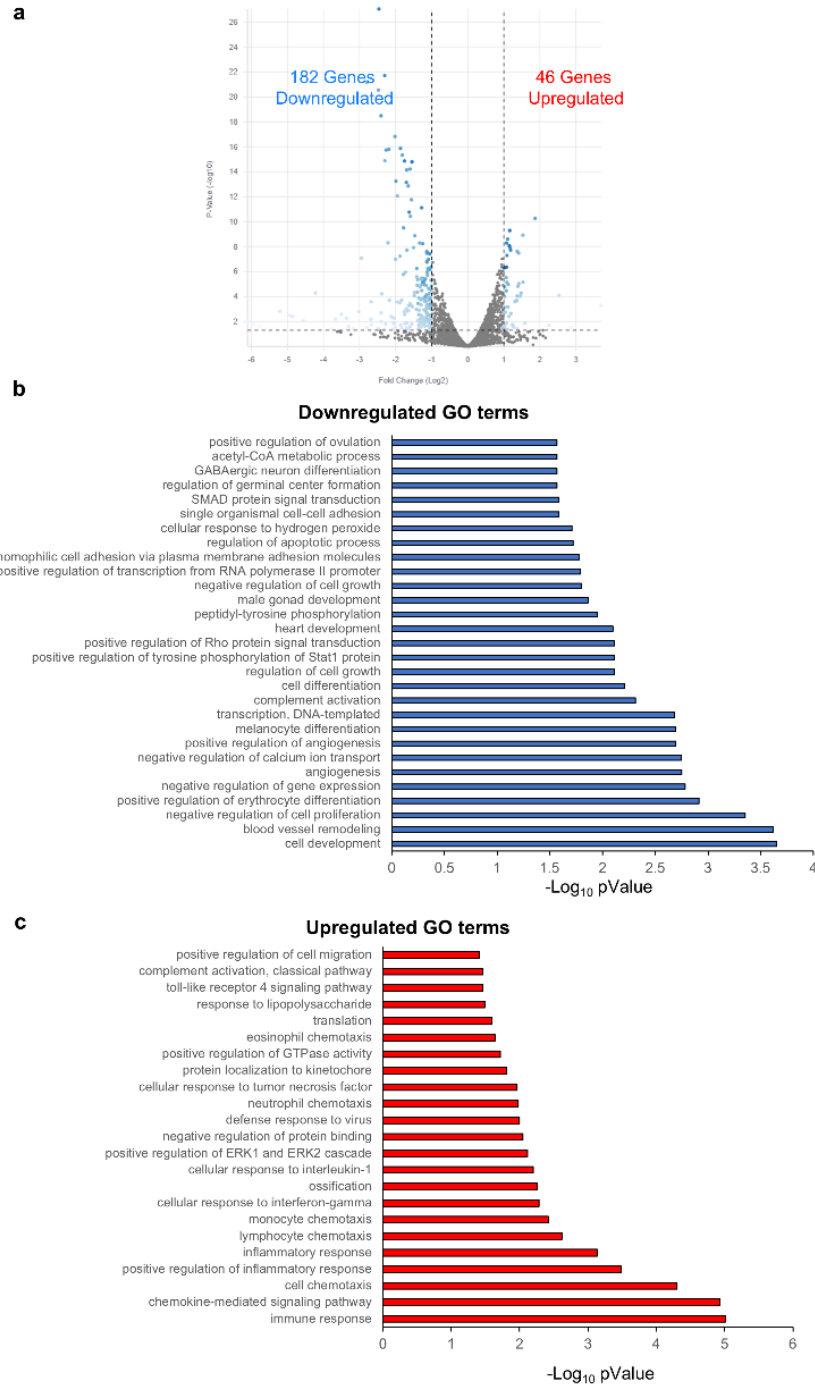
Figure 11: [100] Differential gene expression of cardiac tissue slice with 100 nM Sun compared to control slices. (a) Volcano plot demonstrating significantly changed gene expression. Representative bar graphs of significantly downregulated (b) or upregulated (c) GO terms (n = 2).

2.5. Discussion

The major cause of drug removal from market is due to unforeseen drug-induced cardiotoxicity. [128] This is a major concern with the rapidly growing number of new cancer therapeutics, thus a new field between cardiologist and oncologist has emerged called cardio-oncology. [124] There is an urgent need for a reliable preclinical drug screening platform to accurately detect cardiovascular toxicities associated with these emerging therapeutics before clinical trials. [11, 160]

The use of hiPSC-CMs for drug toxicity testing has been a partial solution to this problem in some studies, however, they do not address the need for a model that can predict functional cardiotoxicity. [55, 136] Additionally, hiPSC-CMs have fetal-like properties and are a single cell model thus they cannot capture the complexity of the 3-dimensional environment of the adult human myocardium. Here we demonstrate that using cardiac tissue slices as an alternative platform for cardiotoxicity detection, we can detect a diverse range of clinically relevant cardiotoxic mechanisms.

2.5.1. Anthracycline – Doxorubicin

Anthracyclines, such as doxorubicin, are a class of antibiotics used to treat breast cancer, lymphoma, leukemia, and sarcoma. [52, 63] Doxorubicin disrupts DNA and RNA synthesis and generates free radicals which induces DNA damage. [52, 135, 201] While doxorubicin is a commonly used and effective anticancer treatment, it has a limited dosage range due to its cardiotoxicity. 5 to 23% of patients who are treated with doxorubicin develop progressive heart failure symptoms and diminished exercise capacity. [27, 166] The toxic mechanism of doxorubicin is still poorly understood, however, literature shows that doxorubicin induces multiple forms of direct

cardiomyocyte damage as a result of free radical accumulation produced by the quinone group. [77] Some studies have reproduced this using hiPSC-CMs. [23, 205]

Consistent with these findings, heart slices can reproduce this known cardiotoxic effect of doxorubicin. The phenotypic damage induced by doxorubicin was shown by a decline in MTT viability, decreased connexin 43 and troponin T expression, reduced contractility, and abolished calcium transient. Transactionally, RNAseq analysis revealed a downregulation in cardiac development, oxidative phosphorylation and cellular division, and mitochondria viability. It also showed an upregulation of genes associated with oxidation/reduction and inflammatory responses.

2.5.2. HER2/neu inhibitor – Trastuzumab

Trastuzumab, a humanized monoclonal antibody targeting HER2/neu receptors, blocks the activation of the HER2/neu receptor, inhibiting epidermal growth factors/HER2 ligand receptor activity thus disrupting the phosphorylation of tyrosine kinases, which are critical regulators of the cell cycle. [163] Trastuzumab treatment typically does no result in cardiac dysfunction, however, in a subset of patients, heart failure can occur. [129] Trastuzumab cardiotoxicity is believed to occur through the disruption of the ERBB2/neuregulin signaling, which is essential for normal myocyte growth, survival, and homeostasis. [167] Recently, hiPSC-CMs have been used to model this detrimental phenotypic and mechanistic effects of trastuzumab treatment. [92, 100]

Heart slices were able to reproduce these findings evidenced by a decline in connexin 43 and troponin T expression and a disruption in calcium homeostasis. Mechanistically, RNA sequencing revealed direct cardiomyocyte damage and a significant downregulation in cardiac contractile gene expression.

41

2.5.3. VEGF inhibitor – Sunitinib

Sunitinib, a tyrosine kinase inhibitor (TKI), specifically inhibits vascular endothelial growth factor (VEGF) which in turn inhibits angiogenesis. Patients treated with sunitinib develop hypertension, cardiomyopathy, and vascular disease. [145] Additionally, 10 to 15% of patients develop cardiac systolic dysfunction which is believed to be due to a disruption of the coronary microvascular pericytes. [31, 124, 180] Since this is not a direct effect on cardiomyocytes, hiPSC-CMs cannot detect any obvious cardiotoxic effects of nanomolar concentrations with sunitinib treatment. [204]

While heart slices showed no major phenotypic damage in response to sunitinib exposure, they did demonstrate a disruption in calcium handling. Transcriptionally, heart slices treated with 100 nM sunitinib had a disruption in the angiogenic gene expression, which is consistent with the literature and clinically known cardiotoxic effects. [31, 180]

2.6. Conclusion

Overall hiPSC-CMs detected the cardiotoxicity of doxorubicin at nanomolar concentrations but did not detect the cardiotoxicity of sunitinib at this concentration. Heart slices on the other hand were able to replicate the clinically known cardiotoxic effects of each compound: Dox for mitochondrial damage and ROS accumulation, Tras for homeostasis disruption, and Sun for targeting the microvascular. These results suggest that cardiac tissue slices can be a promising platform for investigating cardiotoxic phenotypes and mechanisms of cancer therapeutic testing.

2.7. Limitations

Tissue slices were only exposed to three cardiotoxins and assessed at one time point (48 hours). While this time point demonstrated a significant functional

cardiotoxicity, it may not be an appropriate time point when testing other cancer therapeutics. Additionally, this study only used one functional assessment, calcium transients. Future experiments should be expanded to include either a contractility measurement or electrophysiology assessment.

CHAPTER 3: HEAD-TO-HEAD COMPARISON OF CARDIAC TISSUE SLICES AND HIPSC-CMS TO ASSESS THEIR RELIABILITY IN IDENTIFYING THE CLINICAL CARDIOTOXICITY OF 12 KNOWN CARDIOTOXINS

3.1. Introduction – Chemotherapeutic cardiotoxicities

With the rapidly increasing number of cancer therapeutics, the understanding of potential cardiotoxic drug effects needs to be investigated. Current platforms used in cardio-oncology basic science research are *in vivo* animal models and *in vitro* cell cultures (i.e. hiPSC-CMs). While both platforms are excellent tools for the discovery of mechanisms of action, they are limited in their ability to accurately model the human heart. Here, we proposal that cardiac tissue slices can outperform hiPSC-CMs in detecting cardiotoxic effects of known clinical cardiotoxins.

3.1.1. Anthracyclines – Doxorubicin

Anthracyclines such as doxorubicin (Dox), idarubicin, daunorubicin, and epirubicin, induce energetic/mitochondria damage. [105] Anthracyclines are a class of antibiotics that are used to treat various types of cancer (breast, leukemia, lymphoma) and are the most effective cancer therapy. [52, 184] This classification of drug inhibits topoisomerase II (inhibiting ligase repair of DNA breaks), intercalates DNA base pairs, creates iron-mediated free radicals (inducing more DNA damage), and reduces histones

(further reducing DNA repair). [52, 135, 201] While anthracyclines are highly effective in treating cancer, they cause cardiotoxicity. [27, 51, 103, 105, 158] 5-23% of patients develop HF and LV dysfunction in both short- and long-term exposure to these compounds. [27, 103] The exact cardiotoxic mechanism of this class of therapeutics remains elusive but it is believed to be caused by the accumulation of free radicals (inducing a stress response and DNA damage) and inhibition of DNA repair. [77, 201]

3.1.2. Alkylating agents – Vinorelbine, vincristine, and vinblastine

Another cardiotoxic classification is alkylating agents, such as vinorelbine, vincristine, and vinblastine. [49, 62, 107] Vinca-alkaloids are considered spindle toxins that interfere with beta-tubulin subunit of the alpha/beta-tubulin heterodimer thus inhibiting tubulin polymerization, which is a key protein in microtubule assembly. [62] In cardiomyocytes, there are three distinct populations of microtubules: cortical, interfibrillar, and perinuclear. [25] The cortical microtubules span across the cardiomyocyte perpendicular to myofibrils. [164, 165] They are responsible for mechanotransduction of external cues and regulate ion channels as well as transmembrane proteins. [164, 165] Interfibrillar microtubules are responsible for positioning organelles within the cell, maintaining intercalated disc, and T-tubule and SR membrane regulation. [26, 116, 147, 151, 176, 199, 202] Lastly, perinuclear microtubules surround the nucleus. This type of microtubule is responsible for organizing perinuclear organelles and interacting with the LINC complex that mechanically couples the nucleoskeleton to the microtubule cytoskeleton. [35, 133, 168] A disruption in these microtubules can cause major cellular dysregulation. [49, 62, 107] This category of

therapeutics has been linked to cardiac dysfunction and pulmonary hypertension caused by a disruption in myofilaments. [49, 62, 107]

3.1.3. Tyrosine kinase and VEGF inhibitors – Erlotinib, sunitinib, and nilotinib

Tyrosine kinase (TKI) and vascular endothelial growth factor (VEGF) inhibitors also induce cardiotoxicity. [105] Some common tyrosine kinase and VEGF inhibitors are erlotinib, sunitinib, and nilotinib. [105] Sunitinib binds to the phosphorylation site of the VEGFR receptors, inhibiting the VEGF signaling pathway. [134] In normal VEGF signaling activation one of two pathways can be activated. The first is the PI3K/AKT pathway which increases intracellular calcium, resulting in the activation endothelial nitric oxide (eNOS) synthase which, in turn, increases nitric oxide (NO) production. [20, 137] The other pathway is the mitogen-activated protein kinase (MAPK) pathway which increases intracellular prostacyclin (PGI_2) concentrations. [190] High concentrations of NO or PGI_2 will induce vasorelaxation, increase vascular permeability, and improve endothelial survival and angiogenesis. [134] With the treatment of sunitinib these pathways are inhibited, resulting in low intracellular concentrations of NO and PGI_2 thus inducing vasoconstriction, decreasing vascular permeability, and reducing angiogenesis. [134] Interestingly, in patients treated with sunitinib, there is an increase in endothlian-1 (ET-1) within the circulation, which further increases vasoconstriction. [89, 90] With VEGF having so many influences there are many adverse cardiovascular events of VEGF inhibits. Patients who receive this form of treatment are reported to have hypertension, thromboembolism, and cardiac contractile dysfunction (prolonged QT interval). [105, 145, 195] Nilotinib inhibits the tyrosine kinases BCR-ABL, cKit, and PDG-FR. [130] The only reported cardiovascular effect of this compound is the prolongation of the QT

interval. [88] It should be noted that while sunitinib and nilotinib both induce cardiovascular complications, erlotinib is very well handled in patients and cases of cardiotoxicity are very rare (4 cases reported to date). [42, 102, 125, 140]

3.1.4. Antimetabolites – Milrinone

Antimetabolites, such as cytarabine and milrinone, inhibit DNA and RNA growth by substituting normal building blocks of the RNA/DNA, thus inhibiting the cells during the S phase of mitosis. [132][66] Milrinone is a phosphodiesterase inhibitor that slows the degradation of cyclic AMP. [120] This induces an accumulation of cytosolic cAMP which will activate PKA, L-type calcium channels, and the ryanodine receptor, thus increasing intracellular calcium. [198] Activation of PKA causes the phosphorylation of troponin I, which in turn allows for faster force relaxation and contraction. [12, 198] The commonly reported cardiac effects are ECG changes (ST-segment and T-wave irregularities), chest pain, and myocardial ischemia. [105, 132] [51, 66]

3.1.5. Antiprotozoal – Pentamidine

Pentamidine is an antiprotozoal agent that is used to treat pneumocystis jiroveci pneumonia in patients with immunodeficiency virus infection. [16, 56, 60, 80, 82, 183] While this treatment is an effective alternative to the primary treatment, it does have a large number of adverse consequences. [60] Immediately after treatment patients are reported to experience hallucinations, nausea, vomiting, and hypotension. [60] With just 1 week of treatment, pentamidine induces nephrotoxicity, pancreatitis, and cardiotoxicity. [60, 183] The cardiotoxic events that occur include the prolongation of the QT-interval, torsade de points, sinus bradycardia, and ventricular tachycardia. [16, 56, 60, 80, 82, 183] This is due to the cardiotoxic mechanism of action pentamidine. Pentamidine inhibits the

transcription of the human ether-a-go-go-related gene (hERG), thus reducing the number

of potassium channels on the cell surface. [34, 101, 183] This subsequently blocks the I_{K1}

current, inducing QT prolongation and TdP. [34, 101, 183]

3.1.6. Cytotoxin – Arsenic trioxide

Arsenic trioxide, a natural toxin, has been used for centuries to treat various

diseases, such as myelodysplastic syndrome, leukemia, and many types of cancers. [43,

157, 205] Due to the non-specificity of arsenic trioxide, there is a dosage limit to reduce

the damage to other cells. [29, 76] In the heart, this toxin causes a prolongation of the

QT-interval inducing ventricular arrhythmias. [45] This is hypothesized to be due to

arsenic reducing cardiac phosphorylation, thus decreasing intracellular ATP

concentrations inhibiting the activation of potassium-ATP ion channel. [45]

3.1.7. Other – Endothelin-1

Endothelin-1 (ET-1) is a peptide that has been linked to tumor survival,

proliferation, immune modulation, metastasis, and angiogenesis [154] Over the past 3

decades, ET-1 therapies have been developed to interfere with ET-1 receptor activation.

[7, 153] This has proven to be an effective method in treating various types of cancers but

there are adverse events associated with ET-1 therapies. [7] In the cell, a balance between

NO concentrations and ET-1 binding to its receptor controls contraction and relaxation.

[19] NO contractions directly regulate cGAMP synthesis resulting in the relaxation of the

cell. When there is a higher amount of ET-1 binding to the receptors there will be

increased contraction. [19] Endothelin-1 receptors are expressed throughout the body

leading to both direct and indirect cardiovascular complications. [7] Clinically, these

complications can range from hypertension to ischemic heart failure. [36, 66, 68, 112, 172, 174, 175]

3.1.8. Other – BMS-986094

BMS-986094 (BMS) is an anti-hepatitis C virus therapy that was stopped during phase II clinical trials due to unforeseen cardiotoxic events. [3, 178, 185] With long-term treatment, BMS was found to induce a decrease in left ventricular ejection fraction.[3, 185] Through *in vivo* and *in vitro* studies, it was discovered that BMS directly altered CM contractility through the disruption of calcium transients. [161] Additionally, BMS has been reported to induce mitochondrial toxicity with long term exposure in cell cultures, however, this effect has not been reproduced in animals. [9, 46, 53, 117, 161]

3.2. Study Hypothesis

In order to fully evaluate tissue slices as a reliable cardiotoxicity detection screening platform, we hypothesize that cardiac tissue slices can more reliably detect cardiotoxic effects compared to hiPSC-CMs. Here, 12 known cardiotoxic compounds, 1 negative, and 2 positive controls were blinded and tested on cardiac tissue slices. The acute, <1 hour, and subacute, 72 hours, exposure to each compound at four concentrations was evaluated for cardiotoxic effects. Cardiotoxicity for acute exposure was determined by a decline in functionality, evaluated by calcium-transient expression and twitch force measurement. For chronic exposure, the viability, cardiac structure, and transcriptional expression was assessed. Lastly, results obtained from tissue slices were compared to hiPSC-CMs data obtained from CardioExcyte recordings of impedance contractile function over a course of acute, 1 hour, and subacute, 72 hours, of exposure to each compound.

It was found that 2 out of 12 compounds demonstrated cardiotoxicity after 48 to 72 hours of exposure to the clinically relevant dosage in hiPSC-CMs. On tissue slices, 12 out of 12 compounds were detected as cardiotoxic at the clinically relevant dosage, 8 of which were acutely cardiotoxic. Overall, this study demonstrates that heart slices can more accurately detect a diverse range of cardiotoxic effects induced by chemotherapeutics compared to hiPSC-CMs.

3.3. Experimental design

Twelve cardiotoxic compounds, detailed in Table 3, were blindly coded for the study.

3.3.1. Experimental design: Heart Slice

The acute effects of each compound were assessed by evaluating the functionality of the cardiac tissue slices at four different concentrations shown in Table 3. The minimum dosage is based on the C_{max} of the compound. Concentrations are increased by 3X the previous dosage. One tissue slice was initially measured for baseline functionality and the drug was added at increasing concentrations. The functionality assessments used were calcium transient assay and twitch force measurement. The calcium transient assay was performed as described by the manufacturer's protocol. Calcium transient trace data was extracted using ImageJ software and the amplitude was quantified using a custom MATLAB script.

Compound	Classification	Dose 1	Dose 2	Dose 3	Dose 4
Mitochondrial toxin					
Doxorubicin	Anthracyclines	0.1 μM	0.3 μM	1 μM	3 μM
Erlotinib	Kinase inhibitor	0.3 μM	1 μM	3 μM	10 μM
Sunitinib	Tyrosine kinase inhibitor	0.01 μM	0.1 μM	0.3 μM	1 μM
Structural/myofilament					
Vinorelbine	Vinca alkaloid	0.1 μM	0.3 μM	1 μM	3 μM
Endothelin-1	Vasoconstrictor	100 μM	1 nM	30 nM	100 nM
Vincristine	Vinca alkaloid	0.001 μM	0.003 μM	0.1 μM	0.3 μM
Vinblastine	Vinca alkaloid	0.001 μM	0.003 μM	0.01 μM	0.3 μM
Contractility					
BMS-986094	Anti-viral	0.1 μM	0.3 μM	1 μM	3 μM
Milrinone	Antimetabolite	0.1 μM	0.3 μM	3 μM	10 μM
Nilotinib	Kinase inhibitor	0.1 μM	1 μM	3 μM	10 μM
Electro-physiological disturbance					
Pentamidine	Cytotoxin	0.1 μM	0.3 μM	1 μM	3 μM
Arsenic Trioxide	Cytotoxin	0.1 μM	0.3 μM	1 μM	3 μM
None					
Acetaminophen	Analgesics and antipyretics	1 μM	1 μM	1 μM	1 μM

Table 3: **Cancer therapeutic dosages.** 12 known cardiotoxins and 1 negative control for head-to-head comparison of heart slice and hiPSC-CMs. Listed are the compound classification, known cardiotoxic effect, and dosages that were tested. The minimum dosage was determined by the compound's Cmax and the subsequent doses are 3X increases.

Twitch force measurement was recorded by attaching the tissue slices to 3.0 suture and suspending the slice from a force transducer in no BDM Tyrode's solution.

Twitch force measurements were analyzed using a custom MATLAB script to quantify the amplitude.

Subacute exposure to the compounds was performed for 72 hours. The media was changed twice per day, with fresh compound added at each media change. At the end point of the experiment, the tissue slices were collected for structural and transcriptional assessment. Structural assessment consisted of performing immunolabeling for cardiac specific troponin T and gap junction protein connexin 43. Lastly, transcriptional assessment of the exposed tissue slices was quantified by qRT-PCR for Col-1a, Col-3a, TNNT2, a-SMA, and Myh7. The obtained values were normalized to the housekeeping gene GAPDH.

Two-tailed, one-way ANOVA was performed to assess the statistical difference of each dosage compared to control (acute – no dose; subacute – fresh heart slices or day 2 Ace) tissue slices. A significance level of $p < 0.05$ was considered statistically significant.

3.3.2. Experimental design: hiPSC-CM

Nan]i[on 96 well stim plate was coated with PBS containing fibronectin and 1% gelatin overnight. hiPSC-CM cells were seeded at 1 million cells per well with plating media. Media was changed to maintenance media (with serum) after 6 hours. Cells were cultured for 6 days with media change every other day. On day 6, baseline measurements were recorded in triplicate with and without electrical stimulation using a CardioExcyte device. 100 μL of the media from the well was discarded and 100 μL of serum free maintenance media containing the compound was be added. Cells were incubated for 1 hour at 37°C and the acute effects were recorded in triplicate with and without electrical

stimulation. The plate was returned to the incubator and cultured for 3 days with the media changed every day containing fresh compound. After the media was changed on the subsequent days, the plate was incubated for 2 hours prior to recording the measurements.

Each plate contained at most 4 compounds at 4 concentrations, 1 µM of Ace (negative control), and 0.01% DMSO. Data was extracted by Nan]i[on and statistical analysis was performed by our lab. 2-way ANOVA with Dunnett correction was used to evaluate the significance between no dose of each respective concentration (dose 1 at time 0 hour vs dose 1 at time 1 hour, etc.).

3.4. Results

3.4.1. Results: Anthracyclines – Doxorubicin

Anthracyclines induce an accumulation of ROS within the mitochondria of the cells, inducing detrimental DNA damage. [32, 67, 98] Table 4 shows a simplified summary of the results from both the control (Dox) and coded doxorubicin treatment in both tissue slices and hiPSC-CMS. An 'X' indicates a significant decline in the parameter. The contractile function of the tissue slices was significantly lower with doses 1, 3, and 4 with the Dox treatment (Figure 12A; Table 4), however, doxorubicin exposure did not result in a decline (Figure 12C; Table 4). This could possibly be due to a variation in the compound preparation or differences between tissue slice samples. The hiPSC-CMs did not detect acute differences in contractile function with either Dox or doxorubicin treatment (Figures 12B and 12D; Table 4). With subacute exposure, hiPSC-CMs detected a decline in contractility in the high concentrations of both Dox and doxorubicin exposure at 48 hours of exposure and a decline in the low concentrations

after 72 hours of exposure (Figures 12B and 12D; Table 4). These contractile data indicate that heart slices can better detect the cardiotoxicity of the acute exposure to doxorubicin treatment compared to hiPSC-CMs, however, there is a batch-to-batch variation between compounds or tissue samples.

Similar to the data shown in Chapter 2, the calcium transients with both Dox and doxorubicin exposure were completely abolished (Figures 13A and 14A; Table 4), tissue viability significantly declined in all but dose 2 of Dox exposure (Figure 13B; Table 4). There was a significant decline in the structural integrity (Figures 13C and 14C; Table 4) and a disruption in transcriptional expression (Figures 13D and 14D; Table 4). Interestingly, both treatments of doxorubicin demonstrated a colocalization of connexin 43 with the nuclei with the high concentrations. This could be due to the damage to the mitochondria, inhibiting the translocation of the gap junction proteins from the nuclei to the cell surface. Overall, tissue slices were able to reproduce the clinically known cardiotoxic mechanism of doxorubicin treatment of inducing an accumulation of ROS within the cell indicated by the decline in calcium handling, contractile function, tissue viability, structural integrity, and transcriptional expression with subacute exposure.

Left table — Tissue slice Contractility / hiPSC-CMs Contractility

			Anthracyclines	
			Dox	Doxorubicin
Tissue slice	Contractility	Dose 1	X	
		Dose 2		
		Dose 3	X	
		Dose 4	X	
hiPSC-CMs Contractility	0 hr	Dose 1		
		Dose 2		
		Dose 3		
		Dose 4		
	1 hr	Dose 1		
		Dose 2		
		Dose 3		
		Dose 4		
	24 hr	Dose 1		
		Dose 2		
		Dose 3		
		Dose 4		
	48 hr	Dose 1		
		Dose 2		
		Dose 3		X
		Dose 4	X	
	72 hr	Dose 1	X	
		Dose 2		X
		Dose 3	X	X
		Dose 4	X	X

Right table — Tissue slice

			Anthracyclines	
			Dox	Doxorubicin
Tissue slice	Calcium	Dose 1	X	X
		Dose 2	X	X
		Dose 3	X	X
		Dose 4	X	X
	MTT	Dose 1	X	X
		Dose 2		X
		Dose 3	X	X
		Dose 4	X	X
	Structural integrity	Dose 1	X	X
		Dose 2	X	X
		Dose 3	X	X
		Dose 4	X	X
	qRT-PCR	Dose 1	X	X
		Dose 2	X	X
		Dose 3	X	X
		Dose 4	X	X

Table 4: Simplified summary of hiPSC-CM and heart slice acute and subacute exposure to an anthracycline. 'X' indicates a significant decline in the parameter.

Figure 12: **Contractility assessment of cardiac tissue slices and hiPSC-CMs after Dox and doxorubicin exposure.** (A) Contractility amplitude for tissue slices at no dose and doses 1 to 4 of acute Dox exposure. (n = 11-24) (B) hiPSC-CM impedance amplitude for no exposure, 1 hour, 24 hours, 48 hours, and 72 hours of Dox exposure. (n = 4-5) (C) Contractility amplitude for tissue slices at no dose and doses 1 to 4 of acute doxorubicin exposure. (n = 2-10) (D) hiPSC-CM impedance amplitude for no exposure, 1 hour, 24 hours, 48 hours, and 72 hours of doxorubicin exposure. (n = 5)

Figure 13: **Heart slice calcium transient amplitude (acute exposure), viability, structural integrity, and transcriptional expression after subacute exposure of Dox.** (A) Calcium transient amplitude for tissue slices at no dose and doses 1 to 4 of acute Dox exposure. (n = 1-12) (B) Graph depicting MTT viability of no dose to dose 4 Dox treated tissue slices. (n = 3-18) (C) Representative images of troponin-T and connexin 43 of tissue slices treated with low to high concentrations of Dox. (D) qRT-PCR for cardiac remodeling gene expression for Dox treated tissue slices as a fold increase of Ace (Control). (n = 2-3)
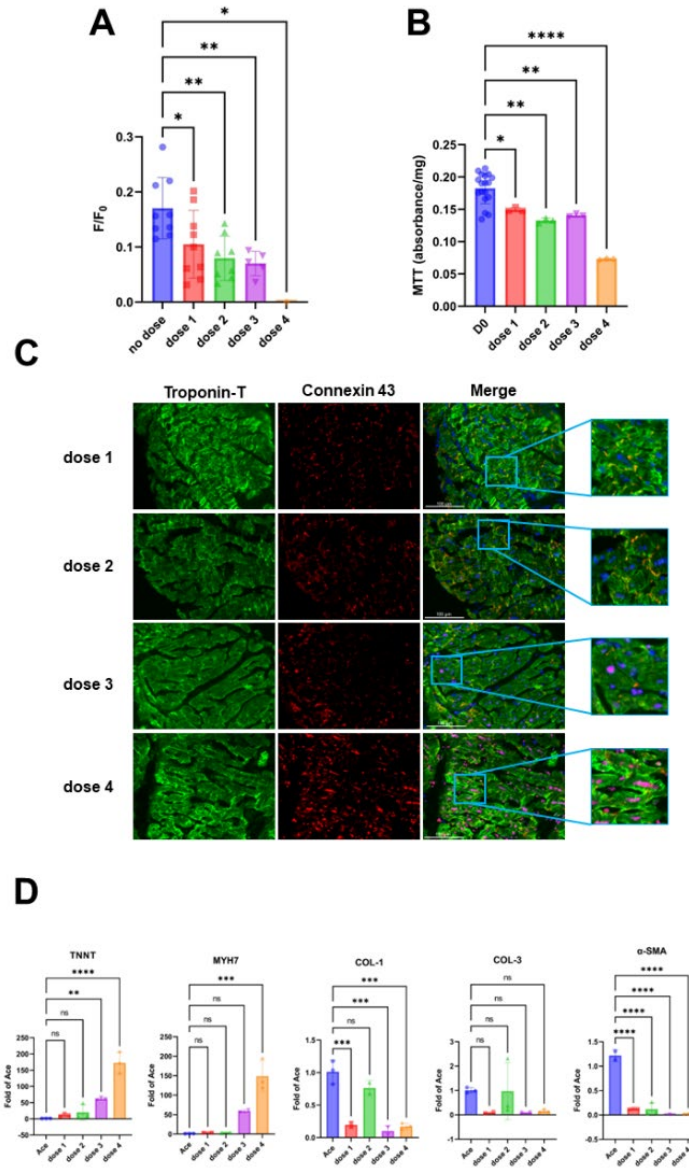
***Figure 14*: Heart slice calcium transient amplitude (acute exposure), viability, structural integrity, and transcriptional expression after subacute exposure of doxorubicin.** (A) Calcium transient amplitude for tissue slices at no dose and doses 1 to 4 of acute doxorubicin exposure. (n = 1-9) (B) Graph depicting MTT viability of no dose to dose 4 doxorubicin treated tissue slices. (n = 3-18) (C) Representative images of troponin-T and connexin 43 of tissue slices treated with low to high concentrations of doxorubicin. (D) qRT-PCR for cardiac remodeling gene expression for doxorubicin treated tissue slices as a fold increase of Ace (Control). (n = 1-3)

3.4.2. Results: TKIs/VEGF inhibitors – Erlotinib, sunitinib, and nilotinib

Table 5 show a simplified summary of the TKI data for heart slices and hiPSC-CMs at acute and subacute exposure to each compound. Of the three TKIs tested, nilotinib was the only compound at all concentrations that induced an acute disruption in contractility in the heart slices (Figure 15; Table 5). This could be due to the mechanism by which nilotinib acts. Nilotinib inhibit the BCR-ABL, cKIT, and PDG-FR pathways which are directly responsible for contractile function. Whereas sunitinib and erlotinib target VEGFR and EGFR having an indirect effect on contractile function which takes time to observe a change in contractility. This is reflected in the hiPSC-CM data for sunitinib which demonstrated a change in contractility after 1 hour, 48 hours, and 72 hours of exposure to the high concentration (Figure 15D; Table 5). The hiPSC-CMs were not able to detect a change in contractility at any time point or compound concentration with nilotinib treatment (Figure 15F; Table 5). This may be due to the immature nature of this cell type.

All three TKIs induced a significant decline in calcium handling (Figures 16A, 17A, and 18A; Table 5). Similar to what was reported in Chapter 2, sunitinib treatment resulted in an almost abolished calcium transients with the clinically relevant dosage and a complete abolishment of the signal with the subsequent concentrations. Also, consistent with the previously reported effect of sunitinib on tissue slices, tissue viability was significantly reduced at all concentrations of sunitinib treatment (Figure 17B; Table 5). Since erlotinib is a milder TKI, there was no significant decline in tissue viability (Figure 16B; Table 5). There was variation in the viability of tissue slices treated with nilotinib with dose 1 and dose 4 inducing a decrease but the other two concentrations not resulting

in a decrease (Figure 18B; Table 5). This may be due to sample variation. Both erlotinib and nilotinib at all concentrations induced a disruption in tissue slice structural integrity (Figures 16C and 18C; Table 5). Sunitinib reproduced the same results seen in Chapter 2 of dose 1 not inducing a significant change in the structural integrity but with increasing concentrations there is a dose dependent decline in troponin T expression (Figure 17C; Table 5). Lastly, the transcriptional expression was disrupted in all three TKIs at all concentrations indicating that all three compounds have a negative effect on cardiac expression.

Overall, tissue slices were able to detect the acute contractility effect of nilotinib while hiPSC-CMs did not detect a difference in contractility with either acute or subacute exposure. Tissue slices demonstrated their ability to reproduce data across separate studies by accurately replicating the effects of sunitinib treatment on tissue slice calcium handling, viability, and structural integrity. Lastly, while erlotinib is a milder TKI when it comes to cardiotoxicity, heart slices were able to detect the acute and subacute cardiotoxic effects of this compound at the clinically relevant concentrations while the hiPSC-CMs did not detect any change (either in the Chapter 2 study with no activation of apoptosis or in the contractility measurement shown in this study).

TKIs/VEGF inhibitors

Tissue slice	Contractility		Erlotinib	Sunitinib	Nilotinib
		Dose 1			X
		Dose 2			X
		Dose 3			X
		Dose 4			X

hiPSC-CMs Contractility			Erlotinib	Sunitinib	Nilotinib
	0 hr	Dose 1			
		Dose 2			
		Dose 3			
		Dose 4			
	1 hr	Dose 1			
		Dose 2			
		Dose 3			
		Dose 4		X	
	24 hr	Dose 1			
		Dose 2			
		Dose 3			
		Dose 4			
	48 hr	Dose 1			
		Dose 2			
		Dose 3			
		Dose 4		X	
	72 hr	Dose 1			
		Dose 2			
		Dose 3			
		Dose 4		X	

TKIs/VEGF inhibitors

Tissue slice			Erlotinib	Sunitinib	Nilotinib
	Calcium	Dose 1	X	X	X
		Dose 2	X	X	X
		Dose 3	X	X	X
		Dose 4	X	X	X
	MTT	Dose 1		X	X
		Dose 2		X	
		Dose 3		X	
		Dose 4		X	X
	Structural integrity	Dose 1	X		X
		Dose 2	X	X	X
		Dose 3	X	X	X
		Dose 4	X	X	X
	qRT-PCR	Dose 1	X	X	X
		Dose 2	X	X	X
		Dose 3	X	X	X
		Dose 4	X	X	X

Table 5: Simplified summary of hiPSC-CM and heart slice acute and subacute exposure to TKI/VEGF inhibitors. 'X' indicates a significant decline in the parameter.
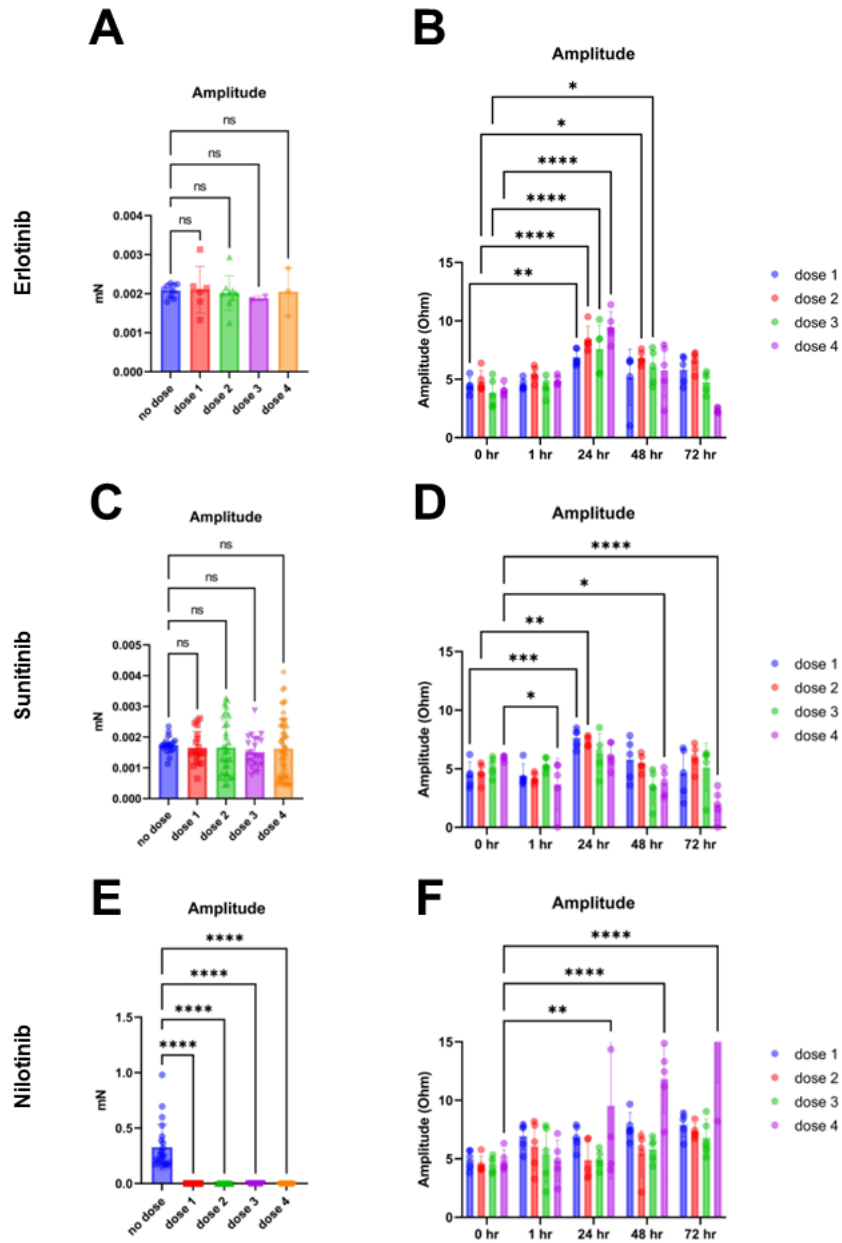
Figure 15: **Contractility assessment of cardiac tissue slices and hiPSC-CMs after erlotinib, sunitinib, and nilotinib exposure.** Contractility amplitude for tissue slices at no dose and doses 1 to 4 of acute erlotinib (A; n = 4-15), sunitinib (C; n = 19-54), and nilotinib (E; n = 22-42) exposure. hiPSC-CM impedance amplitude for no exposure, 1 hour, 24 hours, 48 hours, and 72 hours of erlotinib (B; n = 5), sunitinib (D; n = 5), and nilotinib (F; n = 5) exposure.
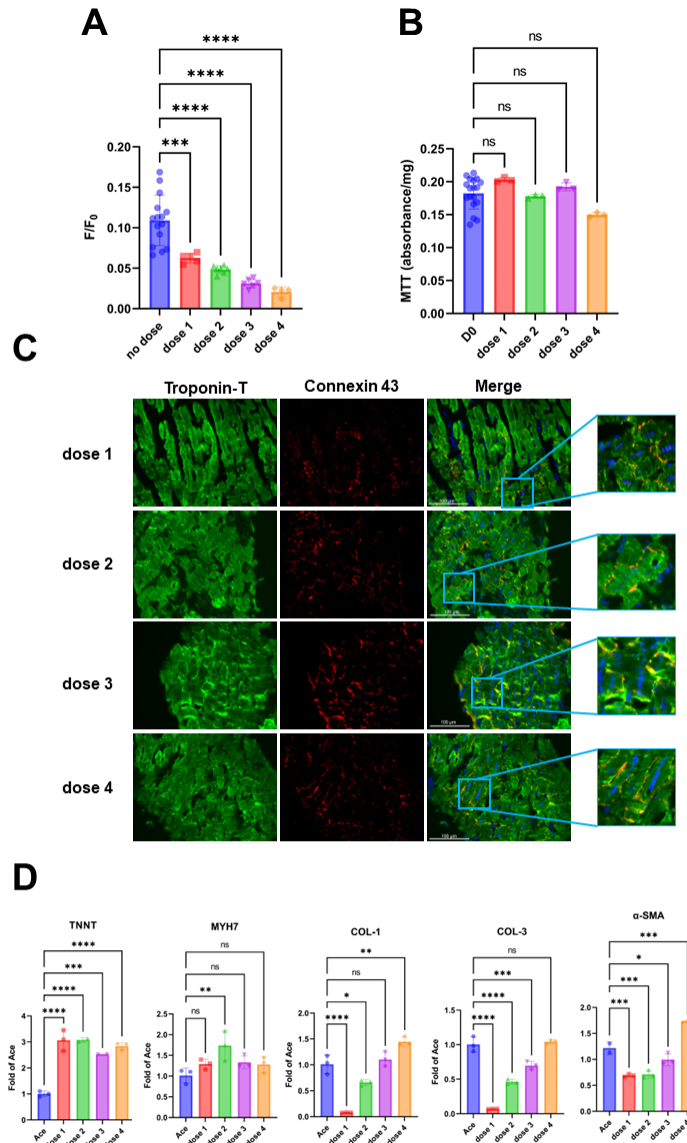
Figure 16: **Heart slice calcium transient amplitude (acute exposure), viability, structural integrity, and transcriptional expression after subacute exposure of erlotinib.** (A) Calcium transient amplitude for tissue slices at no dose and doses 1 to 4 of acute erlotinib exposure. (n = 4-15) (B) Graph depicting MTT viability of no dose to dose 4 erlotinib treated tissue slices. (n = 3-18) (C) Representative images of troponin-T and connexin 43 of tissue slices treated with low to high concentrations of erlotinib. (D) qRT-PCR for cardiac remodeling gene expression for erlotinib treated tissue slices as a fold increase of Ace (Control). (n = 2-3)
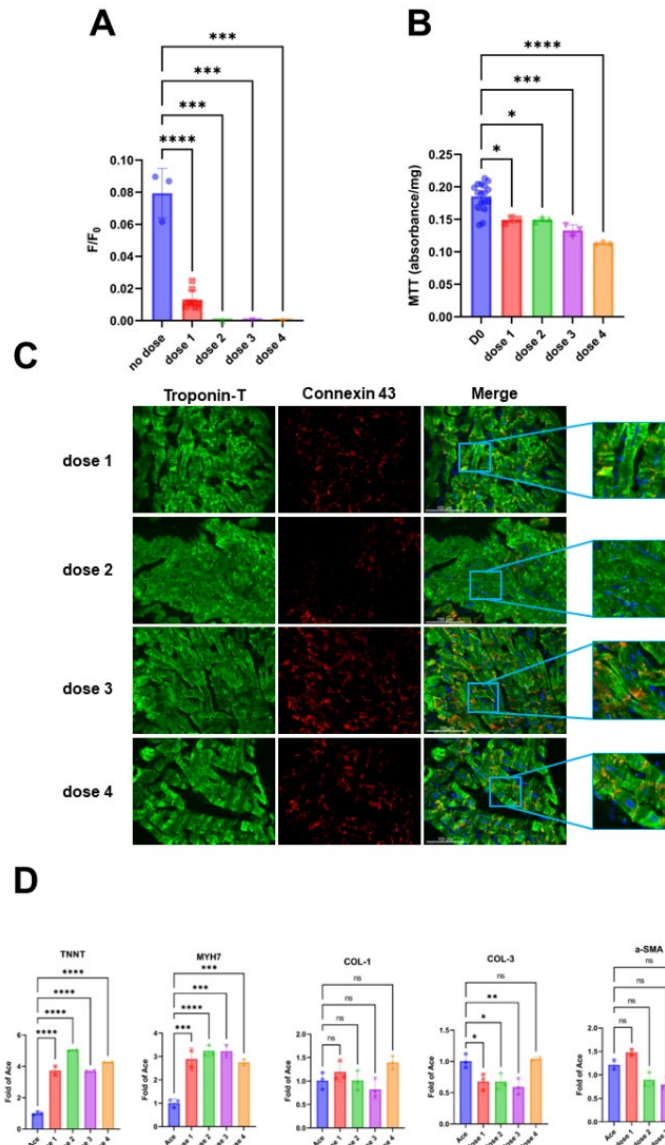
Figure 17: **Heart slice calcium transient amplitude (acute exposure), viability, structural integrity, and transcriptional expression after subacute exposure of sunitinib.** (A) Calcium transient amplitude for tissue slices at no dose and doses 1 to 4 of acute sunitinib exposure. (n = 1-8). (B) Graph depicting MTT viability of no dose to dose 4 sunitinib treated tissue slices. (n = 3-17) (C) Representative images of troponin-T and connexin 43 of tissue slices treated with low to high concentrations of sunitinib. (D) qRT-PCR for cardiac remodeling gene expression for sunitinib treated tissue slices as a fold increase of Act (Control). (n = 2-3)
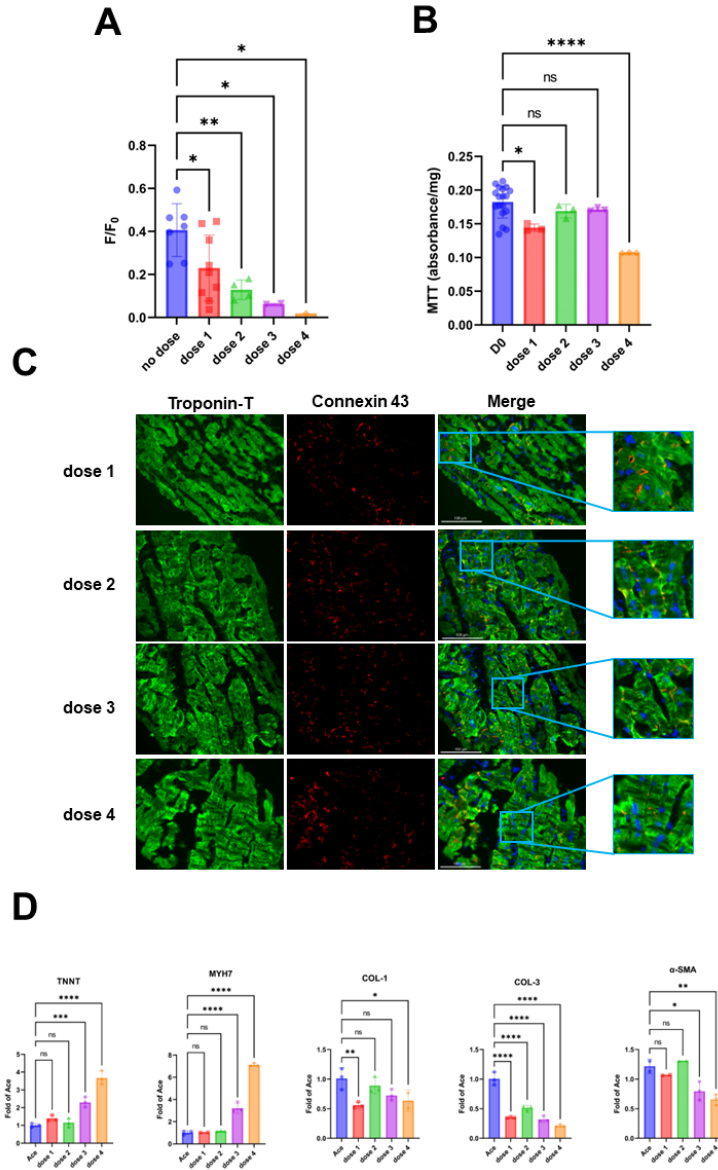
***Figure 18*: Heart slice calcium transient amplitude (acute exposure), viability, structural integrity, and transcriptional expression after subacute exposure of nilotinib.** (A) Calcium transient amplitude for tissue slices at no dose and doses 1 to 4 of acute nilotinib exposure. (n = 1-9). (B) Graph depicting MTT viability of no dose to dose 4 doxorubicin treated tissue slices. (n = 3-18). Representative images of troponin-T and connexin 43 of tissue slices treated with low to high concentrations of nilotinib. (D) qRT-PCR for cardiac remodeling gene expression for nilotinib treated tissue slices as a fold increase of Act (Control). (n = 2-3)

3.4.3. Results: Vinca alkaloids – Vinorelbine, vincristine, and vinblastine

Vinca alkaloids interfere with microtubule assembly and take time to induce a phenotype. Consistent with this knowledge, none of the myofilament toxins induced a decline in contractility within the tissue slices with acute exposure (Figures 19A, 19C, and 19E; Table 6). In the hiPSC-CMs, all three myofilament toxins resulted in a continuous decline in contractile function after 48 hours of exposure (Figures 19B, 19D, and 19F; Table 6).

While a change in contractile function may take time to be observed with vinca alkaloids, changes in ion channel regulation can be reflected acutely. This was seen with all three myofilament toxins (Figures 20A, 21A, and 22A; Table 6). All concentrations of vincristine and only the high concentration of vinorelbine resulted in a decline in tissue viability (Figures 21B and 20B; Table 6). Vinblastine did not result in a decline in tissue viability at any concentration (Figure 22B; Table 6). All three vinca alkaloids resulted in a decline in structural integrity due their interference with the disruption of myofilaments within the cells (Figures 20C, 21C, and 22C; Table 6). Lastly, vinorelbine at all concentrations resulted in altered transcriptional expression while the other two vinca alkaloids at the low concentration showed no change in expression (Figures 20D, 21D, and 22D; Table 6).

Left table — Contractility

Tissue slice / Contractility	Vinca alkaloids		
	Vinorelbine	Vincristine	Vinblastine
Dose 1			
Dose 2			
Dose 3			
Dose 4			

hiPSC-CMs Contractility

Time	Dose	Vinorelbine	Vincristine	Vinblastine
0 hr	Dose 1			
0 hr	Dose 2			
0 hr	Dose 3			
0 hr	Dose 4			
1 hr	Dose 1			
1 hr	Dose 2			
1 hr	Dose 3			
1 hr	Dose 4	X		
24 hr	Dose 1			
24 hr	Dose 2			
24 hr	Dose 3			
24 hr	Dose 4			
48 hr	Dose 1			
48 hr	Dose 2			
48 hr	Dose 3			
48 hr	Dose 4	X		
72 hr	Dose 1			
72 hr	Dose 2	X		
72 hr	Dose 3	X		X
72 hr	Dose 4	X	X	X

Right table — Tissue slice

Assay	Dose	Vinorelbine	Vincristine	Vinblastine
Calcium	Dose 1			X
Calcium	Dose 2		X	X
Calcium	Dose 3		X	X
Calcium	Dose 4	X	X	X
MTT	Dose 1		X	
MTT	Dose 2		X	
MTT	Dose 3		X	
MTT	Dose 4	X	X	
Structural integrity	Dose 1	X	X	X
Structural integrity	Dose 2	X	X	X
Structural integrity	Dose 3	X	X	X
Structural integrity	Dose 4	X	X	X
qRT-PCR	Dose 1	X		
qRT-PCR	Dose 2	X	X	X
qRT-PCR	Dose 3	X	X	X
qRT-PCR	Dose 4	X	X	X

Table 6: Simplified summary of hiPSC-CM and heart slice acute and subacute exposure to vinca alkaloids. 'X' indicates a significant decline in the parameter.
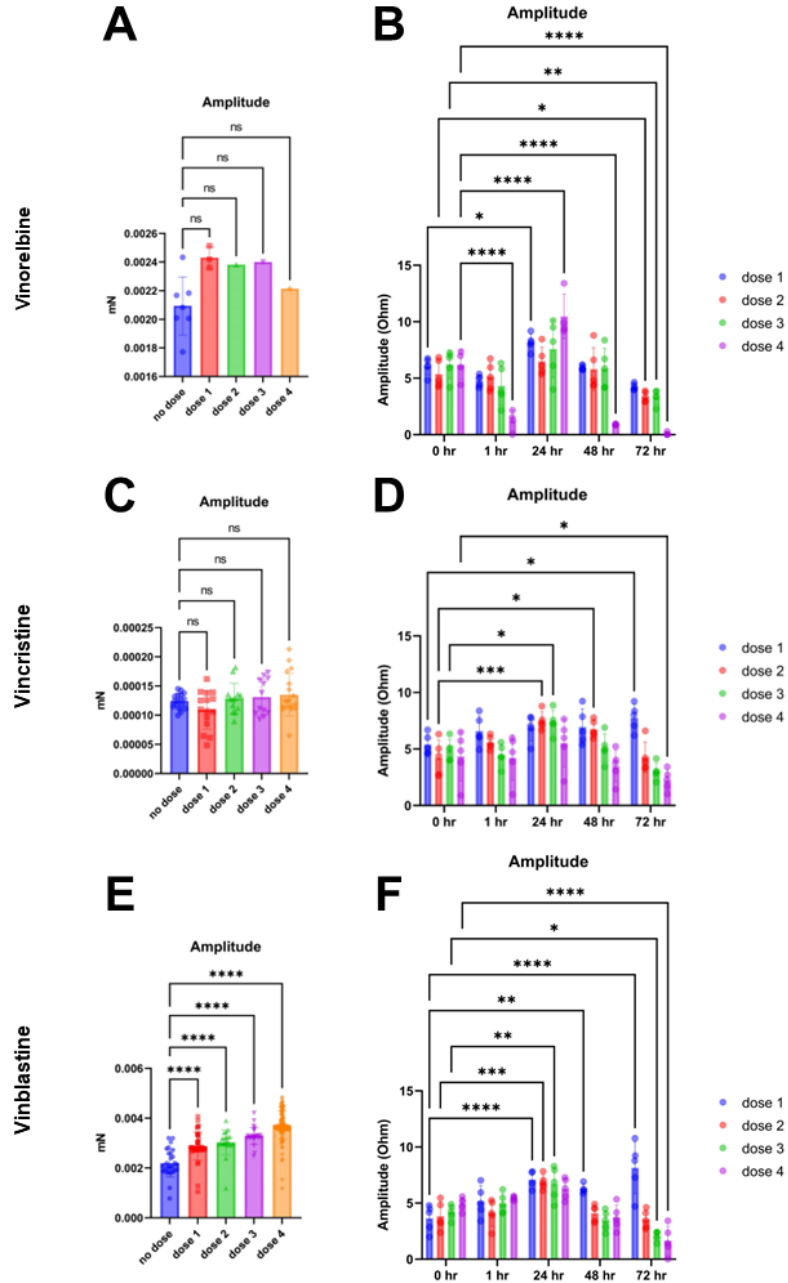
***Figure 19*: Contractility assessment of cardiac tissue slices and hiPSC-CMs after vinorelbine, vincristine, and vinblastine exposure.** Contractility amplitude for tissue slices at no dose and doses 1 to 4 of acute vinorelbine (A; n = 1-7), vincristine (C; n = 12-18), and vinblastine (E; n = 22-115) exposure. hiPSC-CM impedance amplitude for no exposure, 1 hour, 24 hours, 48 hours, and 72 hours of vinorelbine (B; n = 4-5), vincristine (D; n = 5), and vinblastine (F; n = 4-5) exposure.
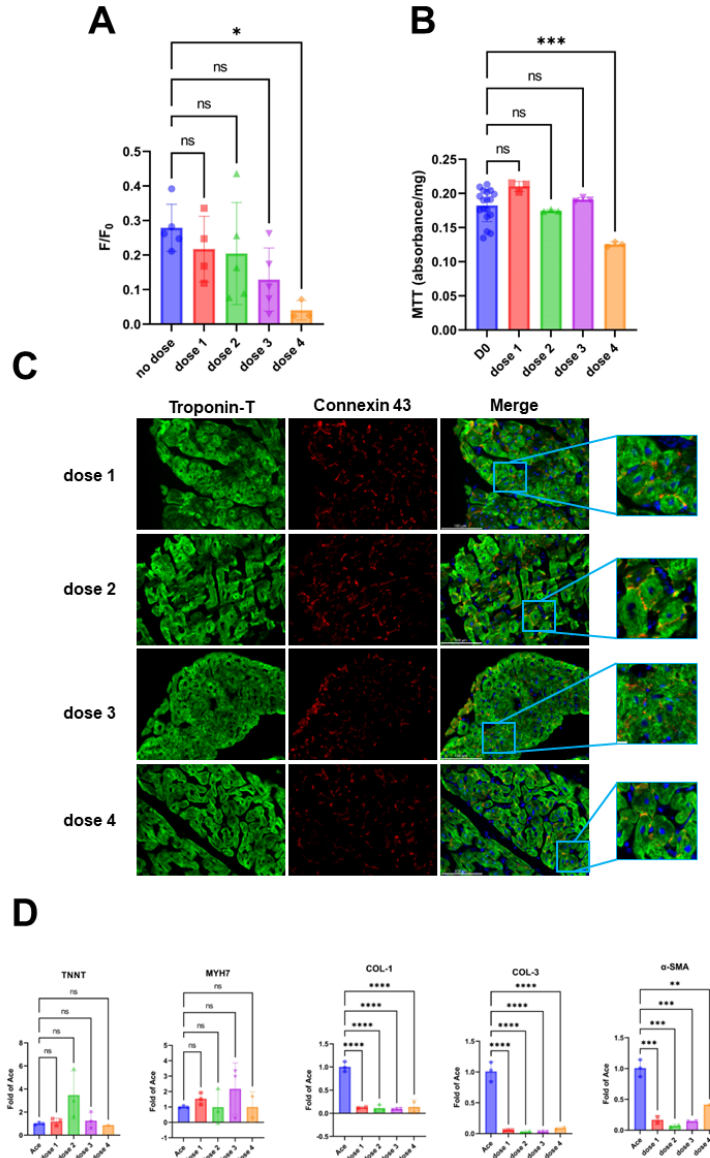
Figure 20: Heart slice calcium transient amplitude (acute exposure), viability, structural integrity, and transcriptional expression after subacute exposure of vinorelbine. (A) Calcium transient amplitude for tissue slices at no dose and doses 1 to 4 of acute vinorelbine exposure. (n = 3-6) (B) Graph depicting MTT viability of no dose to dose 4 of vinorelbine treated tissue slices. (n = 3-18). (C) Representative images of troponin-T and connexin 43 of tissue slices treated with low to high concentrations of vinorelbine. (D) qRT-PCR for cardiac remodeling gene expression for vinorelbine treated tissue slices as a fold increase of Ace (Control). (n = 1-3)
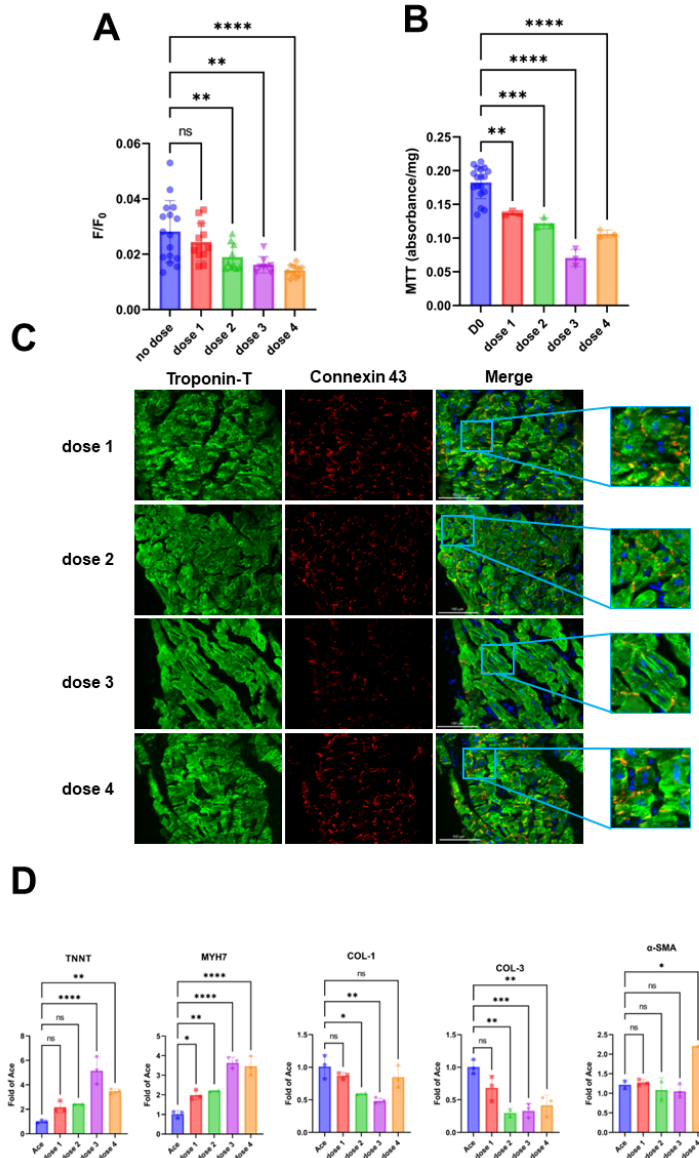
Figure 21: **Heart slice calcium transient amplitude (acute exposure), viability, structural integrity, and transcriptional expression after subacute exposure of vincristine.** (A) Calcium transient amplitude for tissue slices at no dose and doses 1 to 4 of acute vincristine exposure. (n = 8-16) (B) Graph depicting MTT viability of no dose to dose 4 vincristine treated tissue slices. (n = 3-18) (C) Representative images of troponin-T and connexin 43 of tissue slices treated with low to high concentrations of vincristine. (D) qRT-PCR for cardiac remodeling gene expression for vincristine treated tissue slices as a fold increase of Ace (Control). (n = 1-3)
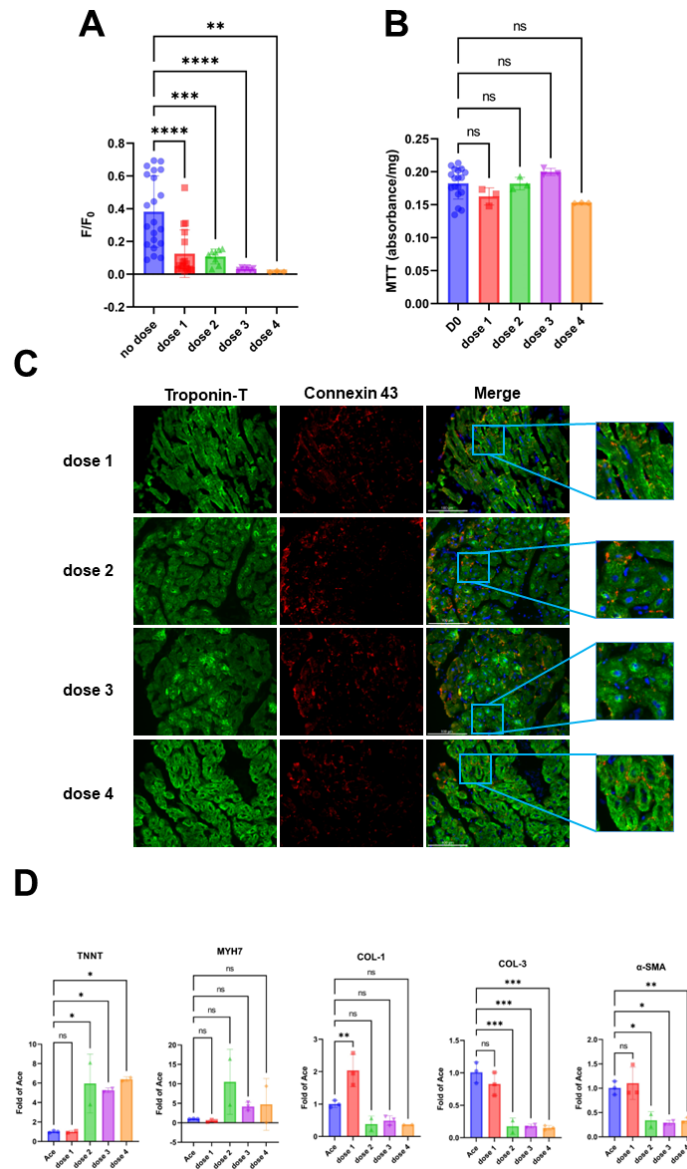
Figure 22: **Heart slice calcium transient amplitude (acute exposure), viability, structural integrity, and transcriptional expression after subacute exposure of vinblastine.** (A) Calcium transient amplitude for tissue slices at no dose and doses 1 to 4 of acute vinblastine exposure. (n = 3-21) (B) Graph depicting MTT viability of no dose to dose 4 vinblastine treated tissue slices. (n = 3-18) (C) Representative images of troponin-T and connexin 43 of tissue slices treated with low to high concentrations of vinblastine. (D) qRT-PCR for cardiac remodeling gene expression for vinblastine treated tissue slices as a fold increase of Ace (Control). (n = 2-3)

3.4.4. Results: Contractility disruptors – BMS-986094, milrinone, and endothelin-1

Table 7 show a simplified summary for the contractility disruptor compounds. None of the three compounds showed a decline in contractility with acute exposure in tissue slices (Figure 23A, 23C, and 23E; Table 7). In the hiPSC-CM data, however, a decline in contractility was observed at the high concentrations after 48 and 72 hours of exposure to BMS-986094 and endothelin-1 (Figure 23B, 23D, and 23F; Table 7). Consistent with the known effect of milrinone to induce an increase in contractility, the heart slices showed a significant increase in the contractility amplitude at dose 1, however, the other 3 concentrations showed no significant change (Figure 23C). This could be due to the first dose causing damage to the tissue slice. The hiPSC-CMs also showed an increase in contractility with milrinone treatment but only in the second dose after 48 and 72 hours of exposure (Figure 23D). Interestingly, the low dosage of ET-1 was the only compound in the hiPSC-CM that resulted in a significant decline in contractility after 48 hours of exposure (Figure 23F; Table 7). This result may be due to variation between wells within the same group.

All three compounds resulted in a decline in calcium amplitude except for dose 1 of ET-1 (Figure 24A, 25A, 26A; Table 7). BMS and milrinone both have a direct effect on calcium handling within the cells and this is reflected here (Figure 24A and 25A). ET-1 has an indirect influence and effects functionality through the balance of NO and ET-1 within the cell therefore it takes time and increased concentrations of ET-1 to see the effect reflected acutely. BMS did not cause a decline in tissue viability at any concentration, but ET-1 caused a significant decline (Figures 24B and 26B; Table 7). Milrinone caused a decrease in viability at dose 1 and 2 but not in the high dosages

(Figure 25B; Table 7). This could be due to sample variation. Lastly, all three compounds caused a disruption in the structural integrity (Figures 24C, 25C, and 26C; Table 7) and transcriptional expression (Figure 24D, 25D, and 26D; Table 7).

Tissue slices were able to detect the clinically reported cardiotoxic effect of BMS and milrinone of directly altering the calcium handling. Additionally, heart slices were able to detect an acute disruption in calcium transients with increased concentrations of ET-1 while hiPSC-CMs were only able to detect a subacute decline in contractility in only the first dose.

Contractility disruptors

Tissue slice – Contractility	BMS-986094	Milrinone	Endothelin-1
Dose 1			
Dose 2			
Dose 3			
Dose 4			

hiPSC-CMs Contractility — Contractility disruptors

		BMS-986094	Milrinone	Endothelin-1
0 hr	Dose 1			
	Dose 2			
	Dose 3			
	Dose 4			
1 hr	Dose 1			
	Dose 2			
	Dose 3			
	Dose 4			
24 hr	Dose 1			
	Dose 2			
	Dose 3			
	Dose 4			
48 hr	Dose 1			X
	Dose 2			
	Dose 3	X		
	Dose 4	X		
72 hr	Dose 1			X
	Dose 2			
	Dose 3	X		
	Dose 4	X		

Tissue slice — Contractility disruptors

		BMS-986094	Milrinone	Endothelin-1
Calcium	Dose 1	X	X	
	Dose 2	X	X	X
	Dose 3	X	X	X
	Dose 4	X	X	X
MTT	Dose 1		X	X
	Dose 2		X	X
	Dose 3			X
	Dose 4			X
Structural integrity	Dose 1	X	X	X
	Dose 2	X	X	X
	Dose 3	X	X	X
	Dose 4	X	X	X
qRT-PCR	Dose 1	X	X	X
	Dose 2	X	X	X
	Dose 3	X	X	X
	Dose 4	X	X	X

Table 7: Simplified summary of hiPSC-CM and heart slice acute and subacute exposure to contractility disruptors. 'X' indicates a significant decline in the parameter.
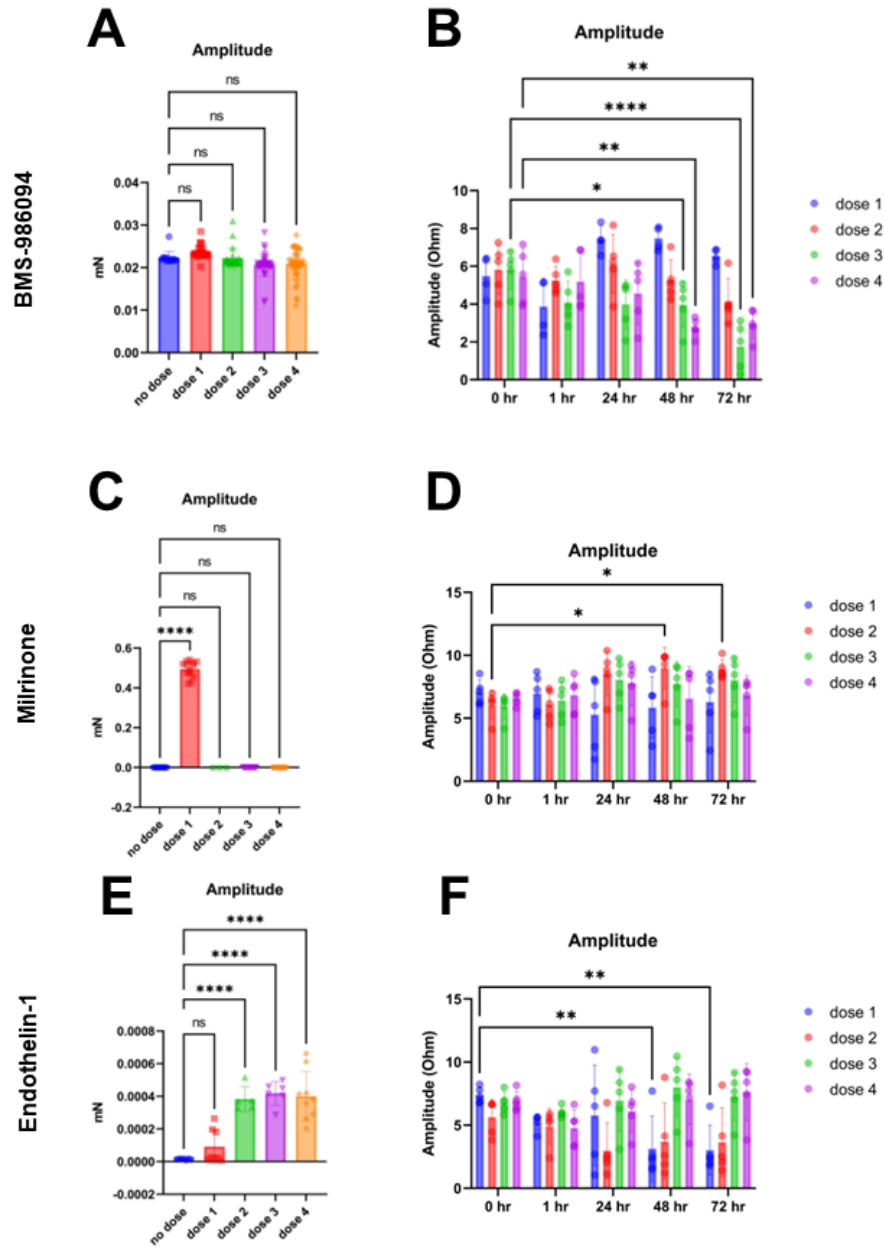
***Figure 23*: Contractility assessment of cardiac tissue slices and hiPSC-CMs after BMS-986094, milrinone, and endothelin-1 exposure.** Contractility amplitude for tissue slices at no dose and doses 1 to 4 of acute BMS-986094 (A; n = 18-45), milrinone (C; n = 3-23), and endothelin-1 (E; n = 5-9) exposure. hiPSC-CM impedance amplitude for no exposure, 1 hour, 24 hours, 48 hours, and 72 hours of BMS-986094 (B; n = 4-5), milrinone (D; n = 5), and endothelin-1 (F; n = 5) exposure.
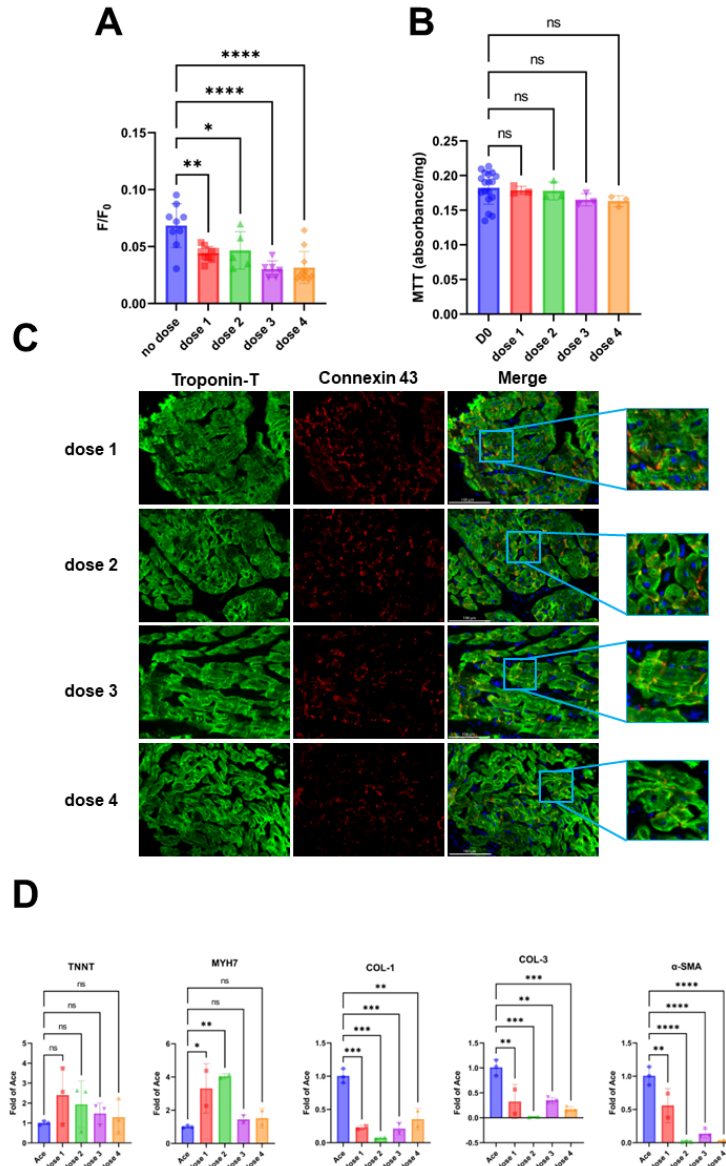
Figure 24: Heart slice calcium transient amplitude (acute exposure), viability, structural integrity, and transcriptional expression after subacute exposure of BMS-986094. (A) Calcium transient amplitude for tissue slices at no dose and doses 1 to 4 of acute BMS-986094 exposure. (n = 5-11) (B) Graph depicting MTT viability of no dose to dose 4 of BMS-986094 treated tissue slices. (n = 3-18) (C) Representative images of troponin-T and connexin 43 of tissue slices treated with low to high concentrations of BMS-986094. (D) qRT-PCR for cardiac remodeling gene expression for BMS-986094 treated tissue slices as a fold increase of Ace (Control). (n = 2-3)
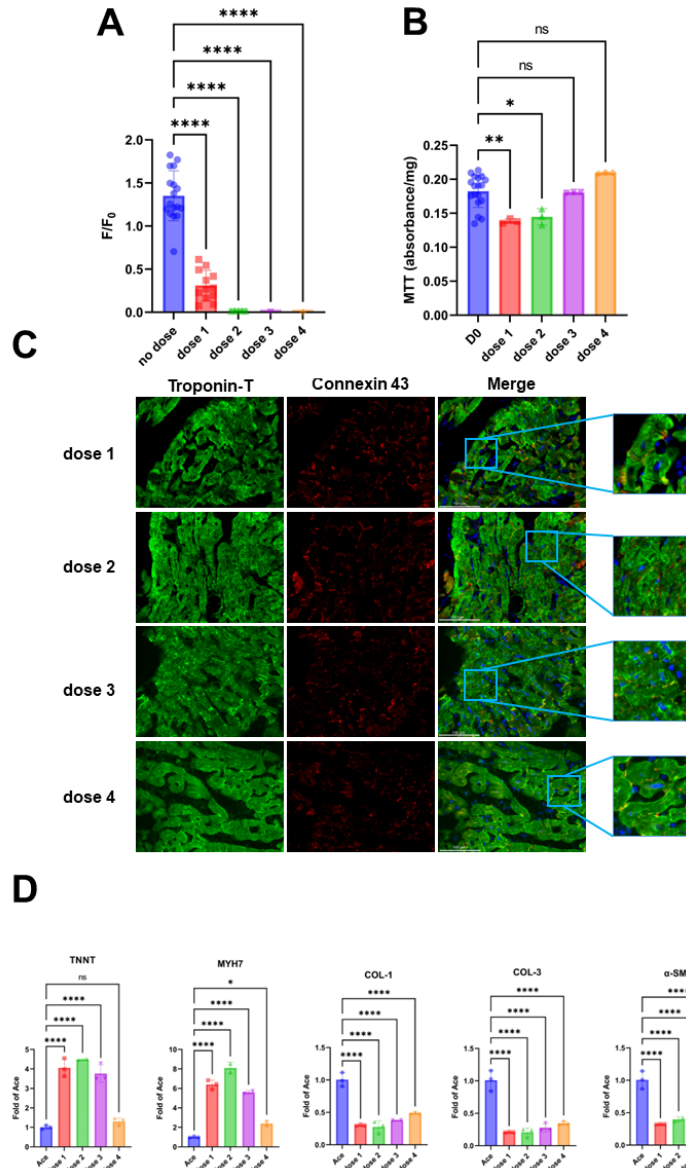
Figure 25: **Heart slice calcium transient amplitude (acute exposure), viability, structural integrity, and transcriptional expression after subacute exposure of milrinone.** (A) Calcium transient amplitude for tissue slices at no dose and doses 1 to 4 of acute milrinone exposure. (n = 1-17) (B) Graph depicting MTT viability of no dose to dose 4 of milrinone treated tissue slices. (n = 3-18) (C) Representative images of troponin-T and connexin 43 of tissue slices treated with low to high concentrations of milrinone. (D) qRT-PCR for cardiac remodeling gene expression for milrinone treated tissue slices as a fold increase of Ace (Control). (n = 2-3)
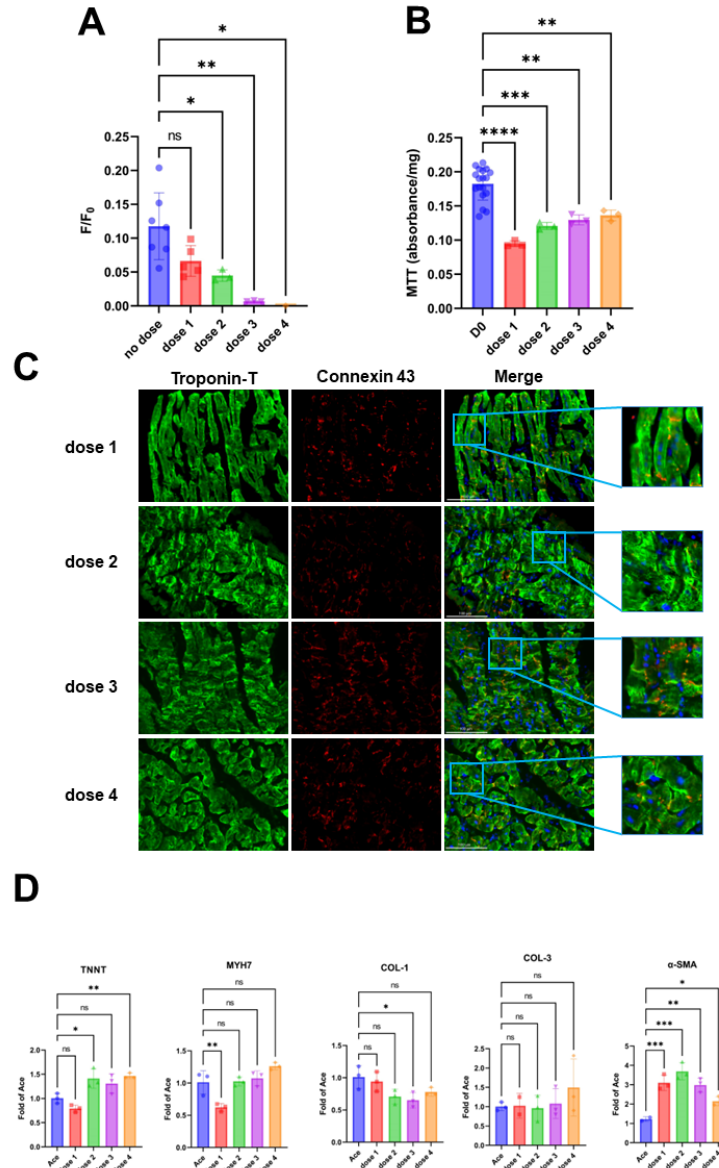
***Figure 26*: Heart slice calcium transient amplitude (acute exposure), viability, structural integrity, and transcriptional expression after subacute exposure of endothelin-1.** (A) Calcium transient amplitude for tissue slices at no dose and doses 1 to 4 of acute endothelin-1 exposure. (n = 1-7) (B) Graph depicting MTT viability of no dose to dose 4 of endothelin-1 treated tissue slices. (n = 3-18) (C) Representative images of troponin-T and connexin 43 of tissue slices treated with low to high concentrations of endothelin-1. (D) qRT-PCR for cardiac remodeling gene expression for endothelin-1 treated tissue slices as a fold increase of Ace (Control). (n = 2-3)

3.4.5. Results: Electrophysiology disruption – Pentamidine and arsenic trioxide

Table 8 show a simplified summary of the electrophysiology disruptor compounds. None of the three compounds resulted in a disruption in contractility in either heart slices or hiPSC-CMs (Figure 27; Table 8). Pentamidine inhibits the transcription of the hERG gene which is responsible for the transcription of potassium ion channels. Since the transcription, translocation, and degradation of proteins all take time to occur, acute exposure to pentamidine would not be detected.

Subacute exposure to Pent at all concentrations showed a decline in calcium transient amplitude, while pentamidine exposure only decreased the calcium amplitude at the high concentrations (Figures 28A and 29A; Table 8). This could be due to a variation in the compound preparation or sample-to-sample variation. The arsenic decreased calcium handling at only the high dose (Figure 30A; Table 8). Only dose 2 of Pent treatment resulted in decreased tissue viability, while doses 1, 2, and 4 of pentamidine decreased the viability (Figures 28B and 29B; Table 8). Arsenic at all concentrations did not induce a decline in tissue viability (Figure 30B; Table 8). This could be due to arsenic toxicity taking months to years of accumulation before any toxic event will occur. All three physiological disruptor compounds at all concentrations resulted in a decline in structural integrity and transcriptional expression, with the exception of dose 4 of arsenic treatment (Figures 28-30C and D; Table 8). The exception for arsenic in the qRT-PCR results can be due to technical error.

Electrophysiology disruptors

Tissue slice	Contractility		Pent	Pentamidine	Arsenic trioxide
Tissue slice	Contractility	Dose 1			
		Dose 2			
		Dose 3			
		Dose 4			

hiPSC-CMs Contractility			Pent	Pentamidine	Arsenic trioxide
hiPSC-CMs Contractility	0 hr	Dose 1			
		Dose 2			
		Dose 3			
		Dose 4			
	1 hr	Dose 1			
		Dose 2			
		Dose 3			
		Dose 4			
	24 hr	Dose 1			
		Dose 2			
		Dose 3			
		Dose 4			
	48 hr	Dose 1			
		Dose 2			
		Dose 3			
		Dose 4			
	72 hr	Dose 1			
		Dose 2			
		Dose 3			
		Dose 4			

Electrophysiology disruptors

Tissue slice			Pent	Pentamidine	Arsenic trioxide
Tissue slice	Calcium	Dose 1	X		
		Dose 2	X		
		Dose 3	X	X	
		Dose 4	X	X	X
	MTT	Dose 1		X	
		Dose 2	X	X	
		Dose 3			
		Dose 4		X	
	Structural integrity	Dose 1	X	X	X
		Dose 2	X	X	X
		Dose 3	X	X	X
		Dose 4	X	X	X
	qRT-PCR	Dose 1	X	X	X
		Dose 2	X	X	X
		Dose 3	X	X	X
		Dose 4	X	X	

Table 8: Simplified summary of hiPSC-CM and heart slice acute and subacute exposure to electrophysiology disruptors. 'X' indicates a significant decline in the parameter.
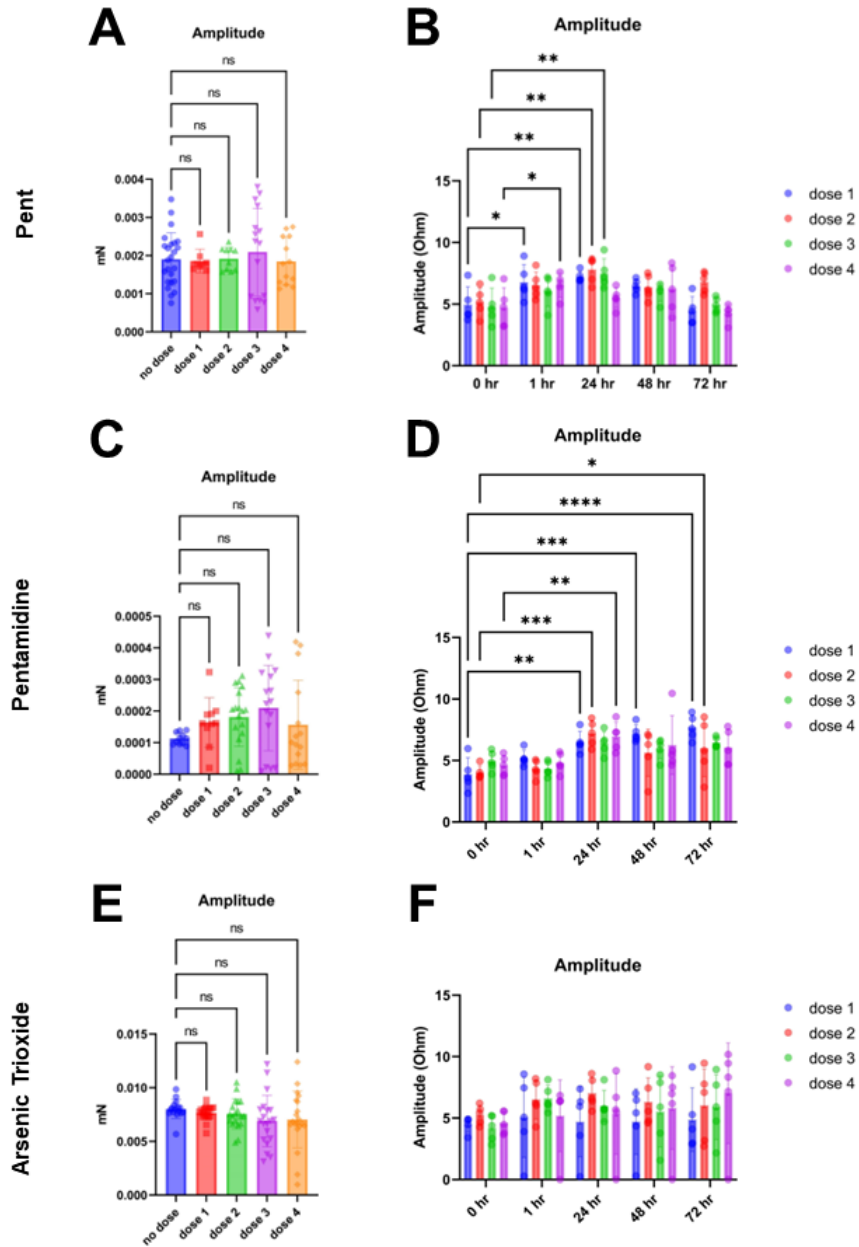
Figure 27: **Contractility assessment of cardiac tissue slices and hiPSC-CMs after Pent, pentamidine, and arsenic trioxide exposure**. Contractility amplitude for tissue slices at no dose and doses 1 to 4 of acute Pent (A; n = 8-24), pentamidine (C; n = 10-18), and arsenic trioxide (E; n = 16-20) exposure. hiPSC-CM impedance amplitude for no exposure, 1 hour, 24 hours, 48 hours, and 72 hours of Pent (B; n = 5), pentamidine (D; n = 5), and arsenic trioxide (F; n = 5) exposure.
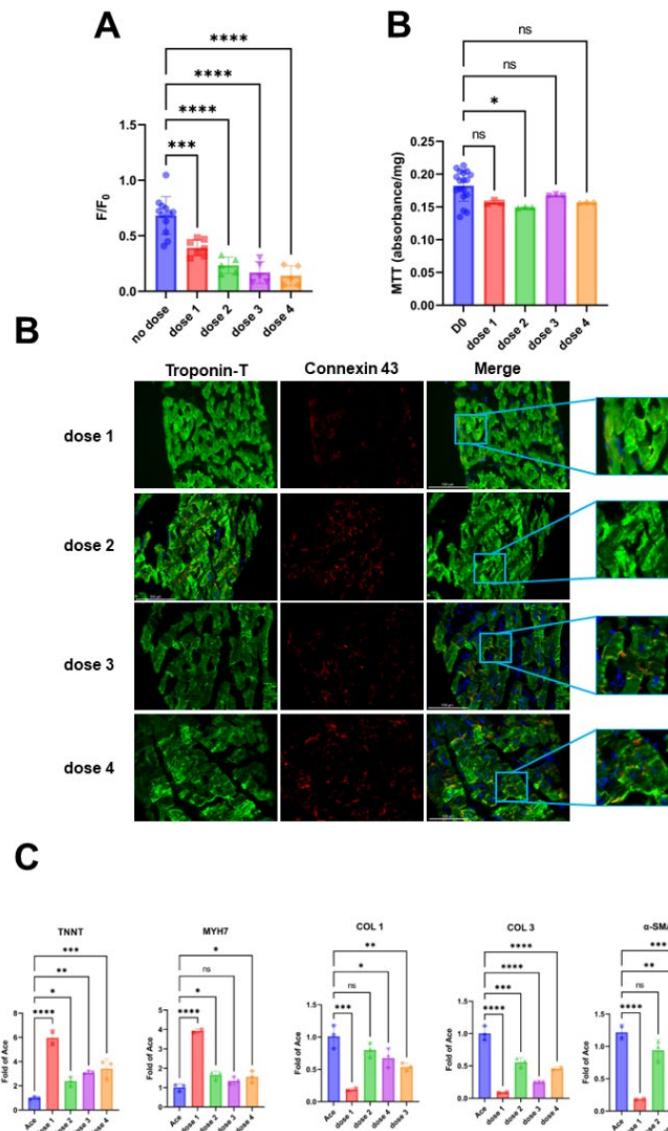
***Figure 28*: Heart slice calcium transient amplitude (acute exposure), viability, structural integrity, and transcriptional expression after subacute exposure of Pent.**

(A) Calcium transient amplitude for tissue slices at no dose and doses 1 to 4 of acute Pent exposure. (n = 5-12) (B) Graph depicting MTT viability of no dose to dose 4 of Pent treated tissue slices. (n = 3-18) (C) Representative images of troponin-T and connexin 43 of tissue slices treated with low to high concentrations of Pent. (D) qRT-PCR for cardiac remodeling gene expression for Pent treated tissue slices as a fold increase of Ace (Control). (n = 2-3)
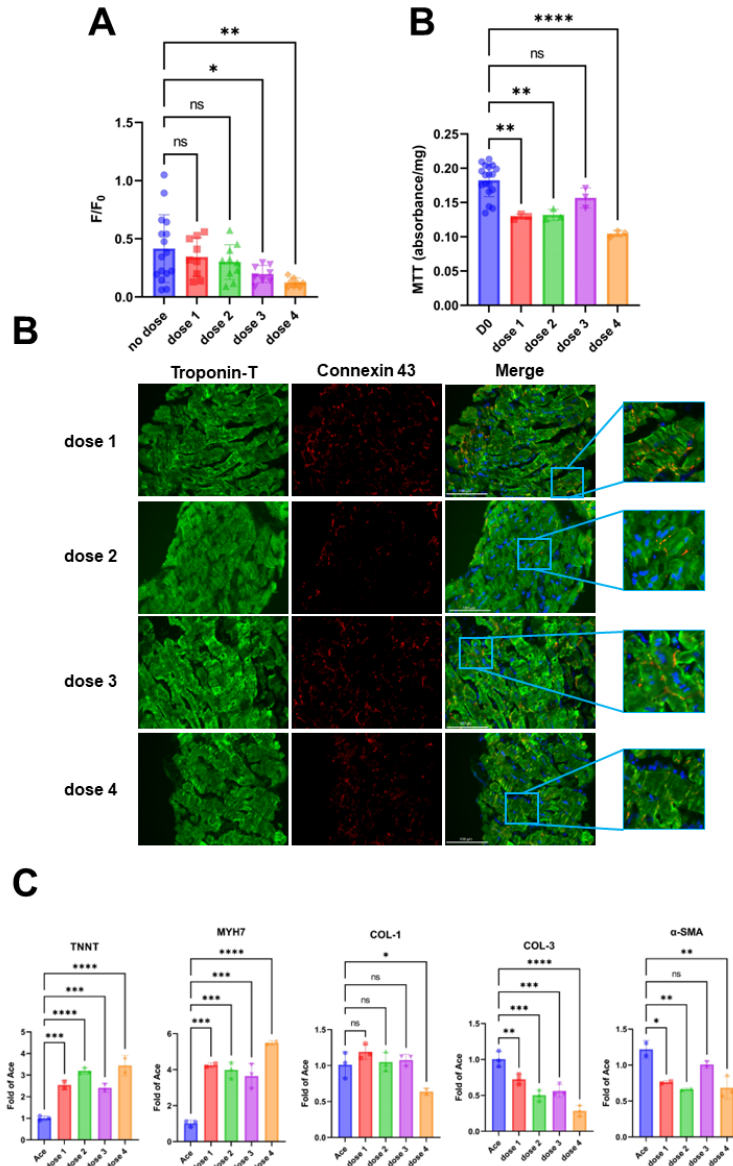
***Figure 29*: Heart slice calcium transient amplitude (acute exposure), viability, structural integrity, and transcriptional expression after subacute exposure of pentamidine.** (A) Calcium transient amplitude for tissue slices at no dose and doses 1 to 4 of acute pentamidine exposure. (n = 8-16) (B) Graph depicting MTT viability of no dose to dose 4 of pentamidine treated tissue slices. (n = 3-18) (C) Representative images of troponin-T and connexin 43 of tissue slices treated with low to high concentrations of pentamidine. (D) qRT-PCR for cardiac remodeling gene expression for pentamidine treated tissue slices as a fold increase of Ace (Control). (n = 2-3)
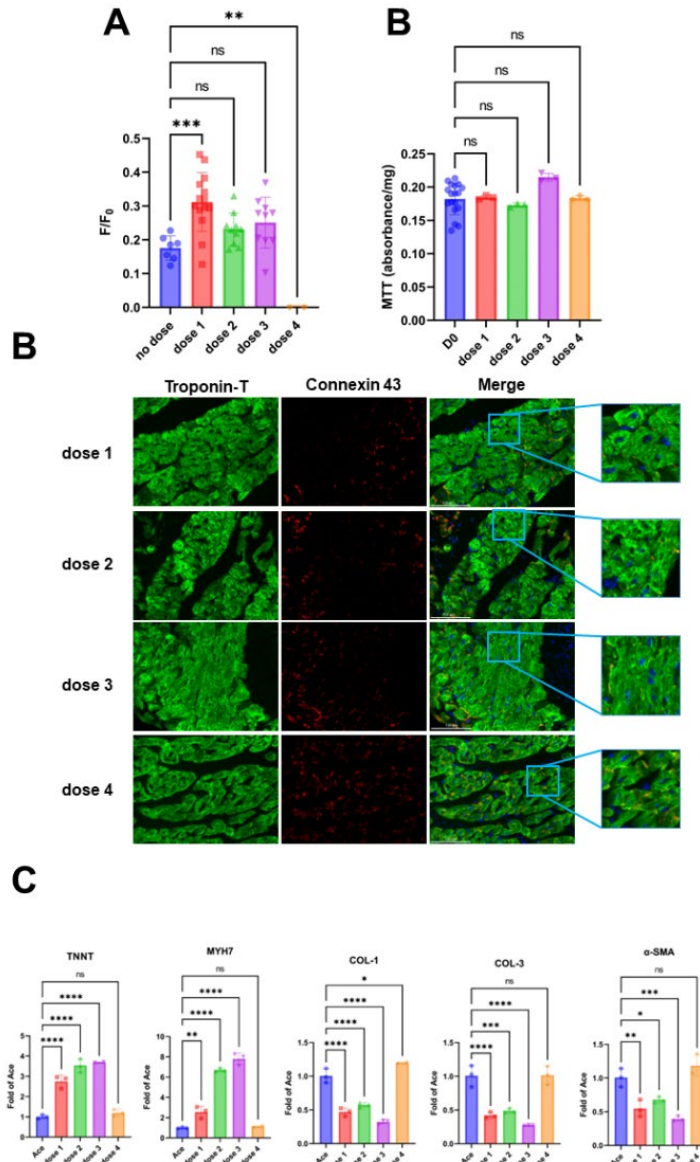
Figure 30: **Heart slice calcium transient amplitude (acute exposure), viability, structural integrity, and transcriptional expression after subacute exposure of arsenic trioxide.** (A) Calcium transient amplitude for tissue slices at no dose and doses 1 to 4 of acute arsenic trioxide exposure. (n = 2-14) (B) Graph depicting MTT viability of no dose to dose 4 of arsenic trioxide treated tissue slices. (n = 3-18) (C) Representative images of troponin-T and connexin 43 of tissue slices treated with low to high concentrations of arsenic trioxide. (D) qRT-PCR for cardiac remodeling gene expression for arsenic trioxide treated tissue slices as a fold increase of Ace (Control). (n = 2-3)

3.5. Discussion

In more recent years, cancer drug development has occurred at a rapid pace, leading to numerous unforeseen consequences. Many patients are exposed to a complex regimen of medications that can have unknown side effects. Additionally, due to many confounding factors such as age, genetics, food consumption or nutritional supplements, adverse drug effects can sometimes be difficult to predict with new therapies. Therefore, it is essential to obtain insight into the mechanism of potential adverse drug events to reduce the risk of detrimental effects in patients.

Many chemotherapeutic treatments have adverse side effects, such as hypertension, thromboembolism, cardiotoxicity, and cardiac contractile dysfunction (prolonged QT interval). [21, 42, 90, 92, 134][105, 145, 195] The most detrimental of these adverse side effects is cardiotoxicity. There are many mechanisms in which to induce cardiotoxicity but the most common forms that appear with chemotherapeutics are toxicities induced through mitochondrial or energetic damage, a disruption in contractile function, a disruption in the electro-physiology, and a direct disruption to the myofilaments.

The hiPSC-CM impedance measurement was the least sensitive assay for detecting the cardiotoxicity of the 12 compounds. The hiPSC-CMs only demonstrated a decline in contractility at the clinically relevant dosage, dose 1, for 2 compounds (Dox and ET-1). This decline in contractility was not observed until 48 hours of exposure to ET-1 and 72 hours of exposure to Dox. Additionally, the hiPSC-CMs were not able to replicate the decline in contractility seen in the Dox treatment within the coded doxorubicin treatment, indicating that this cell type cannot consistently replicate results.

For the heart slice parameters, the immunolabeling and qRT-PCR used to assess the tissue slices after subacute exposure to the compounds were the most sensitive for detecting cardiotoxicities. The qRT-PCR provided a snapshot of the transcriptional cardiac gene expression, while the immunolabeling for connexin 43 and cardiac specific troponin T provided insight into the cardiac protein expression. Transcriptionally, heart slices detected a significant dysregulation in cardiac gene expression in 10 out of the 12 compounds after acute exposure indicating significant damage to the slices. The two compounds that did not show a significant change were vincristine and vinblastine. These two compounds are vinca alkaloids which interfere with the myofilaments within the cells. While the gene expression was not different with these compounds, the structural integrity was significantly disrupted. This indicates that the tissue slices were significantly affected by the compounds at an early timepoint of exposure, causing a change in transcriptional expression prior to the subacute collection timepoint, which is reflected in structural integrity. Either the tissue was damaged beyond compensation (significant cell death), or the compensation was enough, and it returned to normal transcriptional levels.

The MTT viability assay was the least sensitive subacute assay due to the tissue viability being the last indicator for detrimental cardiotoxicity. At the clinically relevant dosage, heart slices detected a significant decline in tissue viability in 7 compounds. The compounds not detected were erlotinib (which is known to be a mild TKI that is not highly cardiotoxic), two spindle toxins (vinorelbine and vinblastine), BMS-986094 (direct influence on calcium handling), and arsenic trioxide (a toxin that requires an accumulation before detrimental effects can be observed).

For the acute functional assays on the tissue slices, the calcium transients were more sensitive to the clinically relevant dosage of the compounds than the contractility measurements. Of the 12 compounds, the tissue slices detected a decline in 8. The four compounds that were not detected were ones that require longer exposure for a change in calcium handling to occur. For example, ET-1 was one of the drugs not acutely detected for calcium handling cardiotoxicity. ET-1 is a compound that effects contractility of the cell through a balance between nitric oxide (NO)/PGI2 and ET-1. With high levels of intracellular ET-1 there will be increased contractility. Arsenic trioxide was another compound not actually detected by the calcium transients due to the nature of the toxin of needing to accumulate within the cell for months to years before a significant toxicity can occur. The last two compounds not detected were vinca alkaloids which target the myofilaments. These spindle toxins require time to alter protein expression thus they are not detected acutely. Vinblastine, one of the three vinca alkaloids tested, did result in a decline in calcium handling with acute exposure. This can be due to vinblastine being more cardiotoxic than the other two compounds and it may be directly inhibiting the treadmilling of the cortical myofilaments which are involved in ion channel regulation.

For the acute contractility measurement, only two of the chemotherapeutics were detected: Dox and nilotinib. It would be expected that doxorubicin causes a decline in cardiac function at the low dose since the compound is well established as a highly cardiotoxic compound. While the tissue slices were able to detect the decline in the control doxorubicin, they did not detect a decline in the coded doxorubicin. This could be due to differences between the preparation of the two compounds. Nilotinib is a TKI that has a direct influence on contractile function unlike the other two TKIs tested. For this

assay, maybe a slightly longer exposure time (1+ hour(s)) to each compound may result in more compounds being detected, such as ET-1, milrinone, or sunitinib.

3.6. Conclusion

To summarize, heart slices were able to reproduce the clinically known effects of 12 out of the 12 compounds, 8 out of these were determined to be cardiotoxic acutely. The hiPSC-CMs were only able to detect the cardiotoxicity of 2 out of the 12 compounds. The calcium transient assessment was the most sensitive assay for acute cardiotoxicity detection, while for subacute cardiotoxic effects, the structural integrity and qRT-PCR assays were most sensitive. These data demonstrate that an intact myocardial slice can consistently detect various cardiotoxic mechanisms of action at both acute and subacute levels as well as out-perform hiPSC-CMs.

3.7. Limitations

A limitation of this study is the time of exposure to each of the compounds. Clinically, the tissue specific toxicity may take months of exposure at the clinical concentrations to become detrimental. The time points for exposure could be extended to 6 days, collecting samples every day to analyze when toxicity starts to occur (specifically with arsenic trioxide and vinorelbine). Additionally, the contractility measurement for the heart slices appears to be less sensitive to short term exposure of the compounds compared to the calcium assay. To improve this parameter, a longer exposure to each concentration of the compounds may be needed.

CHAPTER 4 BIOENGINEERED REVERSE CARDIO-ONCOLOGIC CULTURE SYSTEM TO INVESTIGATE THE CROSSTALK BETWEEN TUMOR CELLS AND CARDIAC TISSUE [3]

4.1. Introduction – Cardio-oncology and reverse cardio-oncology

Recent studies have shown a possible link between cardiovascular disease (CVD) and the development/progression of cancer. [12, 42, 61][6, 64] CVD and cancer are the two leading causes of death, sharing many common risk factors. [14] Whether the relationship between CVD and cancer is due to causality or to the shared risk factors is still under debate. [24] Recent articles, however, suggest that CVD diagnosis subsequent to primary cancer treatment has been associated with cancer progression. [54] Due to these studies, an interest has been invoked to understand the bi-directional relationship between these two diseases. [25]

Current *in vivo* and *in vitro* research has revealed that CVD-induced cancer pathogenesis has been linked with specific CVDs inducing tissue specific tumor development. Koelwyn et al [53] demonstrated that a MI after primary cancer treatment

---

leads to an upregulation of LY6C^{hi} monocytes, promoting breast cancer tumor growth. Meijers et al [64] demonstrated that MI-induced heart failure leads to an increase of circulating SerpinA3, which directly promotes colon cancer pathogenesis. Avraham et al [6] demonstrated that TAC induced mice models displayed larger primary tumors with increased proliferation rates and more metastasis in both lung and breast cancer due to increased periostin release. To further support this emerging field of research, we propose to develop a culture method using cardiac tissue slices and cancer cells to investigate the possible direct effects of CVD on tumor progression.

Our lab recently developed a cardiac tissue culture model (CTCM), shown in Figure 31A, that can emulate the cardiac cycle by subjecting heart slices to dynamic pressure loading with synchronized electrical stimulation set to a physiological frequency (1.2 Hz, 72 beats per minutes). Tissue slices were oversized by 25% by using a 3-D printed apparatus to avoid over-stretching the sample during the diastolic phase (Figure 31B). The electrical stimulation was applied by a C-PACE device controlled by a data acquisition system which was set to send an impulse 100 ms prior to the systolic phase. The CTCM was connected to a programmable pneumatic driver (PPD; LB engineering, Germany) that allows for a cyclic control over the air chamber pressure of the device. As the pressure within the air chamber increases, the flexible silicone membrane will distend, displacing the media under the tissue slice thus inducing a stretch within the tissue. The CTCM was connected to the PPD by an external air line with a pressure probe that allows for the fine pressure tuning ($\pm$ 1 mmHg) and timing ($\pm$ 1 ms) (Figure 31C). Four CTCM devices can be controlled by a single pneumatic drive with each device accommodating 6 tissue slices (Figure 31D).
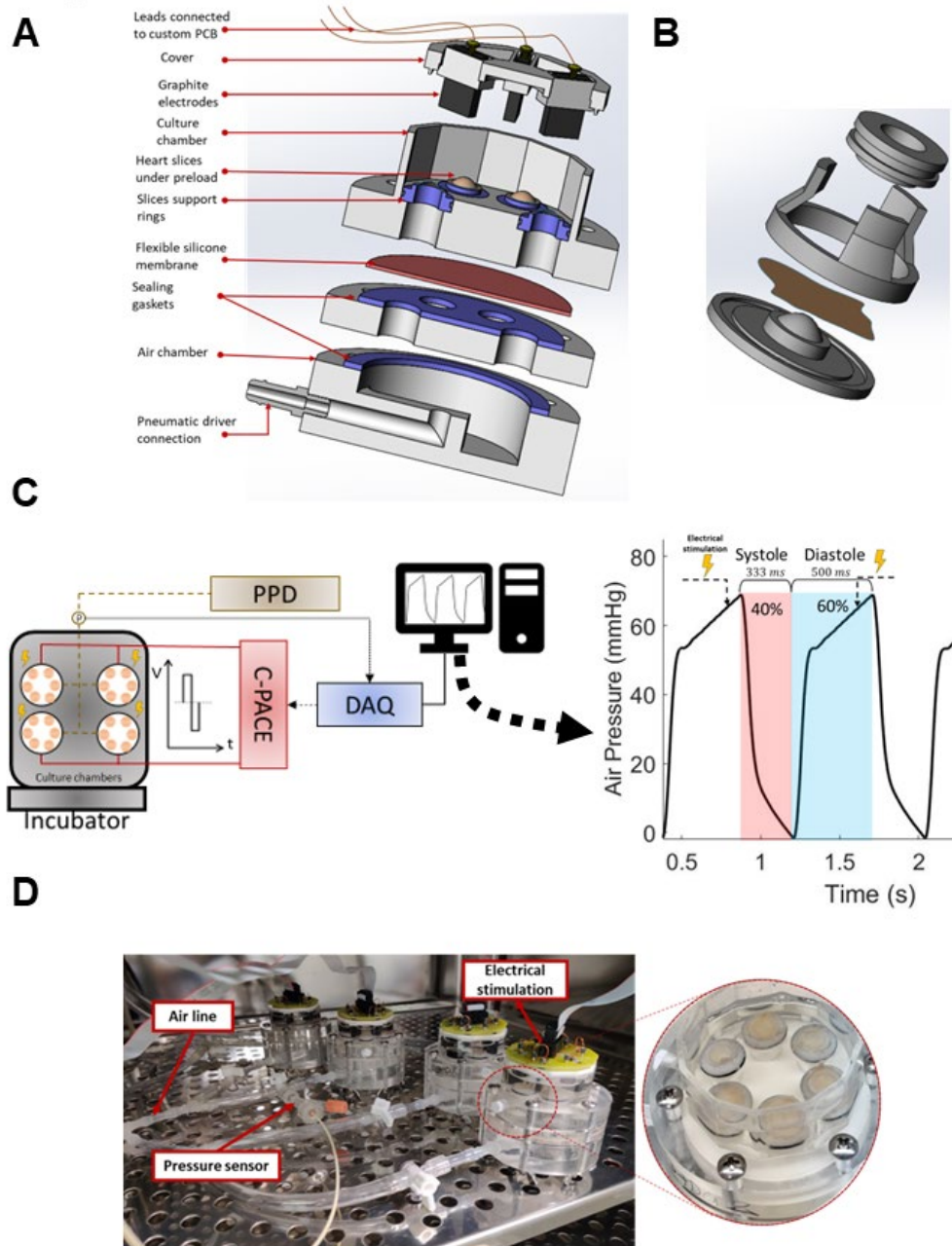
***Figure 31*: Illustration of the cardiac tissue culture model (CTCM).** (A) Exploded

CAD drawing of CTCM device. (B) Schematic illustration of tissue oversizing apparatus,

ring guide, and support ring. (C) A diagram depicting the timing of the electrical

stimulation in relation to the pressure within the air chamber controlled by the

programmable pneumatic driver (PPD). (D) Image of four CTCM devices set up on a

shelf of an incubator.

By setting the PPD to apply pressures of 0 to 80 mmHg, a 25% stretch can be induced within the tissue slice (Figure 32B). This percent stretch corresponds to a physiological sarcomere length of 2.2-2.3 μm, for normal contractile function. [24, 70, 92]
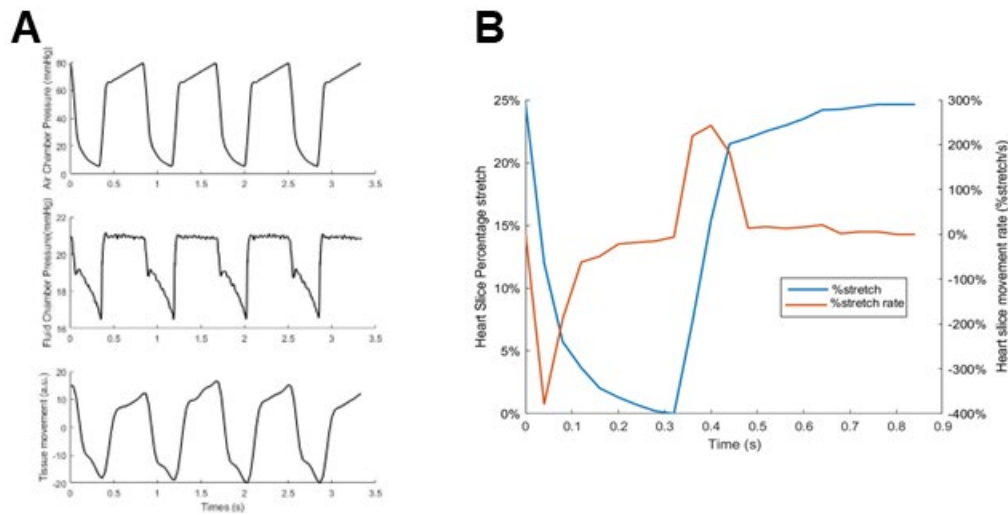
Figure 32: **Characterization of the CTCM and evaluation of the heart slice stretches over time in culture.** (A) Representative traces of the air chamber pressure, fluid chamber pressure, and tissue movement measurements verified that the air chamber pressure changes the fluid chamber pressure, which induces a corresponding tissue slice movement. (B) Representative traces of the percent stretch (blue) of the tissue slices correspond with the percent stretch rate (orange).

When the PPD pressures are increased to apply 0 to 140 mmHg, a 30% stretch of the tissue slice can be achieved, which corresponds to the approach sarcomeric length seen in cardiac hypertrophy. [24, 70, 92] Figure 33 demonstrates that by increasing the pressure by 60 mmHg, tissue slices have an increase in NT-ProBNP (HF biomarker) release at 4 days of culture compared to the control, an increase in cell size, and an increase in NFATC4 activation by 6 days of culture. These results indicate that the

CTCM can emulate the disease condition of over-stretch induced cardiac hypertrophy (OS) in cardiac tissue slices.
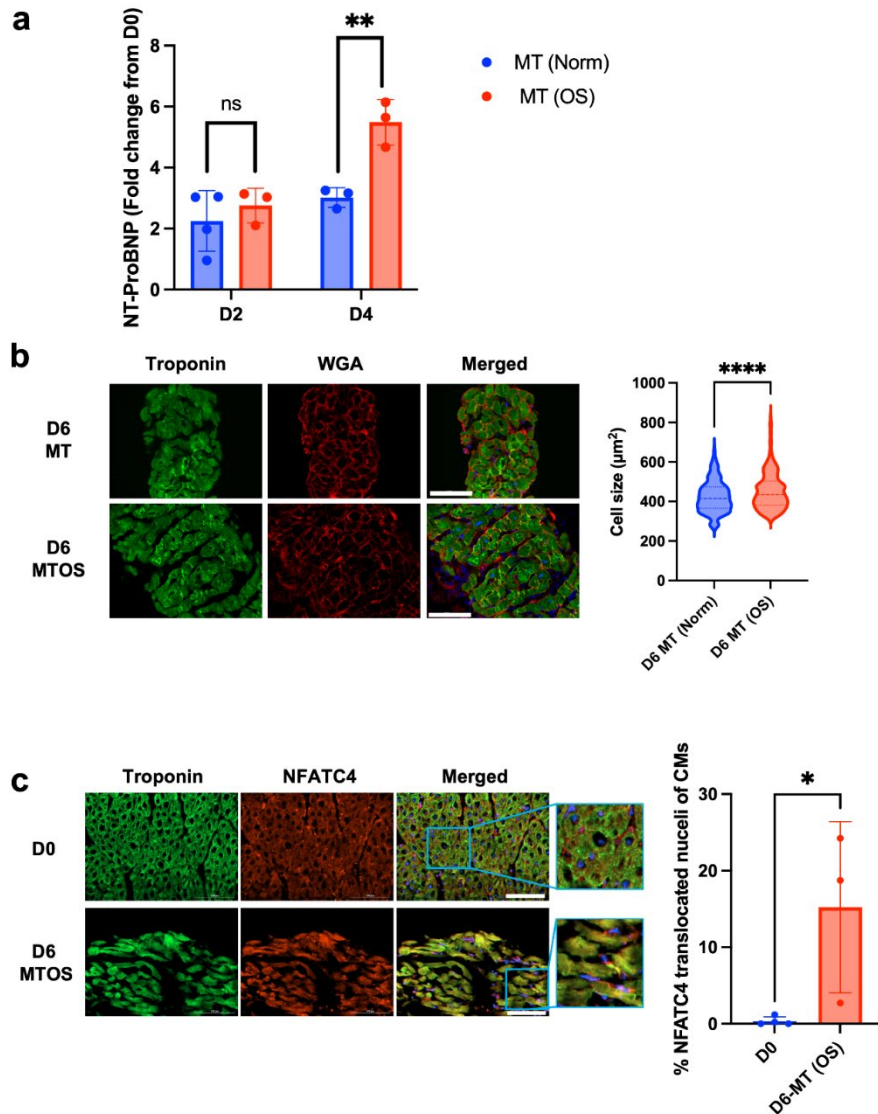
Figure 33: **Induction of over-stretch induced cardiac hypertrophy in cardiac tissue slices.** [103] (A) Bar graph of NT-ProBNP release from normal pressure (0 to 80 mmHg) compared to OS pressure (0 to 140) at 2 and 4 days in culture (n = 3-4). (B) WGA representative images (left) and graphic plot of quantified cell size (n = 330-369 cells). (C) NFATC4 immunolabeling and quantification of the activation. (n = 3).

4.2. Study Hypothesis

In order to investigate the bidirectional relationship between the heart and tumor cells, we hypothesize that a bioengineered bioreactor can be designed to emulate the crosstalk between OS subjected cardiac tissue slices and breast cancer cells.

To address this hypothesis, we developed a novel bioreactor system that allows for continuous media exchange between cardiac tissue slices subjected to over-stretch induced hypertrophy conditions (emulated TAC model) and tumor cells. This system consists of two culture chambers (one for the cardiac tissue slices and one for housing tumor cell insert membranes), a peristaltic pump, and tubing. The culture chamber for the heart slices was designed based on our lab's recently developed cardiac tissue culture model (CTCM). Over-stretch induced hypertrophy (OS) was achieved by utilizing a programmable pneumatic driver (PPD) that can control the pressure within the culture chamber of the tissue slices. Based on prior studies, an increase in the preload from 25% to 32% allows for a similar sarcomere length seen in hypertrophy. [24, 70, 92] To achieve this percent stretch from the tissue slices, the PPD was set to 0 to 140 mmHg. Over-stretch induced hypertrophy was achieved under these conditions verified through an increase in cell size, NT-ProBNP release, and NFATC4 activation shown in Figure 33.

To obtain a continuous media exchange between the heart slices subjected to OS conditions and the tumor cells, flexible tubing will be connected between the culture chambers. The fluid flow rate will be controlled by a peristaltic pump which will allow for an ample amount of fluid exchange experienced by the tumor cells and tissue slices. To assess if the bioreactor system achieved a crosstalk between the two cell types, Ki67, a proliferation marker, immunolabeling of the tumor cells will be performed.

Additionally, media collections once a day for a course of 3 days will be analyzed for periostin release, a biomarker identified as an excreted protein from the heart that may induce tumor cell proliferation.

4.3. Experimental design

A bioengineered flow loop system was designed to emulate the bi-directional communication between CVD and cancer. This device models the effects of over-stretch induced hypertrophy conditions (emulated TAC model) on heart slices accelerating breast cancer tumor growth. This was performed by modifying our recently developed CTCM that emulates the cardiac cycle by utilizing a PPD. The advantage to using the CTCM is that the PPD can be set to any desired pressure and cycle time to induce specific disease conditions. Figure 34 depicts the overall bioreactor setup showing the fluid flow being controlled by a peristaltic pump. Media will be syphoned from a media reserve by the pump into the CTCM culture chamber. From the CTCM culture chamber, the fluid will flow into the cancer cell culture chamber then back into the media reservoir where it will be recirculated through the system. A one-way valve will be placed prior to the CTCM culture chamber to ensure one-directional flow. To account for the height of the CTCM culture chamber, the pump, media reservoir, and cancer cell culture chamber will be placed on platforms to reduce any height differences.
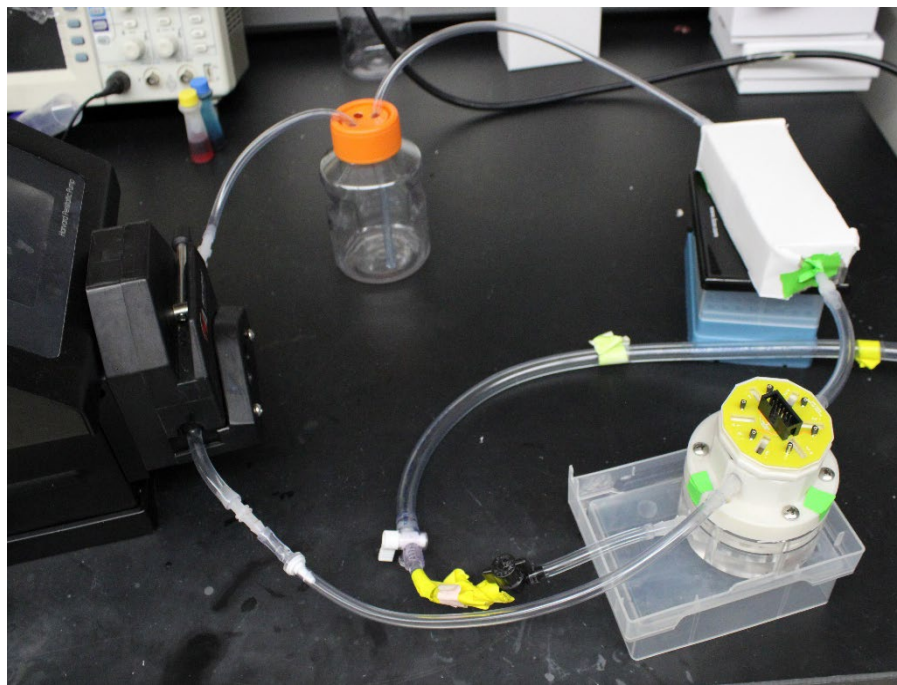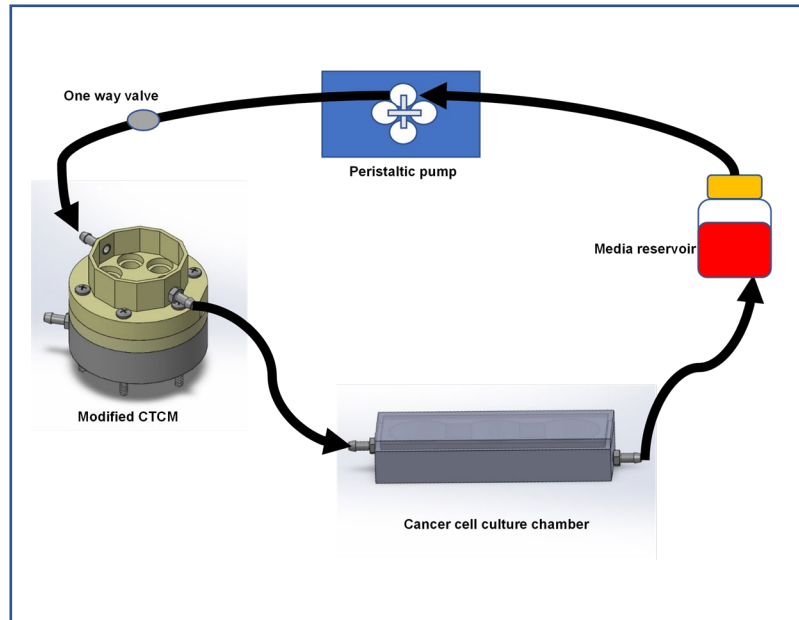
***Figure 34*: Overall CVD-Tumor Bioreactor system.** (Top) Schematic representation of overall bioreactor system setup. (Bottom) CVD-Tumor bioreactor setup.

The schematic shown in Figure 35 and Figure 36 demonstrates that by adding an inlet and outlet channel into the culture chamber of the CTCM fluid flow through the device can be achieved.
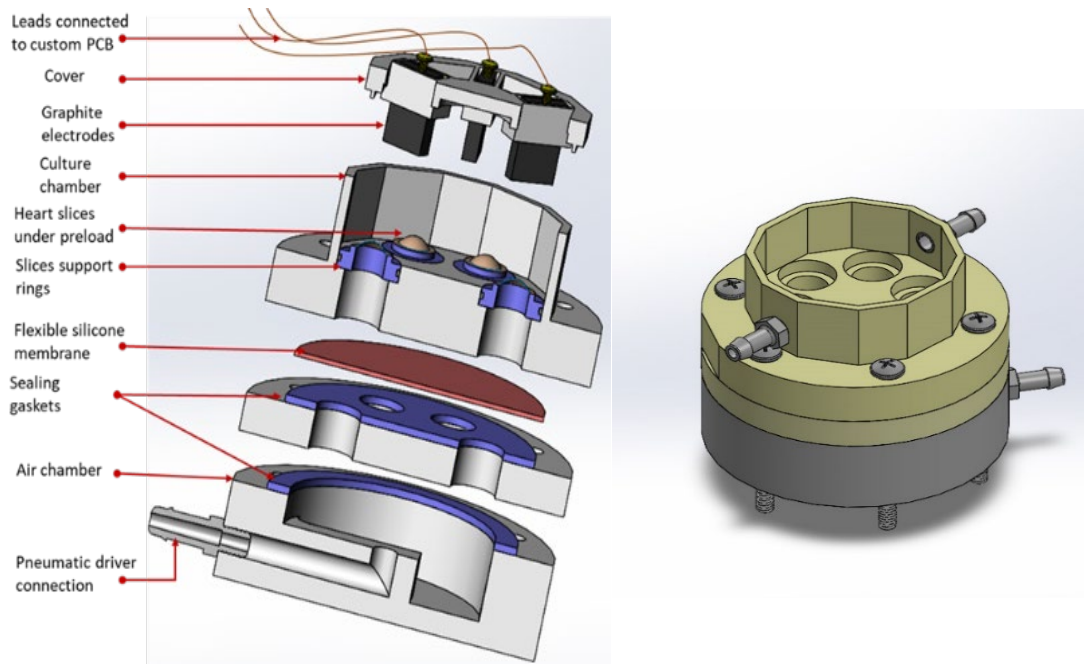
Figure 35: **Modified CTCM device.** (Left) Original CTCM design. [118] (Right) Proposed modification to the CTCM culture chamber. Barb connectors are inserted into the culture chamber of the CTCM device allowing for fluid circulation through the system.
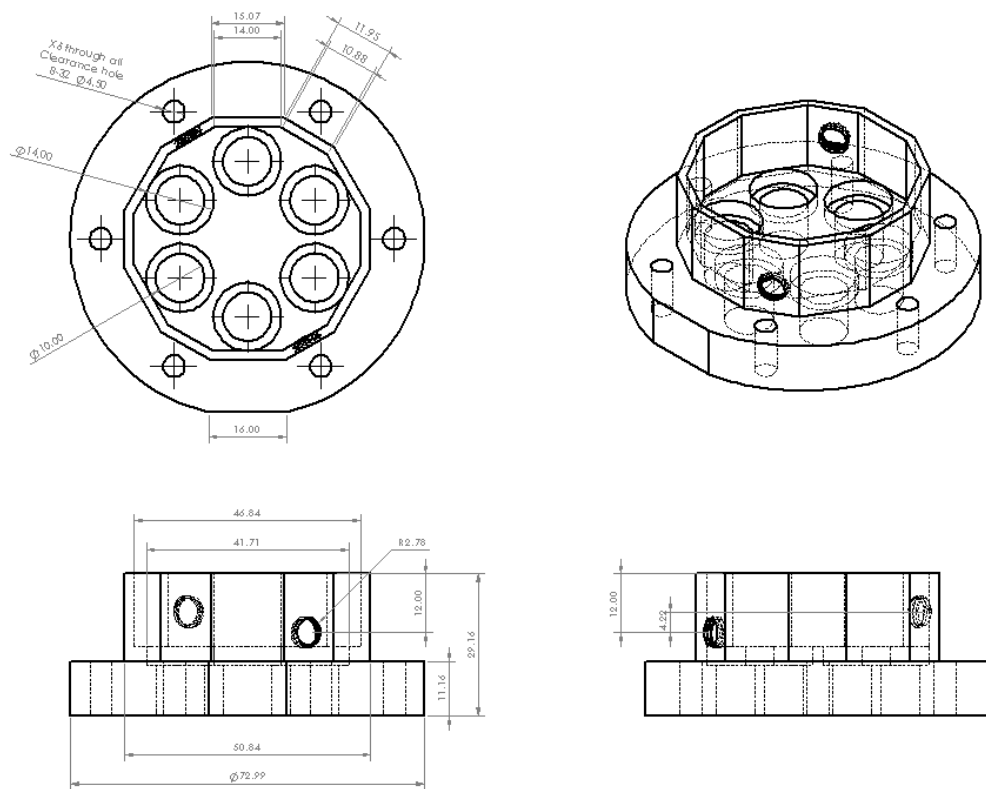
Figure 36: Modified CTCM tissue slice culture chamber schematic with dimensions.

Figure 37 depicts the cancer cell culture chamber. In this chamber, 3 μm pore cell culture inserts (Celltreat, Cat# 230609) shown in Figure 37 (right, bottom), will be placed into the culture device wells and tubing will be attached to barb connectors to allow fluid circulation. The pore size of the culture insert is small enough to prevent the migration of the tumor cells through it, while allowing for paracrine factors, such as periostin, to freely enter the wells. The culture chambers will be 3D printed using PLA filament.
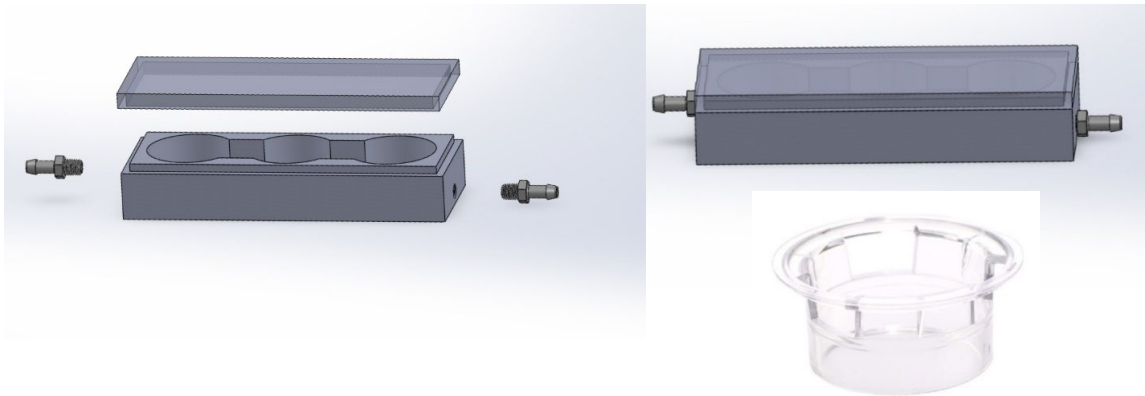
Figure 37: **Cancer cell culture chamber** (left – exploded view; right, top – assembled view) and cell culture insert (right, bottom). Fluid flow will be allowed through the culture chamber by attaching tubing to the barb connectors on either side of the device. The cell culture inserts will be placed into the culture wells of the cancer cell culture chamber.

Before validating the new device with tissue/cells, a fluid flow simulation and mock loop will be performed to characterize the fluid dynamics of the system. SolidWorks' FloXpress CFD package will be used to establish the flow distribution within the bioreactor. The flow distribution will also be observed in a mock loop run. To characterize the flow distribution in the system, food dye will be added to the circulating fluid and a top-down camera recording of the CTCM culture chamber will be assessed.

Lastly, to verify that this system can be used to study over-stretch induced hypertrophy (OS) induced tumorigenesis, experiments using human heart slices and breast cancer cells will be performed. The culture conditions that will be used are depicted in Figure 38. The control for the induction of pressure overload in heart slice will be tissue cultured under normal cyclic pressures (0 to 80 mmHg). Next, to induce OS in tissue slices, the PPD will be set to a pressure of 0 to 140 mmHg. Periostin protein release will be assessed by ELISA protein assay from collected media. Periostin is the protein identified in Avraham et al [5] study as the potential excreted factor in TAC models that induces breast and lung tumorigenesis. The control for the breast cancer cells will be a 6-well culture plate with cell inserts containing tumor cells. This will allow for a baseline for the normal proliferation rate of these cells. An intermediate culture will be prepared to test whether continuous exposure to factors released from the OS-heart slices are necessary for an increase in proliferation of the cancer cells. An additional intermediate culture of cancer cells supplemented with 1 mL of Norm-CTCM media will serve as a control. To these cultures, 1 mL of media from the respective tissue slice culture will be added to the cancer cell wells twice per day. The last culture condition is a coculture within the proposed bioreactor. To assess cancer cell proliferation, immunolabeling for Ki67 will be performed. The Ki67 protein is expressed only during active cell cycle phases and has been associated with the growth of malignant tumor cell populations. [50, 93, 106] The experiment will be run for 3 days with tumor cell proliferation analyzed every day.
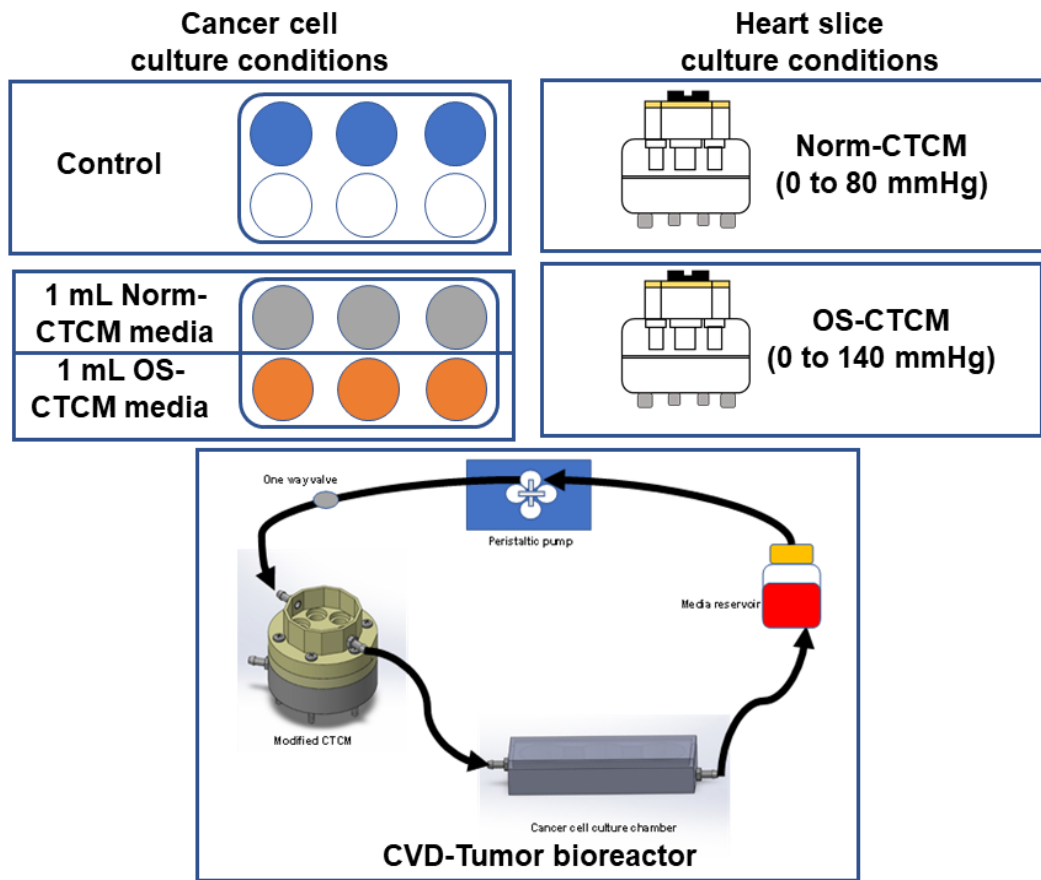
Figure 38: **Culture conditions.** 6 culture conditions will be used to investigate CVD-tumorigenesis.

4.4. Results

To characterize the flow disruption, a mock flow loop was set up for the system. The culture chamber of the CTCM device was 3D printed using PLA filament. Barb connectors were inserted into the device at the inlet and outlet and tubing was attached. To be able to record the top-down video of the flow distribution, the graphite electrodes were secured to the bottom of the culture chamber with double-sided tape. The electrodes were positioned perpendicular to the culture wall at a distance of 5.85 mm. Utilizing a peristaltic pump, water was flowed at 27 mL/min into the tissue culture chamber. A DSLR camera (Cannon Rebel T7i, Cannon, Tokyo, Japan) was used with a Navitar Zoom 7000 18-108mm Macro Lens, (Navitar, San Francisco, CA) to record the videos. A polarizing filter lens was added to reduce light reflection off the surface of the water. The camera was set to record at 30 fps.

Video 1 shows a top-down recording of the CTCM culture chamber without mechanical stimulation. Red colored dye was added to the water reservoir followed by blue dye to again visualize the flow into the chamber. It was observed that there was a slow disruption and a vortex formation in the center of the chamber which delayed the fluid clearing from the chamber.

Video 2 demonstrates the same culture setup as in Video 1 with mechanical stimulation being applied. The mechanical stimulation was set to a pulsatile pressure of 0 to 140 mmHg to emulate over-stretch induced cardiac hypertrophy. It was observed that the fluid exchange occurred at a faster rate due to the mixing effect induced by the mechanical stimulation of the 6 silicone tissue slices. After 10 to 15 seconds there is a full exchange of the media indicated by the even distribution of the dye throughout the

chamber. However, similar to without mechanical stimulation, there is a vortex formation within the center of the chamber.

To prevent the vortex formation and to obtain a uniform flow distribution, a hexagon shaped baffle (Figure 39) was placed into the center of the CTCM culture chamber with the flat face parallel to the inlet as shown in Video 3. The hexagon baffle was 3-D printed using PLA filament. It was observed that the dye distributed across all six tissue slices without any evident stagnation.
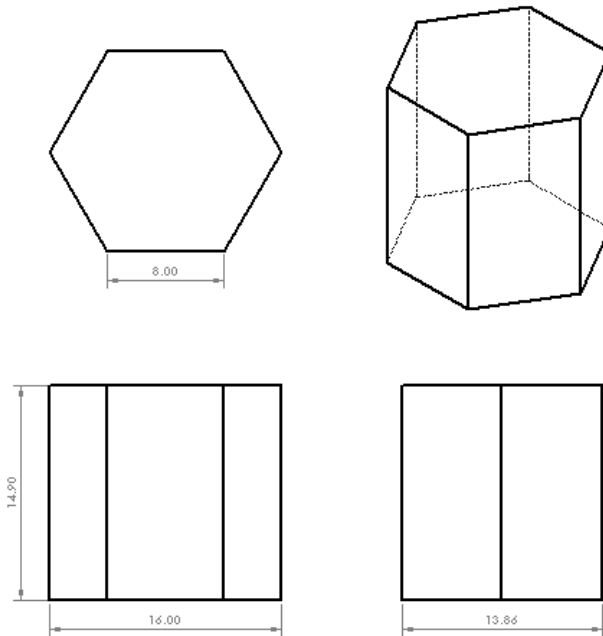
Figure 39: **Hexagon baffle drawing with dimensions.**

Lastly, to verify that factors released by each individual tissue slice can be transferred from the area of the tissue to the outlet, each silicone membrane was marked with black Sharpie. The culture chamber was then filled with water and the water was exchanged with 100% ethanol to dissolve the Sharpie. Videos 4 and 5 demonstrate that both without and with the hexagon baffle there was displacement of factors at each silicone tissue slice. The system without the hexagon baffle again presented with the vortex formation within the center of the culture chamber, however, with time, the area cleared.

As an additional verification of the mock loop run, a CFD was performed using SolidWorks FloXpress. The flow rate was set to the same rate used in the mock run (27 mL/min), a laminar flow was assumed, and the system was evaluated at a fully developed steady state. Figure 40 shows that the hexagon shaped baffle directed the fluid flow away from the center of the culture chamber, allowing for an even exchange across each tissue slice.
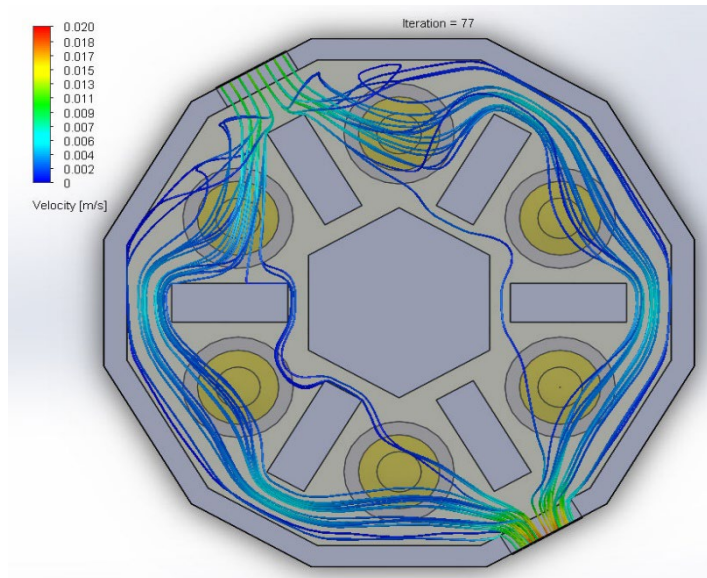
Figure 40: **CFDs of tissue culture chamber with hexagon baffle.** CFD result displaying pipelines of fluid flow through tissue culture chamber at 27 mL/min with hexagon baffle.

4.5. Conclusion

A novel bioreactor system was designed to allow for the continuous media exchange between cardiac tissue slices subjected to over-stretch induced hypertrophy conditions (OS; emulated TAC model) and tumor cells. OS within the tissue slices was achieved by modifying our lab's recently developed CTCM system. The characterization of the fluid flow through the culture chamber was performed using SolidWork's FloXpress CFD software and mock loop runs with the addition of dye. By adding a baffle within the center of the tissue slice culture chamber, a uniform exchange of solution across all 6 tissue slices was established. Overall, this study designed a novel bioreactor system that can be used as a platform to investigate the potential crosstalk between cardiac tissue and tumor cells.

4.6. Limitations

The major limitation of this study going forward will be the media composition. The metabolic demand of heart slices requires additional nutrients of FBS, FGF, and VEGF to maintain tissue viability in culture. For other cell types, certain FBS concentrations are required to induce specific phenotypes. For example, in MCF7 breast cancer cell line, a 10% FBS concentration is needed to maintain a differentiated phenotype. For the case of this cell line, the culture media that is used for the heart slices contains this concentration of FBS. However, if this system is to adapt to coculture other cell lines, media optimization will be necessary.

CHAPTER 5: CONCLUSIONS

5.1. Summary

Recently, the rapid pace of cancer therapeutic development has led to numerous unforeseen consequences on heart function, such as the development of arrythmias or myocardial infarctions. To address these adverse cardiac events, an emerging research field termed cardio-oncology has been established. Additionally, a new subfield of cardio-oncology dubbed reverse cardio-oncology has started to evolve. This new subfield aims to address the research question of whether cardiovascular disease can induce tumorigenesis or accelerated tumor growth. To support the field of cardio-oncology, a more accurate testing platform is needed to identify the toxic mechanisms of chemotherapeutics, characterize possible adverse drug effects, and address the possibility of CVD influencing tumorigenesis or accelerated tumor growth. While both *in vivo* and *in vitro* models have been of paramount importance in the discovery and detection of many cardiotoxic effects and mechanisms of action, they fall short of accurately replicating the response of the adult human myocardium. To address this, we hypothesize that cardiac tissue slices can emulate the complexity of the human heart. 300 μm thin tissue slices have several advantages such as expressing an organotypic structure and can reliably replicate cardiomyocyte functional and transcriptional expression. Our group developed a culture system for heart slices that enables functional and structural viability

of the tissue slices for 6 days using continuous electrical stimulation and enriched media. To fully emulate the cardiac cycle, our group incorporated mechanical and humoral stimulation to the system further extending the culture life to 12 days.

In this dissertation, three studies were performed to evaluate cardiac tissue slices as a potential platform to study cardio-oncology and reverse cardio-oncology related research questions.

Firstly, to test whether cardiac tissue slices could be used in cardiotoxicity screening, slices were evaluated for their ability to detect three known cardiotoxic cancer therapeutics that induce cardiotoxicity through different mechanisms. Tissue slices and hiPSC-CMs were treated with doxorubicin (an anthracycline), trastuzumab (HER2/neu inhibitor) and sunitinib (TKI) for 48 hours. hiPSC-CMs detected the cardiotoxicity of doxorubicin at nanomolar concentrations but did not detect the cardiotoxic effects of sunitinib at this concentration. Heart slices on the other hand were able to replicate the clinically known toxic effects of each compound: Dox for mitochondrial damage and ROS accumulation, Tras for homeostasis disruption, and Sun for targeting the microvascular. Overall, these results suggest that cardiac tissue slices can be a promising platform for investigating the cardiotoxic phenotypes and mechanisms of cancer therapeutics.

Secondly, to validate that cardiac tissue slices can more accurately detect cardiotoxicities compared to hiPSC-CMs, a larger range of clinically established cardiotoxic anti-cancer drugs were tested. 12 compounds, 2 positive, and 1 negative control were blindly tested at acute, < 1-hour, and subacute, 72-hour, exposure on both hiPSC-CMs and heart slices. 2 out of 12 compounds were detected as cardiotoxic after 48

to 72 hours of exposure to the clinically relevant dosage in hiPSC-CMs. On tissue slices, 12 out of 12 compounds were determined to be cardiotoxic at the clinically relevant dosage, 8 of which were detected acutely. Overall, this study demonstrates that heart slices can more accurately detect a diverse range of cardiotoxic effects induced by chemotherapeutics compared to hiPSC-CMs.

Lastly, to investigate the crosstalk between CVD and tumorigenesis a co-culture bioreactor was designed. This novel bioreactor system would allow for continuous media exchange between cardiac tissue slices subjected to over-stretch induced hypertrophy conditions (OS; emulated TAC model) and tumor cells. OS within the tissue slices was achieved by modifying our lab's recently developed CTCM system. The characterization of the fluid flow through the culture chamber was performed using SolidWork's FloXpress CFD software and mock loop runs with the addition of dye. By adding a hexagon shaped baffle within the center of the tissue slice culture chamber, a uniform exchange of solution across all 6 tissue slices was established. Overall, this study designed a novel bioreactor system that can be used as a platform to investigate the potential crosstalk between cardiac tissue and tumor cells.

This dissertation outlined how cardiac tissue slices are an effective platform for cardiotoxicity screening and can more accurately detect clinically known cardiotoxic effects compared to hiPSC-CMs (specifically a disruption in functionality). Additionally, a novel CVD-tumor bioreactor was designed providing a platform to investigate the crosstalk between tumor cells and cardiac tissue.

5.2. Future work

5.2.1. Transswell culture of cardiac tissue slices as a potential platform for cardiotoxicity detection prior to clinical trials

As the two studies detailed here have demonstrated, cardiac tissue slices can outperform the most commonly used platform in drug screening, hiPSC-CMs. Due to the current drug screening process (lack of test on human samples prior to clinical trials), 28% of drug withdrawals are due to undetected cardiotoxicities. To further reduce the risk to patients and improve the efficacy of the drug screening process, human heart slices can be an easy, medium throughput addition for FDA drug approval to obtain results from human samples prior to clinical trials.

A simplified culture method of cardiac tissue slices that consists of just optimized nutrient rich culture media and electrical stimulation is the ideal platform for incorporating into other laboratories. There are only 3 uncommon instruments used in this process that can be purchased at a relatively low price: the vibratome for tissue slice acquisition, the C-pace stimulation and 6-well electrode lids for electrical stimulation, and the force transducer for contractility measurements.

Recently, both the transwell and CTCM tissue slice culture systems developed by our lab were licensed by Anabios. This company will use these two platforms as a drug screening platform available for companies to test for cardiotoxicities of new therapeutics.

5.2.2. Bioengineered reverse cardio-oncologic culture system

Future work will consist of running the CVD-tumor bioreactor system with breast cancer cells and human heart slices. These experiments will be performed as detailed in

Chapter 4's methods section. If periostin is not released from the OS-CTCM culture set at 0 to 140 mmHg, the pressures will be increased until periostin release is observed without significantly damaging the tissue slices. Alternatively, 3 days may not be a sufficient amount of time to either induce hypertrophy in the heart slices or observe an increase in tumor cell proliferation rate. To address this possibility the culture time will be extended to 6 days.

If a hypertrophic model cannot induce tumor cell proliferation or stimulate the release of periostin, an MI model will be used instead. One of two methods can be used to obtain MI tissue slices. The first will be to induce MI in a pig model, isolate the heart and culture slices cut from the border zone of the infarction. The second method could be to emulate an MI environment. This can be achieved by treating the tissue slices with acidic Tyrode's solution and incubating the slices with 1% oxygen for 1 hour. Once it is verified that the tissue slices can emulate a MI-damaged area of the heart, the culture chamber design for a flow loop system can be fabricated. In this design, fluid will flow into the culture chamber under the tissue slices. The tissue slices will be held in the center of the chamber and to prevent the tissue slices from falling from their slots, a thin 3D printed bridge support will be inserted. Electrical stimulation will be applied to the tissue slices by graphite electrodes on either side of the tissue. The cancer cell culture chamber will be the same as described above. For cancer cell proliferation, Ki67 expression will be quantified.

CHAPTER 6: METHODS

6.1. Heart tissue collection from pigs

Thirteen pigs were used in the current study. All animal procedures were in accordance with the institutional guidelines and approved by the University of Louisville Institutional Animal Care and Use Committee. The aortic arch was clamped, and hearts were perfused with 1L of sterile cardioplegia solution (110 mM NaCl, 1.2 mM CaCl2, 16 mM KCl, 16 mM MgCl2, 10 mM NaHCO3, 5 units/ml heparin, pH to 7.4); the hearts were preserved in ice-cold cardioplegic solution until transported to the lab on ice (less than 10 minutes).

6.2. Fabrication of CTCM device

The CTCM devices were designed in SolidWorks Computer-Aided Design (CAD) software. The culture chamber, separating plate, and air chamber were manufactured using CNC (computer numerical control) machining out of clear acrylic plastic. The 7 mm support rings were center-lathed from high-density poly-ethylene plastic (HDPE) and fitted with an O-ring groove to accommodate silicone O-rings for sealing the media below. A thin silicone membrane was used to separate the culture chamber from the separating plate. The silicone membrane was laser-cut out of a 0.02'' silicone sheet, durometer 35A. The bottom and top silicone gaskets were laser-cut from a

1/16'' silicone sheet, durometer 50A. 316L stainless steel screws and wing nuts were used to hold the device together and to create an air-tight seal.

A custom printed circuit board (PCB) was designed to integrate with the C-PACE-EM system. Swiss machine header outlets on the PCB are connected to a graphite electrode via silver-plated copper wires and 0-60 bronze screws threaded into the electrodes. The PCB fits into a 3-D printed device cover.

The CTCM device is controlled by a programmable pneumatic driver (PPD) that can induce a controlled cyclic pressure similar to the cardiac cycle. As the pressure within the air chamber increases, the flexible silicone membrane will distend upward, displacing the culture medium under the tissue slices. The tissue slices will then be stretched by this fluid displacement, mimicking physiological cardiac stretch during diastole. At the peak of diastole, electrical stimulation is applied through the graphite electrodes, and the air chamber pressure is decreased, allowing the tissue slices to contract. Within the air line, there is a hemostatic valve with a pressure probe sensor that detects the pressure of the air system. The pressure detected by the pressure sensor is fed into a data acquisition device connected to a laptop. This allows for the continuous monitoring of the pressures within the air chamber. When the maximum air chamber pressure (80 mmHg for norm and 140 mmHg for OS) is reached, the data acquisition device sends a signal to the C-PACE-EM system inducing a 2 ms biphasic electrical voltage signal set at 4 V.

6.3. Heart slice culture

Heart slices were obtained, and 6-well culture conditions were performed as described below: the collected heart is transferred from the transfer container to a tray

containing cold (4°C) Cardioplegia solution. The left ventricle is isolated using sterile blades and cut into 1-2 cm^3 blocks. These tissue blocks are attached to tissue supports using tissue glue and placed into the tissue bath of a vibrating microtome containing Tyrode's solution with continuous oxygenation (3 g/L 2,3-butanedione monoxime (BDM), 140 mM NaCl (8.18 g), 6 mM KCl (0.447 g), 10 mM D-glucose (1.86 g), 10 mM HEPES (2.38 g), 1 mM MgCl2 (1 mL of 1 M solution), 1.8 mM CaCl2 (1.8 mL of 1 M solution), up to 1 L of ddH2O). The vibrating microtome is set to cut 300 μm slices at a frequency of 80 Hz, horizontal vibration amplitude of 2 mm, and advance speed of 0.03 mm/s. The tissue bath is surrounded by ice to maintain a chilled solution and keep the temperature at 4°C. Tissue slices are transferred from a microtome bath to a holding bath containing continuously oxygenated Tyrode's solution on ice until enough slices are obtained for one culture plate. For transwell culture conditions, tissue slices are adhered to sterilized polyurethane 6 mm wide supports and placed into 6-well culture plates containing 6 mL of optimized culture media (Medium 199, 1x ITS supplement, 10% FBS, 5 ng/mL VEGF, 10 ng/mL FGF-basic, and 2X Antibiotic-Antimycotic). Electrical stimulation (10 V, paced at 1.2 Hz) was applied to the tissue slices through C-Pace lids. The culture media is oxygenated before every media change three times a day. Tissue slices were cultured in an incubator set to 37°C with 5% CO$_2$.

For the CTCM culture, the tissue slices were positioned on a custom 3-D printed apparatus within a petri dish containing modified Tyrode's solution. The device is designed to oversize the heart slice by 25% of the support ring area. This is done to ensure that the heart slice is not over-stretched once it has been transferred from the Tyrode's solution to culture media and during the diastolic phase. Using histoacryl glue,

the 300 μm thick slices were fixed to 7-mm diameter support rings. Once the tissue slice was attached to the support ring, the excess tissue was trimmed off, and the attached tissue slice was placed back into the Tyrode's solution bath on ice (4°C) until enough slices were prepared for one device. The processing time should not exceed 2 hours in total for all devices. Once 6 tissue slices were attached to their support rings, the CTCM device was assembled. The CTCM culture chamber was prefilled with 21 mL of pre-oxygenated culture media. The tissue slices were transferred into the culture chamber, and all air bubbles were carefully removed with a pipette. Then the tissue slice was guided to a well and gently pressed into place. Lastly, the electrode cover was placed onto the device, and the device was transferred to an incubator. The CTCM was then connected to the air tubes and the C-PACE-EM system. The pneumatic driver was switched on and the airflow valve opened to the CTCM device. The C-PACE-EM system was set to provide 4 V at 1.2 Hz at 2 ms biphasic stimulation. The culture medium was changed twice daily, and the electrodes were replaced once a day to avoid graphite buildup from the electrodes. If necessary, the tissue slices can be removed from their culture wells to displace any air bubbles that may be trapped below. The CTCM devices were cultured in an incubator set to 37°C with 5% CO_2.

6.4. Heart slice fixation and mounting

Heart slices were fixed in 4% paraformaldehyde for 48 hours. Fixed tissue underwent dehydration in 10% then 20% sucrose for 1 hour, followed by 30% sucrose overnight. The slices were then embedded in an optimal cutting temperature compound (OCT compound) and gradually frozen in an isopentane/dry ice bath. OCT embedded blocks were stored at -80°C until sectioning. Slides were prepared in 8 μm thick sections.

6.5. Immunostaining

To remove the OCT from the heart slices, the slides were heated on a heat block for 5 minutes at 95°C. 1 mL of PBS was added to each slide and incubated at room temperature for 30 minutes. Sections were then permeabilized by setting for 15 minutes with 0.1% Triton-X in PBS at room temperature. To prevent non-specific antibody binding to the samples, 1 mL of 3% BSA solution was added to the slides and incubated for 1 hour at room temperature. The BSA was then discarded, and the slides were washed with PBS. Using a wax pen, each sample was marked off. The primary antibodies (1:200 dilution in 1% BSA) (Connexin 43 (Abcam; #AB11370), NFATC4 (Abcam; #AB99431) and Troponin-T (Thermo Scientific; #MA5-12960), were added to the section for 90 minutes, followed by the secondary antibodies (1:200 dilution in 1% BSA) Anti-mouse Alexa Fluor 488 (Thermo Scientific; #A16079), Anti-rabbit Alexa Fluor 594 (Thermo Scientific; #T6391) for another 90 minutes separated by three washes with PBS. To distinguish the target staining from the background, we only used a secondary antibody as a control. Finally, the DAPI nuclear stain was added, and the slides were mounted in vectashield (Vector Laboratories) and sealed with nail polish. Immunofluorescence imaging was performed using a Cytation 1 high content imager (20X lens magnification) and a Keyence microscope using 40X lens magnification.

For WGA staining, WGA-Alexa Fluor 555 (Thermo Scientific; #W32464) was used at 5 µg/mL in PBS and was applied to fixed sections for 30 minutes at room temperature. The slides were then washed with PBS, and Sudan Black was added to each slide and incubated for 30 minutes. The slides were then washed with PBS and

vectashield mounting media was added. Slides were imaged on a Keyence microscope using 40X lens magnification.

6.6. MTT assay

CyQUANT™ MTT Cell Viability Assay (Invitrogen, Carlsbad, CA; catalog # V13154) was used according to the manufacturer's protocol with some modifications. In details, a 6 mm surgical punch was used to ensure similar tissue size when performing the MTT assay. The tissues were each placed in a well of a 12 well plates containing MTT substrate according to the manufacturer's protocol. The slices were incubated for 3 hours at 37°C and viable tissue metabolized the MTT substrate creating a purple formazan compound. The MTT solution was replaced with 1 ml of DMSO and incubated at 37°C for 15 minutes to extract the purple formazan from the heart slices. Samples were diluted to 1:10 in DMSO within a clear bottom 96 well plate, and the intensity of the purple color was measured using a Cytation plate reader (BioTek) at 570nm. The readings were normalized to the weight of each heart slice.

6.7. Caspase-3/7

For fluorescent imaging of apoptosis, the Incucyte Caspase-3/7 Green dye (Essen Bioscience 4440) was added to the media/drug cocktail at a concentration of 5 μM for the duration of the assay. Analysis of apoptosis using the Caspase 3/7 fluorescent dye was performed using Incucyte® S3 Live Cell Analysis System (Essen Bioscience / Sartorius) running version 2019A (20,191.1.6976.19779). Parameters were set to quantify green fluorescent intensity metrics and areas of high signal intensity indicated cell death.

6.8. RNAseq

RNA was isolated from the heart slices by using the Qiagen miRNeasy Micro Kit, #210874, following the manufacturer's protocol after homogenizing tissue in Trizol. RNAseq library preparation, sequencing, and data analysis were performed as described below:

1 μg RNA per sample was used as input material for the RNA library preparations. Sequencing libraries were generated using NEBNext UltraTM RNA Library Prep Kit for Illumina (NEB, USA) following manufacturer's recommendations and index codes were added to attribute sequences to each sample. Briefly, mRNA was purified from total RNA using poly-T oligo-attached magnetic beads. Fragmentation was carried out using divalent cations under elevated temperature in NEBNext First Strand Synthesis Reaction Buffer (5X). First strand cDNA was synthesized using random hexamer primer and M-MuLV Reverse Transcriptase (RNase H). Second strand cDNA synthesis was subsequently performed using DNA Polymerase I and RNase H. Remaining overhangs were converted into blunt ends via exonuclease/polymerase activities. After adenylation of 3' ends of DNA fragments, NEBNext Adaptor with hairpin loop structure were ligated to prepare for hybridization. In order to select cDNA fragments of preferentially 150~200 bp in length, the library fragments were purified with AMPure XP system (Beckman Coulter, Beverly, USA). Then 3 μL USER Enzyme (NEB, USA) was used with size-selected, adaptor ligated cDNA at 37ºC for 15 min followed by 5 min at 95ºC before PCR. Then PCR was performed with Phusion High-Fidelity DNA polymerase, Universal PCR primers and Index (X) Primer. At last, PCR products were purified (AMPure XP system) and library quality was assessed on the

Agilent Bioanalyzer 2100 system. Then the cDNA libraries are sequenced using Novaseq sequencer. Original image data file from Illumina is transformed to raw reads by CASAVA base recognition (Base Calling). Raw data are stored in FASTQ(fq) format files, which contain sequences of reads and corresponding base quality. HISAT2 is selected to map the filtered sequenced reads to the reference genome Sscrofa11.1. In general, HISAT2 supports genomes of any size, including those larger than 4 billion bases and most of the parameters are set to default. Spliced reads of RNA Seq data can be effectively aligned using HISAT2, which is the fastest system currently available, with equal or better accuracy than any other method.

The abundance of transcript reflects gene expression level directly. Gene expression level is estimated by the abundance of transcripts (count of sequencing) that mapped to genome or exon. Read counts is proportional to gene expression level, gene length and sequencing depth. FPKM (Fragments Per Kilobase of transcript sequence per Millions base pairs sequenced) were calculated and differential expression P-values were determined using DESeq2 package. Then, we calculated the false discovery rates (FDRs) for each P-value with the Benjamini-Hochberg method 9 based on the built-in R function "p.adjust".

6.9. qRT-PCR

The RNA extracted from heart slices, was converted to cDNA at 200 ng/µL concentration using Thermo's SuperScript IV Vilo Master mix (Thermo, Cat # 11756050). qRT-PCR was run using Applied Biosystems microamp Endura plate optical 384-well clear reaction plate (Thermo, Cat # 4483319) with microamp optical adhesive film (Thermo, Cat # 4311971). The reaction mixture is consisted of 5 µL Taqman Fast

Advanced Master mix (Thermo, Cat # 4444557), 0.5 μL Taqman Primer, and 3.5 μL H$_2$O per well were mixed. The standard qPCR cycle was run, and CT values were measured using an Applied Biosystems Quantstudio 5 Real-Time PCR instrument (384-well block; Product #A28135). Taqman primers were purchased from Thermo (GAPDH (Ss03375629_u1), COL1A2 (Ss03375009_u1), COL3A1 (Ss04323794_m1), ACTA2 (Ss04245588_m1), TNNT (Ss004953568_g1), and MYH7 (Ss03392424_mH). All sample CT values were normalized to the housekeeping gene GAPDH.

6.10. NT-ProBNP ELISA Assay

NT–ProBNP release in the culture media was assessed using an NT-ProBNP kit (pigs) (Cat # MBS2086979, MyBioSource) according to the manufacturer protocol. Briefly, 250 μL of each sample and standard were added to each well in duplicate. Immediately following the addition of the samples, 50 μL of Detection Reagent A was added per well. The plate was shaken gently and sealed with a Plate Sealer. The plate was then incubated for 1 hour at 37°C. Then, the solution was aspirated, and the wells were washed with 350 μL of 1X Wash Solution 4 times, letting the Wash Solution incubate for 1-2 minutes each time. Next, 100 μL of Detection Reagent B was added per well and sealed with a Plate sealer. The plate was gently shaken and incubated at 37°C for 30 minutes. The solution was aspirated, and the wells were washed with 350 μL of 1X Wash Solution 5 times. 90 μL of Substrate Solution was added to each well, and the plate was sealed. The plate was incubated for 10-20 minutes at 37°C. 50 μL of Stop Solution was added per well. The plate was immediately measured using a Cytation plate reader (BioTek) set at 450 nm.

6.11. Calcium-transient assessment

Heart slices were loaded with Fluo-4 for 30 minutes at room temperature before being transferred to the imaging chamber. The loading solution contained a 1:10 mixture of 5mM Fluo-4 AM in dry DMSO and PowerloadTM concentrate (Invitrogen), which was diluted 100-fold into extracellular Tyrode's solution (NaCl 140 mM; KCl 4.5 mM; glucose 10 mM; HEPES 10 mM; MgCl2 1 mM; CaCl2 1.8 mM; 2× Antibiotic-Antimycotic; pH 7.4). An additional 20min were allowed for de-esterification before recordings were made. Contractions and calcium transients were evoked by applying voltage pulses at 1 Hz between platinum wires placed on either side of the heart slice and connected to a field stimulator (IonOptix, Myopacer). Fluo-4 fluorescence transients were recorded via a standard filter set (#49011 ET, Chroma Technology). Resting fluorescence was recorded after cessation of pacing, and background light was obtained after removing the heart slice from the field of view at the end of the experiment. All analyses of calcium transients were based on calcium transients recorded from single cardiomyocytes within the heart slice and the calcium transient's amplitude was assessed as the average of 10 consecutive beats from each cell. Calcium transients and amplitude was assessed following normalization to the basal florescence of each cell and represented as F/F0.

6.12. Force transducer contractility measurement

Video 6 provides a detailed walkthrough of the force transducer setup.

A day before the experiment the following materials are prepared. 1 cm wide by 0.5 cm high triangle foil supports are cut out, anchor supports are 3-D printed, and standard sized staples are bent into square shaped hooks. 1.25" long 3-0 suture is fixed to the top half of the foil triangle and an anchor support. Next a 3.25" long suture is attached

to another foil triangle and a hook. The force transducer is connected to a bridge amplifier. The bridge amplifier is then connected to a data acquisition device which records the data sent to LabChart program on a laptop. The force transducer is calibrated using a two-point calibration method prior to each experiment.

Tissue slices are obtained using the method detailed above and transferred to a petri dish containing no BDM Tyrode's solution for 20 minutes. The tissue slice are then transferred to a lid of a petri dish and cut to a 1 cm by 1 cm sized square. Perpendicular to the fiber alignment within the tissue slice, the base of the triangular supports are adhered using histoacryl glue. The slice is gently transferred to the tissue bath containing 30 mL no BDM Tyrode's solution. The anchor is pressed into the slot in the bottom of the tissue bath and the tissue bath is secured directly underneath the force transducer cantilever. The suture length attached to the anchor is adjusted to a length that will allow for the hook to be placed onto the cantilever without applying excess stretch to the tissue slice. The graphite electrodes are inserted into their slots in the tissue bath and the hook is placed onto the cantilever. The electrical stimulation is set to apply 10 V at a 0.2 Hz frequency.

The tissue slice length is then adjusted until the slice is taut and a contractile signal is detected but the tissue slices are not overstretched. Typically, the slice will produce better contractile data if allowed to hang in the taut position with electrical stimulation for 10 to 15 minutes prior to recording.

6.13. Calcium analysis code

ImageJ was used to extract the transient intensity of the calcium videos for each cell. The intensity data was normalized to the background signal and passed into the code

below. The code finds the minimum and maximum peaks and calculates the amplitude,

downstroke and upstroke velocity, and the cycle time.

Calcium data extraction:

```matlab
close all
clear
clc

%load file in

a = readtable('template_1_Ca.xlsx');

%Prompts user for frame rate input
prompt = {'Enter frame rate:'};
dlgtitle = 'Input';
dims = 1;
definput = {'10'};
FrameRate = inputdlg(prompt,dlgtitle,dims,definput);

FrameRate = str2double(FrameRate);

%plot each column
for i = 1:width(a)

    figure(i)
    Trace = table2array(a(:,i));
    hold on
    plot(Trace)

    %find max peaks
    [pks, index] = findpeaks(Trace);
    scatter(index,pks,'b')

    %invert
    min_Trace = max(Trace)-(Trace);

    %find min peaks
    [pks_min, index_min] = findpeaks(min_Trace);

    %now find the actual peaks of the min from Trace
    pks_min = Trace(index_min);
    scatter(index_min,pks_min)

    %Pre-allocate/clear arrays
    amplitude = [ ];
    upstroke = [ ];
    downstroke = [ ];

    %Find the amplitude of each (min to max? start of contraction)
```

```matlab
    %first check if we start at a peak on valley
    if index(1) < index_min(1) %then skip the first peak
        for b = 2:length(pks)-1
            [amplitude(b-1)] = (pks(b)-pks_min(b-1))/pks_min(b-1);
            [upstroke(b-1)] = amplitude(b-1)/((index(b)-index_min(b-
1))/FrameRate);
            [upstrokeTime(b-1)] = (index(b)-index_min(b-1))/FrameRate;
            [downstroke(b-1)] = ((pks(b)-
pks_min(b))/pks_min(b))/((index_min(b)-index(b))/FrameRate);
            [downstrokeTime(b-1)] = (index_min(b)-index(b))/FrameRate;
        end
    else %don't skip first peak
        for c = 1:length(pks)-1
            [amplitude(c)] = (pks(c)-pks_min(c))/pks_min(c);
            [upstroke(c)] = amplitude(c)/((index(c)-index_min(c))/FrameRate);
            [upstrokeTime(c)] = (index(c)-index_min(c))/FrameRate;
            [downstroke(c)] = ((pks(c)-pks_min(c+1))/pks_min(c+1)) /
((index_min(c+1)-index(c))/FrameRate);
            [downstrokeTime(c)] = (index_min(c+1)-index(c))/FrameRate;
        end
    end

    %take average for this cell
    [average_amp(i)] = mean(amplitude);
    [average_up(i)] = mean(upstroke);
    [average_down(i)] = mean(downstroke);
    [average_up_Time(i)] = mean(upstrokeTime);
    [average_down_Time(i)] = mean(downstrokeTime);

    hold off

    %Convert index to seconds
    for D = 1:length(index)
        T_Sec(D) = index(D)/FrameRate; %frames/sec
    end

    Diff_T_Sec = diff(T_Sec);
    [average_Time(i)] = mean(Diff_T_Sec);

    %is it in sycn with the electrical stim (1.2 Hz--> 0.833 seconds)
        %Within 25% consistency?
    for E = 1:length(Diff_T_Sec)

        PlusPoint = 0.833 + (0.25*0.833);
        MinusPoint = 0.833 - (0.25*0.833);

        if Diff_T_Sec(E) < PlusPoint && Diff_T_Sec(E)> MinusPoint %index is
within the 5% range of 1.2 Hz
            Consist(E) = 1;
        elseif Diff_T_Sec(E) > PlusPoint %took longer
            Consist(E) = 2;
        else % Shorter
            Consist(E) = 0;
        end
    end
```

```matlab
    %Find the number of 1's
    o = 0;

    for Y = 1:length(Consist)
        if Consist(Y) == 1
            o = o + 1;
        end
    end

    %percent of points that are consist for that cell
    [Consist_Average(i)] = (o / length(Consist))* 100;

    %What is the # of beats that have a longer time between transients
    r = 0;

    for QQ = 1:length(Consist)
        if Consist(QQ) == 2
            r = r + 1;
        end
    end

    %percent longer transients
    [Percent_Slow_Trans(i)] = (r / length(Consist)) * 100;

    [Percent_Fast_Trans(i)] = 100 -
    (Consist_Average(i)+Percent_Slow_Trans(i));

end

    average_up_Time = average_up_Time';
    average_down_Time = average_down_Time';

CopyMe =
[average_amp;average_up;average_down;average_Time;Consist_Average;Percent_Slow
_Trans;Percent_Fast_Trans]';
```

6.14. Contractility analysis code

Contractile data is extracted from the data recorded by the force transducer. The

data is saved as a .mat file and read by the "Data extraction and peak detection/selection"

code. In this code the data is analyzed by each timepoint marker that is placed at each

recording, indicating when certain compounds or concentrations are added. The

maximum and minimum peaks are detected by controlling the minimum threshold and

distance between peaks. If these values cannot be adjusted to accurately detect all desired

peaks, then manual section can be performed and the minimum or maximum "select peaks" code can be run. Once all the desired minimum and maximum peaks are stored then the "analysis" code can be run to extract the contraction amplitude, upstroke and downstroke velocities, and cycle time.

Data extraction and peak detection/selection

```
close all
clear
clc

%read in file
a = load('datafile.mat');

%% Change me to the recorded trace
point = 6;

% collecting the data and converting time
Dose = a.data(a.datastart(point):a.dataend(point));

t=0:1/1000:length(Dose)/1000-1/1000; %converting the sampling frame to time

figure(1);
hold on
plot(Dose)

% set max threshold
max_Threshold = max(Dose) - (0.31 * max(Dose)); %0.25

%find max peaks with a threshold and min distance for close peaks
[pks, index] = findpeaks(Dose,'MinPeakHeight',max_Threshold,
'MinPeakDistance', 1500);
scatter(index,pks,'o')

hold off

%Now for the min peaks
%first invert the trace
DoseI = max(Dose)-(Dose);

figure(2)
hold on
plot(DoseI)

min_Threshold = max(DoseI) - (0.4*max(DoseI));

%Now find min peaks with a threshold and min distance for close peaks
```

```
[pks_min, index_min] = findpeaks(DoseI,'MinPeakHeight',min_Threshold,
'MinPeakDistance',2500);
scatter(index_min,pks_min,'magenta')

hold off
```

Select max peaks (if necessary)

```
close all

%We know the position saved ss
index = flip(ss(:,1))';
pks = flip(ss(:,2));

figure (3)
hold on
plot(Dose)
scatter(index,pks)

hold off
```

Select min peaks (if necessary)

```
close all

%We know the position saved as ss
index_min = flip(ss(:,1))';
pks_min = flip(ss(:,2));

figure (3)
hold on
plot(DoseI)
scatter(index_min,pks_min)

hold off

[pks_min] = [0];

%find the actual pks
for f = 1:length(index_min)
    [pks_min(f)] = Dose(index_min(f));
end

figure(4)
hold on
plot(Dose)
scatter(index,pks,'p')
scatter(index_min,pks_min,'o')
hold off
```

Analysis

```matlab
%Find the amplitude of each (min to max? start of contraction)
    %first check if we start at a peak on valley
    if index(1) < index_min(1) %then skip the first peak
        for b = 2:length(pks)-1
            [amplitude(b-1)] = ((pks(b)-pks_min(b-1))/pks_min(b-1))*0.0098;

            %contraction speed (mg/sec)
            [contraction_speed(b-1)]  = (amplitude(b-1)/((index(b)-
index_min(b-1))/1000))*0.0098;
            [contraction_time(b-1)]  = ((index(b)-index_min(b-1))/1000);

            %relaxation speed
            [relaxtion_speed(b-1)] = (((pks(b)-pks_min(b))/pks_min(b)) /
((index_min(b)-index(b))/1000))*0.0098;
            [relaxtion_time(b-1)] = ((index_min(b)-index(b))/1000);

        end
    else %don't skip first peak
        for c = 1:length(pks)-1
            [amplitude(c)] = ((pks(c)-pks_min(c))/pks_min(c))*0.0098;

            %contraction speed
            [contraction_speed(c)] = (amplitude(c)/((index(c)-
index_min(c))/1000))*0.0098;
            [contraction_time(c)] = ((index(c)-index_min(c))/1000);

            %relaxation speed
            [relaxtion_speed(c)] = (((pks(c)-pks_min(c+1))/pks_min(c+1)) /
((index_min(c+1)-index(c))/1000))*0.0098;
            [relaxtion_time(c)] = ((index_min(c+1)-index(c))/1000);
        end
    end


% convert index to seconds
for y = 1:length(index)
    [index_sec(y)] = index(y)/1000;
end

%cycle time (in sec)
[cycle] = diff(index_sec);

%calc. regularity
for E = 1:length(cycle)

        PlusPoint = 5 + (0.25*5);
        MinusPoint = 5 - (0.25*5);
```

```matlab
        if cycle(E) < PlusPoint && cycle(E)> MinusPoint %index is within the
75% range of 1.2 Hz
            Consist(E) = 1;
        elseif cycle(E) > PlusPoint %took longer
            Consist(E) = 2;
        else % Shorter
            Consist(E) = 0;
        end
end


    %Find the number of 1's
    o = 0;

    for Y = 1:length(Consist)
        if Consist(Y) == 1
            o = o + 1;
        end
    end

    %percent of points that are consist for that cell
    Consist_Average = (o / length(Consist))* 100;

    %What is the # of beats that have a longer time between transients
    r = 0;

    for QQ = 1:length(Consist)
        if Consist(QQ) == 2
            r = r + 1;
        end
    end

    %percent longer transients
    Percent_Slow = (r / length(Consist)) * 100;

    Percent_Fast = 100 - (Consist_Average+Percent_Slow);

    AboutMe = [amplitude;contraction_speed;relaxtion_speed]';
    APercentages = [Consist_Average;Percent_Slow;Percent_Fast]';

    cycle = cycle';

    times = [contraction_time;relaxtion_time]';
```

REFERENCES

1. A. R. Parrish NGS, R. D. Spall, R. T. Dorr,t C. L. Krumdieck, A. J. Gandolfi, and K. Brendel (1992) Organ culture of rat myocardial slices: an alternative in vitro tool in organ-specific toxicology. Toxicology Methods 2:101-111

2. Aboumsallem JP, Moslehi J, de Boer RA (2020) Reverse cardio-oncology: cancer development in patients with cardiovascular disease. J Am Heart Assoc 9:e013754 doi:10.1161/JAHA.119.013754

3. Ahmad T, Yin P, Saffitz J, Pockros PJ, Lalezari J, Shiffman M, Freilich B, Zamparo J, Brown K, Dimitrova D, Kumar M, Manion D, Heath-Chiozzi M, Wolf R, Hughes E, Muir AJ, Hernandez AF (2015) Cardiac dysfunction associated with a nucleotide polymerase inhibitor for treatment of hepatitis C. Hepatology 62:409-416 doi:10.1002/hep.27488

4. Ahmed RE, Anzai T, Chanthra N, Uosaki H (2020) A brief review of current maturation methods for human induced pluripotent stem cells-derived cardiomyocytes. Front Cell Dev Biol 8:178 doi:10.3389/fcell.2020.00178

5. Avraham S, Abu-Sharki S, Shofti R, Haas T, Korin B, Kalfon R, Friedman T, Shiran A, Saliba W, Shaked Y, Aronheim A (2020) Early cardiac remodeling promotes tumor growth and metastasis. Circulation 142:670-683 doi:10.1161/CIRCULATIONAHA.120.046471

6. Barbey JT, Pezzullo JC, Soignet SL (2003) Effect of arsenic trioxide on qt interval in patients with advanced malignancies. J Clin Oncol 21:3609-3615 doi:10.1200/JCO.2003.10.009

7. Barton M, Yanagisawa M (2019) Endothelin: 30 years from discovery to therapy. Hypertension 74:1232-1265 doi:10.1161/HYPERTENSIONAHA.119.12105

8. Barton PJ, Felkin LE, Birks EJ, Cullen ME, Banner NR, Grindle S, Hall JL, Miller LW, Yacoub MH (2005) Myocardial insulin-like growth factor-i gene expression during recovery from heart failure after combined left ventricular assist device and clenbuterol therapy. Circulation 112:I46-50 doi:10.1161/01.CIRCULATIONAHA.105.525873

9. Baumgart BR, Wang F, Kwagh J, Storck C, Euler C, Fuller M, Simic D, Sharma S, Arnold JJ, Cameron CE, Van Vleet TR, Flint O, Bunch RT, Davies MH, Graziano MJ, Sanderson TP (2016) Effects of bms-986094, a guanosine nucleotide analogue, on mitochondrial dna synthesis and function. Toxicol Sci 153:396-408 doi:10.1093/toxsci/kfw135

10. Beavers CJ, Rodgers JE, Bagnola AJ, Beckie TM, Campia U, Di Palo KE, Okwuosa TM, Przespolewski ER, Dent S, American Heart Association Clinical Pharmacology C, Cardio-Oncology Committee of the Council on Clinical C, Council on G, Precision M, the Council on Peripheral Vascular D (2022) Cardio-oncology drug interactions: a scientific statement from the american heart association. Circulation:CIR0000000000001056 doi:10.1161/CIR.0000000000001056

11. Bellinger AM, Arteaga CL, Force T, Humphreys BD, Demetri GD, Druker BJ, Moslehi JJ (2015) Cardio-oncology: how new targeted cancer therapies and precision medicine can inform cardiovascular discovery. Circulation 132:2248-2258 doi:10.1161/CIRCULATIONAHA.115.010484

12. Bers DM (2008) Calcium cycling and signaling in cardiac myocytes. Annu Rev Physiol 70:23-49 doi:10.1146/annurev.physiol.70.113006.100455

13. Berton G, Cordiano R, Cavuto F, Bagato F, Segafredo B, Pasquinucci M (2018) Neoplastic disease after acute coronary syndrome: incidence, duration, and features: the abc-4* study on heart disease. J Cardiovasc Med (Hagerstown) 19:546-553 doi:10.2459/JCM.0000000000000701

14. Beuckelmann DJ, and Wier, W. G. (1988) Mechanismof release of calcium from sarcoplasmic reticulum of guinea-pig cardiac cells. J. Physiol 405:233-255 doi:10.1113/jphysiol.1988.sp017331

15. Beuckelmann DJ, Näbauer, M., and Erdmann, E. (1992) Intracellular calcium handling in isolated ventricular myocytes from patients with terminal heart failure. Circulation 85:1046-1055 doi:10.1161/01.cir.85.3.1046

16. Bibler MR, Chou TC, Toltzis RJ, Wade PA (1988) Recurrent ventricular tachycardia due to pentamidine-induced cardiotoxicity. Chest 94:1303-1306 doi:10.1378/chest.94.6.1303

17. Bird S (2003) The human adult cardiomyocyte phenotype. Cardiovascular Research 58:423-434 doi:10.1016/s0008-6363(03)00253-0

18. Boffetta P, Malhotra J (2018) Impact of heart failure on cancer incidence: a complicated question. J Am Coll Cardiol 71:1511-1512 doi:10.1016/j.jacc.2018.02.015

19. Bohm F, Pernow J (2007) The importance of endothelin-1 for vascular dysfunction in cardiovascular disease. Cardiovasc Res 76:8-18 doi:10.1016/j.cardiores.2007.06.004

20. Bouloumié A S-KV, Busse R (1999) Vascular endothelial growth factor up-regulates nitric oxide synthase expression in endothelial cells. Cardiovasc Res 41:773-780

21. Bowles EJ, Wellman R, Feigelson HS, Onitilo AA, Freedman AN, Delate T, Allen LA, Nekhlyudov L, Goddard KA, Davis RL, Habel LA, Yood MU, McCarty C, Magid DJ, Wagner EH, Pharmacovigilance Study T (2012) Risk of heart failure in breast cancer patients after anthracycline and trastuzumab treatment: a retrospective cohort study. J Natl Cancer Inst 104:1293-1305 doi:10.1093/jnci/djs317

22. Brandenburger M, Wenzel J, Bogdan R, Richardt D, Nguemo F, Reppel M, Hescheler J, Terlau H, Dendorfer A (2012) Organotypic slice culture from human adult ventricular myocardium. Cardiovasc Res 93:50-59 doi:10.1093/cvr/cvr259

23. Burridge PW, Li YF, Matsa E, Wu H, Ong SG, Sharma A, Holmstrom A, Chang AC, Coronado MJ, Ebert AD, Knowles JW, Telli ML, Witteles RM, Blau HM, Bernstein D, Altman RB, Wu JC (2016) Human induced pluripotent stem cell-derived cardiomyocytes recapitulate the predilection of breast cancer patients to doxorubicin-induced cardiotoxicity. Nat Med 22:547-556 doi:10.1038/nm.4087

24. Callaghan NI, Lee SH, Hadipour-Lakmehsari S, Lee XA, Ahsan Siraj M, Driouchi A, Yip CM, Husain M, Simmons CA, Gramolini AO (2020) Functional culture and in vitro genetic and small-molecule manipulation of adult mouse cardiomyocytes. Commun Biol 3:229 doi:10.1038/s42003-020-0946-9

25. Caporizzo MA, Chen CY, Prosser BL (2019) Cardiac microtubules in health and heart disease. Exp Biol Med (Maywood) 244:1255-1272 doi:10.1177/1535370219868960

26. Caporizzo MA, Chen CY, Salomon AK, Margulies KB, Prosser BL (2018) Microtubules provide a viscoelastic resistance to myocyte motion. Biophys J 115:1796-1807 doi:10.1016/j.bpj.2018.09.019

27. Cardinale D, Colombo A, Lamantia G, Colombo N, Civelli M, De Giacomi G, Rubino M, Veglia F, Fiorentini C, Cipolla CM (2010) Anthracycline-induced cardiomyopathy: clinical relevance and response to pharmacologic therapy. J Am Coll Cardiol 55:213-220 doi:10.1016/j.jacc.2009.03.095

28. Celes MR, Malvestio LM, Suadicani SO, Prado CM, Figueiredo MJ, Campos EC, Freitas AC, Spray DC, Tanowitz HB, da Silva JS, Rossi MA (2013) Disruption of calcium homeostasis in cardiomyocytes underlies cardiac structural and functional changes in severe sepsis. PLoS One 8:e68809 doi:10.1371/journal.pone.0068809

29. Chen B, Liu Q, Popowich A, Shen S, Yan X, Zhang Q, Li XF, Weinfeld M, Cullen WR, Le XC (2015) Therapeutic and analytical applications of arsenic binding to proteins. Metallomics 7:39-55 doi:10.1039/c4mt00222a

30. Chen X, Cordes JS, Bradley JA, Sun Z, Zhou J (2006) Use of arterially perfused rabbit ventricular wedge in predicting arrhythmogenic potentials of drugs. J Pharmacol Toxicol Methods 54:261-272 doi:10.1016/j.vascn.2006.02.005

31. Chintalgattu V, Rees ML, Culver JC, Goel A, Jiffar T, Zhang J, Dunner K, Jr., Pati S, Bankson JA, Pasqualini R, Arap W, Bryan NS, Taegtmeyer H, Langley RR, Yao H, Kupferman ME, Entman ML, Dickinson ME, Khakoo AY (2013) Coronary microvascular pericytes are the cellular target of sunitinib malate-induced cardiotoxicity. Sci Transl Med 5:187ra169 doi:10.1126/scitranslmed.3005066

32. Clark M, Steger-Hartmann T (2018) A big data approach to the concordance of the toxicity of pharmaceuticals in animals and humans. Regul Toxicol Pharmacol 96:94-105 doi:10.1016/j.yrtph.2018.04.018

33. Cohen JB, Geara AS, Hogan JJ, Townsend RR (2019) Hypertension in cancer patients and survivors: epidemiology, diagnosis, and management. JACC CardioOncol 1:238-251 doi:10.1016/j.jaccao.2019.11.009

34. Cordes JS, Sun Z, Lloyd DB, Bradley JA, Opsahl AC, Tengowski MW, Chen X, Zhou J (2005) Pentamidine reduces herg expression to prolong the qt interval. Br J Pharmacol 145:15-23 doi:10.1038/sj.bjp.0706140

35. Crisp M, Liu Q, Roux K, Rattner JB, Shanahan C, Burke B, Stahl PD, Hodzic D (2006) Coupling of the nucleus and cytoplasm: role of the linc complex. J Cell Biol 172:41-53 doi:10.1083/jcb.200509124

36. Czopek A, Moorhouse R, Guyonnet L, Farrah T, Lenoir O, Owen E, van Bragt J, Costello HM, Menolascina F, Baudrie V, Webb DJ, Kluth DC, Bailey MA, Tharaux PL, Dhaun N (2019) A novel role for myeloid endothelin-b receptors in hypertension. Eur Heart J 40:768-784 doi:10.1093/eurheartj/ehy881

37. de Boer RA, Aboumsallem JP, Bracun V, Leedy D, Cheng R, Patel S, Rayan D, Zaharova S, Rymer J, Kwan JM, Levenson J, Ronco C, Thavendiranathan P, Brown SA (2021) A new classification of cardio-oncology syndromes. Cardiooncology 7:24 doi:10.1186/s40959-021-00110-1

38. de Boer RA, Hulot JS, Tocchetti CG, Aboumsallem JP, Ameri P, Anker SD, Bauersachs J, Bertero E, Coats AJS, Celutkiene J, Chioncel O, Dodion P, Eschenhagen T, Farmakis D, Bayes-Genis A, Jager D, Jankowska EA, Kitsis RN, Konety SH, Larkin J, Lehmann L, Lenihan DJ, Maack C, Moslehi JJ, Muller OJ, Nowak-Sliwinska P, Piepoli MF, Ponikowski P, Pudil R, Rainer PP, Ruschitzka F, Sawyer D, Seferovic PM, Suter T, Thum T, van der Meer P, Van Laake LW, von Haehling S, Heymans S, Lyon AR, Backs J (2020) Common mechanistic pathways in cancer and heart failure. a scientific roadmap on behalf of the translational research committee of the heart failure association (hfa) of the european society of cardiology (ESC). Eur J Heart Fail 22:2272-2289 doi:10.1002/ejhf.2029

39. de Boer RA, Meijers WC, van der Meer P, van Veldhuisen DJ (2019) cancer and heart disease: associations and relations. Eur J Heart Fail 21:1515-1525 doi:10.1002/ejhf.1539

40. Denning C, Borgdorff V, Crutchley J, Firth KS, George V, Kalra S, Kondrashov A, Hoang MD, Mosqueira D, Patel A, Prodanov L, Rajamohan D, Skarnes WC, Smith JG, Young LE (2016) Cardiomyocytes from human pluripotent stem cells: from laboratory curiosity to industrial biomedical platform. Biochim Biophys Acta 1863:1728-1748 doi:10.1016/j.bbamcr.2015.10.014

41. DENNIS J. SLAMON MD, PH.D., BRIAN LEYLAND-JONES, M.D., STEVEN SHAK, M.D., HANK FUCHS, M.D., VIRGINIA PATON, PHARM.D., ALEX BAJAMONDE, PH.D., THOMAS FLEMING, PH.D., WOLFGANG EIERMANN, M.D., JANET WOLTER, M.D., MARK PEGRAM, M.D., JOSE BASELGA, M.D., AND LARRY NORTON, M.D (2001) Use of chemotherapy plus a monoclonal antibody against her2 for metastatic breast cancer that overexpresses HER2. The New England Journal of Medicine 344:783-792

42. Ding S, Long F, Jiang S (2016) Acute myocardial infarction following erlotinib treatment for nsclc: a case report. Oncol Lett 11:4240-4244 doi:10.3892/ol.2016.4508

43. Ding W, Zhang L, Kim S, Tian W, Tong Y, Liu J, Ma Y, Chen S (2015) Arsenic sulfide as a potential anticancer drug. Mol Med Rep 11:968-974 doi:10.3892/mmr.2014.2838

44. Dipla K, Mattiello, J. A., Jeevanandam, V., Houser, S. R., and Margulies, K. B. (1998) Myocyte recovery after mechanical circulatory support in humans with end-stage heart failure. Circulation 97:2316-2322 doi:10.1161/01.cir.97.23.2316

45. Drolet B, Simard C, Roden DM (2004) Unusual effects of a QT-prolonging drug, arsenic trioxide, on cardiac potassium currents. Circulation 109:26-29 doi:10.1161/01.CIR.0000109484.00668.CE

46. Feng JY, Xu Y, Barauskas O, Perry JK, Ahmadyar S, Stepan G, Yu H, Babusis D, Park Y, McCutcheon K, Perron M, Schultz BE, Sakowicz R, Ray AS (2016) Role of mitochondrial rna polymerase in the toxicity of nucleotide inhibitors of hepatitis C virus. Antimicrob Agents Chemother 60:806-817 doi:10.1128/AAC.01922-15

47. Fischer C, Milting H, Fein E, Reiser E, Lu K, Seidel T, Schinner C, Schwarzmayr T, Schramm R, Tomasi R, Husse B, Cao-Ehlker X, Pohl U, Dendorfer A (2019) Long-term functional and structural preservation of precision-cut human myocardium under continuous electromechanical stimulation in vitro. Nat Commun 10:117 doi:10.1038/s41467-018-08003-1

48. Fu X, Khalil H, Kanisicak O, Boyer JG, Vagnozzi RJ, Maliken BD, Sargent MA, Prasad V, Valiente-Alandi I, Blaxall BC, Molkentin JD (2018) Specialized fibroblast differentiated states underlie scar formation in the infarcted mouse heart. J Clin Invest 128:2127-2143 doi:10.1172/JCI98215

49. Galano G, Caputo M, Tecce MF, Capasso A (2011) Efficacy and tolerability of vinorelbine in the cancer therapy. Curr Drug Saf 6:185-193 doi:10.2174/157488611797579302

50. Gatter DCBKC (2002) Ki67 protein: the immaculate deception? Histopathology 40:2-11

51. Geisberg CA, Abdallah WM, da Silva M, Silverstein C, Smith HM, Abramson V, Mayer I, Means-Powell J, Freehardt D, White B, Lenihan D, Sawyer DB (2013) Circulating neuregulin during the transition from stage a to stage B/C heart failure in a breast cancer cohort. J Card Fail 19:10-15 doi:10.1016/j.cardfail.2012.11.006

52. Geisberg CA, Sawyer DB (2010) Mechanisms of anthracycline cardiotoxicity and strategies to decrease cardiac damage. Curr Hypertens Rep 12:404-410 doi:10.1007/s11906-010-0146-y

53. Gill M, Horn K, Hennan J, White R, Bounous D, Clark S, Megill JR, Janovitz E, Davies M, Sanderson T, Graziano M (2017) From the cover: investigative nonclinical cardiovascular

safety and toxicology studies with BMS-986094, an NS5B RNA-dependent RNA polymerase inhibitor. Toxicol Sci 155:348-362 doi:10.1093/toxsci/kfw211

54. Gilsbach R, Preissl S, Gruning BA, Schnick T, Burger L, Benes V, Wurch A, Bonisch U, Gunther S, Backofen R, Fleischmann BK, Schubeler D, Hein L (2014) Dynamic DNA methylation orchestrates cardiomyocyte development, maturation and disease. Nat Commun 5:5288 doi:10.1038/ncomms6288

55. Gintant G, Burridge P, Gepstein L, Harding S, Herron T, Hong C, Jalife J, Wu JC (2019) Use of human induced pluripotent stem cell-derived cardiomyocytes in preclinical cancer drug cardiotoxicity testing: a scientific statement from the american heart association. Circ Res 125:e75-e92 doi:10.1161/RES.0000000000000291

56. Girgis I, Gualberti J, Langan L, Malek S, Mustaciuolo V, Costantino T, McGinn TG (1997) A prospective study of the effect of I.V. pentamidine therapy on ventricular arrhythmias and QTC prolongation in HIV-infected patients. Chest 112:646-653 doi:10.1378/chest.112.3.646

57. Glukhov AV, Fedorov VV, Kalish PW, Ravikumar VK, Lou Q, Janks D, Schuessler RB, Moazami N, Efimov IR (2012) Conduction remodeling in human end-stage nonischemic left ventricular cardiomyopathy. Circulation 125:1835-1847 doi:10.1161/CIRCULATIONAHA.111.047274

58. Glukhov AV, Fedorov VV, Lou Q, Ravikumar VK, Kalish PW, Schuessler RB, Moazami N, Efimov IR (2010) Transmural dispersion of repolarization in failing and nonfailing human ventricle. Circ Res 106:981-991 doi:10.1161/CIRCRESAHA.109.204891

59. Goldfracht I, Efraim Y, Shinnawi R, Kovalev E, Huber I, Gepstein A, Arbel G, Shaheen N, Tiburcy M, Zimmermann WH, Machluf M, Gepstein L (2019) Engineered heart tissue models from hiPSC-derived cardiomyocytes and cardiac ECM for disease modeling and drug testing applications. Acta Biomater 92:145-159 doi:10.1016/j.actbio.2019.05.016

60. Gough TAaKA (2005) Early-onset pentamidine-associated second-degree heart block and sinus bradycardia: case report and review of the literature. Pharmacotherapy 25:899-903 doi:10.1592/phco.2005.25.6.899

61. Greenfield JC (1964) Circulatory physiology: cardiac output and its regulation. JAMA 187 doi:10.1001/jama.1964.03060160066027

62. Gregory RK, Smith IE (2000) Vinorelbine--a clinical review. Br J Cancer 82:1907-1913 doi:10.1054/bjoc.2000.1203

63. Groarke J, Tong D, Khambhati J, Cheng S, Moslehi J (2012) Breast cancer therapies and cardiomyopathy. Med Clin North Am 96:1001-1019 doi:10.1016/j.mcna.2012.07.008

64. Guo GR, Chen L, Rao M, Chen K, Song JP, Hu SS (2018) A modified method for isolation of human cardiomyocytes to model cardiac diseases. J Transl Med 16:288 doi:10.1186/s12967-018-1649-6

65. Guth BD, Engwall M, Eldridge S, Foley CM, Guo L, Gintant G, Koerner J, Parish ST, Pierson JB, Ribeiro AJS, Zabka T, Chaudhary KW, Kanda Y, Berridge B (2019) Considerations for an in vitro, cell-based testing platform for detection of adverse drug-induced inotropic effects in early drug development. PART 1: General considerations for development of novel testing platforms. Front Pharmacol 10:884 doi:10.3389/fphar.2019.00884

66. Guzik TJ, Hoch NE, Brown KA, McCann LA, Rahman A, Dikalov S, Goronzy J, Weyand C, Harrison DG (2007) Role of the T cell in the genesis of angiotensin II induced hypertension and vascular dysfunction. J Exp Med 204:2449-2460 doi:10.1084/jem.20070657

67. Gwathmey JK, Tsaioun K, Hajjar RJ (2009) Cardionomics: A new integrative approach for screening cardiotoxicity of drug candidates. Expert Opin Drug Metab Toxicol 5:647-660 doi:10.1517/17425250902932915

68. Haisong Ju RG, Xiaomang You, Sarah Tsang, Mansoor Husain, and Marlene Rabinovitch (2001) Conditional and targeted overexpression of vascular chymase causes hypertension in transgenic mice. PNAS 98:7469-7474

69. Halbert SP, Bruderer, R., and Thompson, A. (1973) Growth of dissociated beating human heart cells in tissue culture. Life sciences 13:969-975 doi:10.1016/0024-3205(73)90087-8

70. Hall JE (2016) Guyton and hall textbook of medical physiology. Elsevier

71. Han X, Rodriguez D, Parker TL (2017) Biological activities of frankincense essential oil in human dermal fibroblasts. Biochim Open 4:31-35 doi:10.1016/j.biopen.2017.01.003

72. Harake D, Franco VI, Henkel JM, Miller TL, Lipshultz SE (2012) Cardiotoxicity in childhood cancer survivors: Strategies for prevention and management. Future Cardiol 8:647-670 doi:10.2217/fca.12.44

73. Harary I, and Farley, B. (1963) In vitro studies on single beating rat heart cells. I.Growth and organization. Exp. Cell Res 29:451-465 doi:10.1016/s0014-4827(63)80008-7

74. Hasin T, Gerber Y, Weston SA, Jiang R, Killian JM, Manemann SM, Cerhan JR, Roger VL (2016) Heart failure after myocardial infarction is associated with increased risk of cancer. J Am Coll Cardiol 68:265-271 doi:10.1016/j.jacc.2016.04.053

75. Hirt MN, Boeddinghaus J, Mitchell A, Schaaf S, Bornchen C, Muller C, Schulz H, Hubner N, Stenzig J, Stoehr A, Neuber C, Eder A, Luther PK, Hansen A, Eschenhagen T (2014) Functional improvement and maturation of rat and human engineered heart tissue by chronic electrical stimulation. J Mol Cell Cardiol 74:151-161 doi:10.1016/j.yjmcc.2014.05.009

76. Hoonjan M, Jadhav V, Bhatt P (2018) Arsenic trioxide: Insights into its evolution to an anticancer agent. J Biol Inorg Chem 23:313-329 doi:10.1007/s00775-018-1537-9

77. Horenstein MS, Vander Heide RS, L'Ecuyer TJ (2000) Molecular basis of anthracycline-induced cardiotoxicity and its prevention. Mol Genet Metab 71:436-444 doi:10.1006/mgme.2000.3043

78. Houser SR, Margulies KB, Murphy AM, Spinale FG, Francis GS, Prabhu SD, Rockman HA, Kass DA, Molkentin JD, Sussman MA, Koch WJ, American Heart Association Council on Basic Cardiovascular Sciences CoCC, Council on Functional G, Translational B (2012) Animal models of heart failure: A scientific statement from the american heart association. Circ Res 111:131-150 doi:10.1161/RES.0b013e3182582523

79. Hughes JP, Rees S, Kalindjian SB, Philpott KL (2011) Principles of early drug discovery. Br J Pharmacol 162:1239-1249 doi:10.1111/j.1476-5381.2010.01127.x

80. J M Wharton PAD, and N Goldschlager (1987) Torsade de pointes during administration of pentamidine isethionate. Am J Med 83:571-576 doi:10.1016/0002-9343(87)90774-1

81. Jackman CP, Carlson AL, Bursac N (2016) Dynamic culture yields engineered myocardium with near-adult functional output. Biomaterials 111:66-79 doi:10.1016/j.biomaterials.2016.09.024

82. Jha TK (1983) Evaluation of diamidine compound (pentamidine isethionate) in the treatment resistant cases of KALA-AZAR Occurring In North Bihar, India. Trans R Soc Trop Med Hyg 77:167-170 doi:10.1016/0035-9203(83)90058-5

83. Jones LW, Haykowsky MJ, Swartz JJ, Douglas PS, Mackey JR (2007) Early breast cancer therapy and cardiovascular injury. J Am Coll Cardiol 50:1435-1441 doi:10.1016/j.jacc.2007.06.037

84. Judd J, Lovas J, Huang GN (2016) Isolation, culture and transduction of adult mouse cardiomyocytes. J Vis Exp doi:10.3791/54012

85. Jung G, Bernstein D (2014) hiPSC modeling of inherited cardiomyopathies. Curr Treat Options Cardiovasc Med 16:320 doi:10.1007/s11936-014-0320-7

86. Kang C, Qiao Y, Li G, Baechle K, Camelliti P, Rentschler S, Efimov IR (2016) Human organotypic cultured cardiac slices: New platform for high throughput preclinical human trials. Sci Rep 6:28798 doi:10.1038/srep28798

87. Kanisicak O, Khalil H, Ivey MJ, Karch J, Maliken BD, Correll RN, Brody MJ, SC JL, Aronow BJ, Tallquist MD, Molkentin JD (2016) Genetic lineage tracing defines myofibroblast origin and function in the injured heart. Nat Commun 7:12260 doi:10.1038/ncomms12260

88. Kantarjian HM, Giles FJ, Bhalla KN, Pinilla-Ibarz J, Larson RA, Gattermann N, Ottmann OG, Hochhaus A, Radich JP, Saglio G, Hughes TP, Martinelli G, Kim DW, Shou Y, Gallagher NJ, Blakesley R, Baccarani M, Cortes J, le Coutre PD (2011) Nilotinib is effective in patients with chronic myeloid leukemia in chronic phase after imatinib resistance or intolerance: 24-month follow-up results. Blood 117:1141-1145 doi:10.1182/blood-2010-03-277152

89. Kappers MH, Smedts FM, Horn T, van Esch JH, Sleijfer S, Leijten F, Wesseling S, Strevens H, Jan Danser AH, van den Meiracker AH (2011) The vascular endothelial growth factor receptor inhibitor sunitinib causes a preeclampsia-like syndrome with activation of the endothelin system. Hypertension 58:295-302 doi:10.1161/HYPERTENSIONAHA.111.173559

90. Kappers MH, van Esch JH, Sluiter W, Sleijfer S, Danser AH, van den Meiracker AH (2010) Hypertension induced by the tyrosine kinase inhibitor sunitinib is associated with increased circulating endothelin-1 levels. Hypertension 56:675-681 doi:10.1161/HYPERTENSIONAHA.109.149690

91. Ke Q, Xiao, Y.-F., Bradbury, J. A., Graves, J. P., Degraff, L. M., Seubert, J. M., et al. (2007) Electrophysiological properties of cardiomyocytes isolated from cyp2j2 transgenic mice. Mol. Pharmacol 72:1063-1073 doi:10.1124/mol.107.035881

92. Kitani T, Ong SG, Lam CK, Rhee JW, Zhang JZ, Oikonomopoulos A, Ma N, Tian L, Lee J, Telli ML, Witteles RM, Sharma A, Sayed N, Wu JC (2019) Human-induced pluripotent stem cell model of trastuzumab-induced cardiac dysfunction in patients with breast cancer. Circulation 139:2451-2465 doi:10.1161/CIRCULATIONAHA.118.037357

93. Kloppel G, Perren A, Heitz PU (2004) The gastroenteropancreatic neuroendocrine cell system and its tumors: The WHO classification. Ann N Y Acad Sci 1014:13-27 doi:10.1196/annals.1294.002

94. Knudsen ES, Witkiewicz AK (2017) The strange case of cdk4/6 inhibitors: mechanisms, resistance, and combination strategies. Trends Cancer 3:39-55 doi:10.1016/j.trecan.2016.11.006

95. Kocadal K, Saygi S, Alkas FB, Sardas S (2019) Drug-associated cardiovascular risks: A retrospective evaluation of withdrawn drugs. North Clin Istanb 6:196-202 doi:10.14744/nci.2018.44977

96. Koelwyn GJ, Aboumsallem JP, Moore KJ, de Boer RA (2022) Reverse cardio-oncology: Exploring the effects of cardiovascular disease on cancer pathogenesis. J Mol Cell Cardiol 163:1-8 doi:10.1016/j.yjmcc.2021.09.008

97. Koelwyn GJ, Newman AAC, Afonso MS, van Solingen C, Corr EM, Brown EJ, Albers KB, Yamaguchi N, Narke D, Schlegel M, Sharma M, Shanley LC, Barrett TJ, Rahman K, Mezzano V, Fisher EA, Park DS, Newman JD, Quail DF, Nelson ER, Caan BJ, Jones LW,

Moore KJ (2020) Myocardial infarction accelerates breast cancer via innate immune reprogramming. Nat Med 26:1452-1458 doi:10.1038/s41591-020-0964-7

98.   Kretzschmar K, Post Y, Bannier-Helaouet M, Mattiotti A, Drost J, Basak O, Li VSW, van den Born M, Gunst QD, Versteeg D, Kooijman L, van der Elst S, van Es JH, van Rooij E, van den Hoff MJB, Clevers H (2018) Profiling proliferative cells and their progeny in damaged murine hearts. Proc Natl Acad Sci U S A 115:E12245-E12254 doi:10.1073/pnas.1805829115

99.   Kroll K, Chabria M, Wang K, Hausermann F, Schuler F, Polonchuk L (2017) Electro-mechanical conditioning of human iPSC-derived cardiomyocytes for translational research. Prog Biophys Mol Biol 130:212-222 doi:10.1016/j.pbiomolbio.2017.07.003

100.   Kurokawa YK, Shang MR, Yin RT, George SC (2018) Modeling trastuzumab-related cardiotoxicity in vitro using human stem cell-derived cardiomyocytes. Toxicol Lett 285:74-80 doi:10.1016/j.toxlet.2018.01.001

101.   Kuryshev YA, Ficker E, Wang L, Hawryluk P, Dennis AT, Wible BA, Brown AM, Kang J, Chen XL, Sawamura K, Reynolds W, Rampe D (2005) Pentamidine-induced long QT syndrome and block of herg trafficking. J Pharmacol Exp Ther 312:316-323 doi:10.1124/jpet.104.073692

102.   Kus T, Aktas G, Sevinc A, Kalender ME, Camci C (2015) Could erlotinib treatment lead to acute cardiovascular events in patients with lung adenocarcinoma after chemotherapy failure? Onco Targets Ther 8:1341-1343 doi:10.2147/OTT.S84480

103.   Laurel J. Steinherz MPGS, MD; Charlotte T.C. Tan, MD; Glenn Heller, PhD; M. Lois Murphy, MD (1991) Cardiac toxicity 4 to 20 years after completing anthracycline therapy. JAMA 266:1672-1677

104.   Lemoine MD, Mannhardt I, Breckwoldt K, Prondzynski M, Flenner F, Ulmer B, Hirt MN, Neuber C, Horvath A, Kloth B, Reichenspurner H, Willems S, Hansen A, Eschenhagen T, Christ T (2017) Human iPSC-derived cardiomyocytes cultured in 3D engineered heart tissue show physiological upstroke velocity and sodium current density. Sci Rep 7:5464 doi:10.1038/s41598-017-05600-w

105.   Lenneman CG, Sawyer DB (2016) Cardio-Oncology: An update on cardiotoxicity of cancer-related treatment. Circ Res 118:1008-1020 doi:10.1161/CIRCRESAHA.115.303633

106.   Li LT, Jiang G, Chen Q, Zheng JN (2015) Ki67 is a promising molecular target in the diagnosis of cancer (review). Mol Med Rep 11:1566-1572 doi:10.3892/mmr.2014.2914

107.   Linschoten M, Kamphuis JAM, van Rhenen A, Bosman LP, Cramer MJ, Doevendans PA, Teske AJ, Asselbergs FW (2020) Cardiovascular adverse events in patients with non-hodgkin lymphoma treated with first-line cyclophosphamide, doxorubicin, vincristine, and prednisone (CHOP) or CHOP with Rituximab (R-CHOP): A systematic review and meta-analysis. The Lancet Haematology 7:e295-e308 doi:10.1016/s2352-3026(20)30031-4

108.   Liu W, Ashford MW, Chen J, Watkins MP, Williams TA, Wickline SA, Yu X (2006) MR tagging demonstrates quantitative differences in regional ventricular wall motion in mice, rats, and men. Am J Physiol Heart Circ Physiol 291:H2515-2521 doi:10.1152/ajpheart.01016.2005

109.   Lou Q, Fedorov VV, Glukhov AV, Moazami N, Fast VG, Efimov IR (2011) Transmural heterogeneity and remodeling of ventricular excitation-contraction coupling in human heart failure. Circulation 123:1881-1890 doi:10.1161/CIRCULATIONAHA.110.989707

110.   Malmborg M, Christiansen CB, Schmiegelow MD, Torp-Pedersen C, Gislason G, Schou M (2018) Incidence of new onset cancer in patients with a myocardial infarction - A

nationwide cohort study. BMC Cardiovasc Disord 18:198 doi:10.1186/s12872-018-0932-z

111. Maria Volkova and Raymond Russell I (2011) Anthracycline cardiotoxicity: Prevalence, pathogenesis and treatment. Current Cardiology Reviews 7:214-220

112. Masashi Yanagisawa HK, Sadao Kimura, Yoko Torno be, Mieko Kobayashi, Youji Mitsui, Yoshio YazakP, Katsutoshi Goto & omoh Masaki (1988) A novel potent vasoconstrictor peptide produced by vascular endothelial cells. Nature 332:411-415

113. Meijers WC, Maglione M, Bakker SJL, Oberhuber R, Kieneker LM, de Jong S, Haubner BJ, Nagengast WB, Lyon AR, van der Vegt B, van Veldhuisen DJ, Westenbrink BD, van der Meer P, Sillje HHW, de Boer RA (2018) Heart failure stimulates tumor growth by circulating factors. Circulation 138:678-691 doi:10.1161/CIRCULATIONAHA.117.030816

114. Meki MH, Miller JM, Mohamed TMA (2021) Heart slices to model cardiac physiology. Front Pharmacol 12:617922 doi:10.3389/fphar.2021.617922

115. Mercuro G, Cadeddu C, Piras A, Dessi M, Madeddu C, Deidda M, Serpe R, Massa E, Mantovani G (2007) Early epirubicin-induced myocardial dysfunction revealed by serial tissue doppler echocardiography: Correlation with inflammatory and oxidative stress markers. Oncologist 12:1124-1133 doi:10.1634/theoncologist.12-9-1124

116. Meunier B, Quaranta M, Daviet L, Hatzoglou A, Leprince C (2009) The membrane-tubulating potential of amphiphysin 2/BIN1 is dependent on the microtubule-binding cytoplasmic linker protein 170 (CLIP-170). Eur J Cell Biol 88:91-102 doi:10.1016/j.ejcb.2008.08.006

117. Meyer JN, Hartman JH, Mello DF (2018) Mitochondrial toxicity. Toxicol Sci 162:15-23 doi:10.1093/toxsci/kfy008

118. Miller JM, Meki MH, Elnakib A, Ou Q, Abouleisa RRE, Tang XL, Salama ABM, Gebreil A, Lin C, Abdeltawab H, Khalifa F, Hill BG, Abi-Gerges N, Bolli R, El-Baz AS, Giridharan GA, Mohamed TMA (2022) Biomimetic cardiac tissue culture model (CTCM) to emulate cardiac physiology and pathophysiology ex vivo. Commun Biol 5:934 doi:10.1038/s42003-022-03919-3

119. Miller JM, Meki MH, Ou Q, George SA, Gams A, Abouleisa RRE, Tang XL, Ahern BM, Giridharan GA, El-Baz A, Hill BG, Satin J, Conklin DJ, Moslehi J, Bolli R, Ribeiro AJS, Efimov IR, Mohamed TMA (2020) Heart slice culture system reliably demonstrates clinical drug-related cardiotoxicity. Toxicol Appl Pharmacol 406:115213 doi:10.1016/j.taap.2020.115213

120. Milton Packer JRC, Richard J. Rodeheffer, Russell J. Ivanhoe, Robert DiBianco, Steven M. Zeldis, Grady H. Hendrix, William J. Bommer, Uri Elkayam, Marrick L. Kukin, George I. Mallis, Josephine A. Sollano, James Shannon, P.K. Tandon, David L. DeMets, and the PROMISE Study Research Group (1991) Effect of oral milrinone on mortality in severe chronic heart failure. N Engl J Med 325:1468-1475 doi:10.1056/NEJM199111213252103

121. Mitcheson J (1998) Cultured adult cardiac myocytes: Future applications, culture methods, morphological and electrophysiological properties. Cardiovasc. Res 39:280-300 doi:10.1016/s0008-6363(98)00128-x

122. Mladenka P, Applova L, Patocka J, Costa VM, Remiao F, Pourova J, Mladenka A, Karlickova J, Jahodar L, Voprsalova M, Varner KJ, Sterba M, Tox OER, Researchers CHK, Collaborators (2018) Comprehensive Review Of Cardiovascular Toxicity Of Drugs And Related Agents. Med Res Rev 38:1332-1403 doi:10.1002/med.21476

123. Monte FD, Harding, S. E., Schmidt, U., Matsui, T., Kang, Z. B., Dec, G. W., et al. (1999) Restoration of contractile function in isolated cardiomyocytes from failing human hearts by gene transfer of SERCA2A. Circulation 100:2308-2311 doi:10.1161/01.cir.100.23.2308

124. Moslehi JJ (2016) Cardiovascular toxic effects of targeted cancer therapies. N Engl J Med 375:1457-1467 doi:10.1056/NEJMra1100265

125. Nagashio K, Tajiri K, Sato K, Ieda M (2021) Erlotinib-induced cardiomyopathy in a patient with metastatic non-small cell lung cancer. Int Heart J 62:1171-1175 doi:10.1536/ihj.21-130

126. Nunes SS, Miklas JW, Liu J, Aschar-Sobbi R, Xiao Y, Zhang B, Jiang J, Masse S, Gagliardi M, Hsieh A, Thavandiran N, Laflamme MA, Nanthakumar K, Gross GJ, Backx PH, Keller G, Radisic M (2013) Biowire: A platform for maturation of human pluripotent stem cell-derived cardiomyocytes. Nat Methods 10:781-787 doi:10.1038/nmeth.2524

127. O'Shea C, Holmes AP, Winter J, Correia J, Ou X, Dong R, He S, Kirchhof P, Fabritz L, Rajpoot K, Pavlovic D (2019) Cardiac optogenetics and optical mapping - overcoming spectral congestion in all-optical cardiac electrophysiology. Front Physiol 10:182 doi:10.3389/fphys.2019.00182

128. Onakpoya IJ, Heneghan CJ, Aronson JK (2016) Post-marketing withdrawal of 462 medicinal products because of adverse drug reactions: A systematic review of the world literature. BMC Med 14:10 doi:10.1186/s12916-016-0553-2

129. Onitilo AA, Engel JM, Stankowski RV (2014) Cardiovascular toxicity associated with adjuvant trastuzumab therapy: Prevalence, patient characteristics, and risk factors. Ther Adv Drug Saf 5:154-166 doi:10.1177/2042098614529603

130. Orphanos GS, Ioannidis GN, Ardavanis AG (2009) Cardiotoxicity induced by tyrosine kinase inhibitors. Acta Oncol 48:964-970 doi:10.1080/02841860903229124

131. Ou Q, Jacobson Z, Abouleisa RRE, Tang XL, Hindi SM, Kumar A, Ivey KN, Giridharan G, El-Baz A, Brittian K, Rood B, Lin YH, Watson SA, Perbellini F, McKinsey TA, Hill BG, Jones SP, Terracciano CM, Bolli R, Mohamed TMA (2019) Physiological biomimetic culture system for pig and human heart slices. Circ Res 125:628-642 doi:10.1161/CIRCRESAHA.119.314996

132. P. Alter MH, M. Soufi, J.R. Schaefer and B. Maisch (2006) Cardiotoxicity of 5-Fluorouracil. Cardiovascular & Hematological Agents in Medicinal Chemistry 4:1-5

133. Padmakumar VC, Libotte T, Lu W, Zaim H, Abraham S, Noegel AA, Gotzmann J, Foisner R, Karakesisoglou I (2005) The inner nuclear membrane protein SUN1 mediates the anchorage of NESPRIN-2 to the nuclear envelope. J Cell Sci 118:3419-3430 doi:10.1242/jcs.02471

134. Pandey AK, Singhi EK, Arroyo JP, Ikizler TA, Gould ER, Brown J, Beckman JA, Harrison DG, Moslehi J (2018) Mechanisms of VEGF (vascular endothelial growth factor) inhibitor-associated hypertension and vascular disease. Hypertension 71:e1-e8 doi:10.1161/HYPERTENSIONAHA.117.10271

135. Pang B, Qiao X, Janssen L, Velds A, Groothuis T, Kerkhoven R, Nieuwland M, Ovaa H, Rottenberg S, van Tellingen O, Janssen J, Huijgens P, Zwart W, Neefjes J (2013) Drug-induced histone eviction from open chromatin contributes to the chemotherapeutic effects of doxorubicin. Nat Commun 4:1908 doi:10.1038/ncomms2921

136. Pang L, Sager P, Yang X, Shi H, Sannajust F, Brock M, Wu JC, Abi-Gerges N, Lyn-Cook B, Berridge BR, Stockbridge N (2019) Workshop report: FDA workshop on improving cardiotoxicity assessment with human-relevant platforms. Circ Res 125:855-867 doi:10.1161/CIRCRESAHA.119.315378

137. Papapetropoulos A G-CG, Madri JA, Sessa WC (1997) Nitric oxide production contributes to the angiogenic properties of vascular endothelial growth factor in human endothelial cells. J Clin Invest 100:3131-3139 doi:10.1172/JCI119868

138.   Parikh SS, Zou, S. Z., and Tung, L (1993) Contraction and relaxation of isolated cardiac myocytes of the frog under varying mechanical loads. Circ. Res 72:297-311 doi:10.1161/01.res.72.2.297

139.   Pentassuglia L, Sawyer DB (2009) The role of NEUREGULIN-1BETA/ERBB signaling in the heart. Exp Cell Res 315:627-637 doi:10.1016/j.yexcr.2008.08.015

140.   Pinquie F, de Chabot G, Urban T, Hureaux J (2016) Maintenance treatment by erlotinib and toxic cardiomyopathy: A case report. Oncology 90:176-177 doi:10.1159/000444186

141.   Pitoulis FG, Watson SA, Perbellini F, Terracciano CM (2020) Myocardial slices come to age: An intermediate complexity in vitro cardiac model for translational research. Cardiovasc Res 116:1275-1287 doi:10.1093/cvr/cvz341

142.   Plana JC, Galderisi M, Barac A, Ewer MS, Ky B, Scherrer-Crosbie M, Ganame J, Sebag IA, Agler DA, Badano LP, Banchs J, Cardinale D, Carver J, Cerqueira M, DeCara JM, Edvardsen T, Flamm SD, Force T, Griffin BP, Jerusalem G, Liu JE, Magalhaes A, Marwick T, Sanchez LY, Sicari R, Villarraga HR, Lancellotti P (2014) Expert consensus for multimodality imaging evaluation of adult patients during and after cancer therapy: A report from the american society of echocardiography and the european association of cardiovascular imaging. J Am Soc Echocardiogr 27:911-939 doi:10.1016/j.echo.2014.07.012

143.   Pointon A, Harmer AR, Dale IL, Abi-Gerges N, Bowes J, Pollard C, Garside H (2015) Assessment of cardiomyocyte contraction in human-induced pluripotent stem cell-derived cardiomyocytes. Toxicol Sci 144:227-237 doi:10.1093/toxsci/kfu312

144.   Ponce R (2011) ICH S9: Developing anticancer drugs, one year later. Toxicol Pathol 39:913-915 doi:10.1177/0192623311416263

145.   Pouessel D, Culine S (2008) High frequency of intracerebral hemorrhage in metastatic renal carcinoma patients with brain metastases treated with tyrosine kinase inhibitors targeting the vascular endothelial growth factor receptor. Eur Urol 53:376-381 doi:10.1016/j.eururo.2007.08.053

146.   Powell T, and Twist, V. W. (1976) A rapid technique for the isolation and purification of adult cardiac muscle cells having respiratory control and a tolerance to calcium. Biochem. Biophys. Res. Commun 72:327-333 doi:10.1016/0006-291x(76)90997-9

147.   Prosser BL WC, Lederer W. (2011) X-ROS signaling: Rapid mechanochemo transduction in heart. Science 333:1440-1445

148.   Qiao Y, Dong Q, Li B, Obaid S, Miccile C, Yin RT, Talapatra T, Lin Z, Li S, Li Z, Efimov IR (2019) Multiparametric slice culture platform for the investigation of human cardiac tissue physiology. Prog Biophys Mol Biol 144:139-150 doi:10.1016/j.pbiomolbio.2018.06.001

149.   Qinghui Ou RREA, Xian-Liang Tang, Hamzah R. Juhardeen, Moustafa H. Meki, Jessica M. Miller, Guruprasad Giridharan, Ayman El-Baz, Roberto Bolli, Tamer M. A. Mohamed (2021) Slicing and culturing pig hearts under physiological conditions. J Vis Exp.

150.   Roberts MA, Tran D, Coulombe KL, Razumova M, Regnier M, Murry CE, Zheng Y (2016) Stromal cells in dense collagen promote cardiomyocyte and microvascular patterning in engineered human heart tissue. Tissue Eng Part A 22:633-644 doi:10.1089/ten.TEA.2015.0482

151.   Robison P, Caporizzo MA, Ahmadzadeh H, Bogush AI, Chen CY, Margulies KB, Shenoy VB, Prosser BL (2016) Detyrosinated microtubules buckle and bear load in contracting cardiomyocytes. Science 352:aaf0659 doi:10.1126/science.aaf0659

152. Ronaldson-Bouchard K, Ma SP, Yeager K, Chen T, Song L, Sirabella D, Morikawa K, Teles D, Yazawa M, Vunjak-Novakovic G (2018) Advanced maturation of human cardiac tissue grown from pluripotent stem cells. Nature 556:239-243 doi:10.1038/s41586-018-0016-3

153. Rosano L, Bagnato A (2016) Endothelin therapeutics in cancer: Where are we? Am J Physiol Regul Integr Comp Physiol 310:R469-475 doi:10.1152/ajpregu.00532.2015

154. Rosano L, Spinella F, Bagnato A (2013) Endothelin 1 in cancer: Biological implications and therapeutic opportunities. Nat Rev Cancer 13:637-651 doi:10.1038/nrc3546

155. Ruan JL, Tulloch NL, Razumova MV, Saiget M, Muskheli V, Pabon L, Reinecke H, Regnier M, Murry CE (2016) Mechanical stress conditioning and electrical stimulation promote contractility and force maturation of induced pluripotent stem cell-derived human cardiac tissue. Circulation 134:1557-1567 doi:10.1161/CIRCULATIONAHA.114.014998

156. Salama G, Bett GC (2014) Sex differences in the mechanisms underlying long QT syndrome. Am J Physiol Heart Circ Physiol 307:H640-648 doi:10.1152/ajpheart.00864.2013

157. SAMUEL WAXMAN KCA (2001) History of the development of arsenic derivatives in cancer therapy. The Oncologist 6:3-10

158. Shan K LA, Young JB (1996) Anthracycline-induced cardiotoxicity. Ann Intern Med 125:47-58

159. Sharma A, McKeithan WL, Serrano R, Kitani T, Burridge PW, Del Alamo JC, Mercola M, Wu JC (2018) Use of human induced pluripotent stem cell-derived cardiomyocytes to assess drug cardiotoxicity. Nat Protoc 13:3018-3041 doi:10.1038/s41596-018-0076-8

160. Sheng CC, Amiri-Kordestani L, Palmby T, Force T, Hong CC, Wu JC, Croce K, Kim G, Moslehi J (2016) 21ST century Cardio-Oncology: Identifying cardiac safety signals in the era of personalized medicine. JACC Basic Transl Sci 1:386-398 doi:10.1016/j.jacbts.2016.05.008

161. Shota Yanagida AS, Sayo Hayashi, Atsushi Ono, and Yasunari Kanda (2021) Chronic cardiotoxicity assessment of BMS-986094, a guanosine nucleotide analogue, using human iPS cell-derived cardiomyocytes. J. Toxicol. Sci. 46:359-369

162. Sirenko O, Cromwell EF, Crittenden C, Wignall JA, Wright FA, Rusyn I (2013) Assessment of beating parameters in human induced pluripotent stem cells enables quantitative in vitro screening for cardiotoxicity. Toxicol Appl Pharmacol 273:500-507 doi:10.1016/j.taap.2013.09.017

163. Slamon DJ, Leyland-Jones, B., Shak, S., Fuchs, H., Paton, V., Bajamonde, A., Fleming, T., Eiermann, W., Wolter, J., Pegram, M., Baselga, J., Norton, L. (2001) Use of chemotherapy plus a monoclonal antibody against HER2 for metastatic breast cancer that overexpresses HER2. N. Engl. J. Med 344:783-792

164. Steele DF, Eldstrom J, Fedida D (2007) Mechanisms of cardiac potassium channel trafficking. J Physiol 582:17-26 doi:10.1113/jphysiol.2007.130245

165. Steele DF, Fedida D (2014) Cytoskeletal roles in cardiac ion channel expression. Biochim Biophys Acta 1838:665-673 doi:10.1016/j.bbamem.2013.05.001

166. Steinherz LJ, Steinherz, P.G., Tan, C.T., Heller, G., Murphy, M.L. (1991) Cardiac Toxicity 4 To 20 Years After Completing Anthracycline Therapy. JAMA 266:1672-1677

167. Steven A. Crone Y-Yz, Lian Fan, Yusu Gu, Susumu Minamisawa, Yang Liu, Kirk L. Peterson, Ju Chen, Ronald Kahn, Gianluigi Condorelli, John Ross Jr, Kenneth R. Chien & Kuo-Fen Lee (2002) ERBB2 is essential in the prevention of dilated cardiomyopathy. Nature Medicine 8:459-465

168. Stroud MJ (2018) Linker of nucleoskeleton and cytoskeleton complex proteins in cardiomyopathy. Biophys Rev 10:1033-1051 doi:10.1007/s12551-018-0431-6

169. Swain SM, Whaley FS, Ewer MS (2003) Congestive heart failure in patients treated with doxorubicin: A retrospective analysis of three trials. Cancer 97:2869-2879 doi:10.1002/cncr.11407

170. Takahashi K, Tanabe K, Ohnuki M, Narita M, Ichisaka T, Tomoda K, Yamanaka S (2007) Induction of pluripotent stem cells from adult human fibroblasts by defined factors. Cell 131:861-872 doi:10.1016/j.cell.2007.11.019

171. Talman V, Kivela R (2018) Cardiomyocyte-endothelial cell interactions in cardiac remodeling and regeneration. Front Cardiovasc Med 5:101 doi:10.3389/fcvm.2018.00101

172. Tamis-Holland JE, Jneid H, Reynolds HR, Agewall S, Brilakis ES, Brown TM, Lerman A, Cushman M, Kumbhani DJ, Arslanian-Engoren C, Bolger AF, Beltrame JF, American Heart Association Interventional Cardiovascular Care Committee of the Council on Clinical C, Council on C, Stroke N, Council on E, Prevention, Council on Quality of C, Outcomes R (2019) Contemporary diagnosis and management of patients with myocardial infarction in the absence of obstructive coronary artery disease: A scientific statement from the american heart association. Circulation 139:e891-e908 doi:10.1161/CIR.0000000000000670

173. Tandon N, Cannizzaro C, Chao PH, Maidhof R, Marsano A, Au HT, Radisic M, Vunjak-Novakovic G (2009) Electrical stimulation systems for cardiac tissue engineering. Nat Protoc 4:155-173 doi:10.1038/nprot.2008.183

174. Thygesen K (2019) 'Ten Commandments' for the fourth universal definition of myocardial infarction 2018. Eur Heart J 40:226 doi:10.1093/eurheartj/ehy856

175. Thygesen K, Alpert JS, Jaffe AS, Chaitman BR, Bax JJ, Morrow DA, White HD, Executive Group on behalf of the Joint European Society of Cardiology /American College of Cardiology /American Heart Association /World Heart Federation Task Force for the Universal Definition of Myocardial I (2018) Fourth universal definition of myocardial infarction. J Am Coll Cardiol 72:2231-2264 doi:10.1016/j.jacc.2018.08.1038

176. Tsutsui H IK, Cooper G. (1993) Cytoskeletal role in the contractile dysfunction of hypertrophied myocardium. Science 260:682-687

177. Tytgat J (1994) How to isolate cardiac myocytes. Cardiovasc. Res. 28:280-283 doi:10.1093/cvr/28.2.280

178. Ucciferri C, Occhionero A, Vecchiet J, Falasca K (2018) Cardiac toxicity associated with hcv direct antiviral agents. Mediterr J Hematol Infect Dis 10:e2018069 doi:10.4084/MJHID.2018.069

179. Unverferth BJ, Magorien RD, Balcerzak SP, Leier CV, Unverferth DV (1983) Early changes in human myocardial nuclei after doxorubicin. Cancer 52:215-221 doi:10.1002/1097-0142(19830715)52:2<215::Aid-cncr2820520206>3.0.Co;2-f

180. Uraizee I, Cheng, S., Moslehi, J. (2011) Reversible cardiomyopathy associated with sunitinib and sorafenib. N. Engl. J. Med. 365:1649-1650

181. Van Norman GA (2019) Limitations of animal studies for predicting toxicity in clinical trials: Is it time to rethink our current approach? JACC Basic Transl Sci 4:845-854 doi:10.1016/j.jacbts.2019.10.008

182. Van Norman GA (2020) Limitations of animal studies for predicting toxicity in clinical trials: Part 2: Potential alternatives to the use of animals in preclinical trials. JACC Basic Transl Sci 5:387-397 doi:10.1016/j.jacbts.2020.03.010

183. Varkevisser R, Houtman MJ, Linder T, de Git KC, Beekman HD, Tidwell RR, Ijzerman AP, Stary-Weinzinger A, Vos MA, van der Heyden MA (2013) Structure-activity relationships

of pentamidine-affected ion channel trafficking and dofetilide mediated rescue. Br J Pharmacol 169:1322-1334 doi:10.1111/bph.12208

184.   Vasanthakumar A, Kattusamy K, Prasad R (2013) Regulation of daunorubicin biosynthesis in streptomyces peucetius - feed forward and feedback transcriptional control. J Basic Microbiol 53:636-644 doi:10.1002/jobm.201200302

185.   Vernachio JH, Bleiman B, Bryant KD, Chamberlain S, Hunley D, Hutchins J, Ames B, Gorovits E, Ganguly B, Hall A, Kolykhalov A, Liu Y, Muhammad J, Raja N, Walters CR, Wang J, Williams K, Patti JM, Henson G, Madela K, Aljarah M, Gilles A, McGuigan C (2011) INX-08189, a phosphoramidate prodrug of 6-O-METHYL-2'-C-METHYL guanosine, is a potent inhibitor of hepatitis C virus replication with excellent pharmacokinetic and pharmacodynamic properties. Antimicrob Agents Chemother 55:1843-1851 doi:10.1128/AAC.01335-10

186.   Waliany S, Sainani KL, Park LS, Zhang CA, Srinivas S, Witteles RM (2019) Increase in blood pressure associated with tyrosine kinase inhibitors targeting vascular endothelial growth factor. JACC CardioOncol 1:24-36 doi:10.1016/j.jaccao.2019.08.012

187.   Wang D, Patel C, Cui C, Yan GX (2008) Preclinical assessment of drug-induced proarrhythmias: Role of the arterially perfused rabbit left ventricular wedge preparation. Pharmacol Ther 119:141-151 doi:10.1016/j.pharmthera.2008.02.009

188.   Watson SA, Duff J, Bardi I, Zabielska M, Atanur SS, Jabbour RJ, Simon A, Tomas A, Smolenski RT, Harding SE, Perbellini F, Terracciano CM (2019) Biomimetic electromechanical stimulation to maintain adult myocardial slices in vitro. Nat Commun 10:2168 doi:10.1038/s41467-019-10175-3

189.   Watson SA, Scigliano M, Bardi I, Ascione R, Terracciano CM, Perbellini F (2017) Preparation of viable adult ventricular myocardial slices from large and small mammals. Nat Protoc 12:2623-2639 doi:10.1038/nprot.2017.139

190.   Wheeler-Jones C, Abu-Ghazaleh R, Cospedal R, Houliston RA, Martin J, Zachary I (1997) Vascular endothelial growth factor stimulates prostacyclin production and activation of cytosolic phospholipase a2in endothelial cells via P42/P44 mitogen-activated protein kinase. FEBS Letters 420:28-32 doi:10.1016/s0014-5793(97)01481-6

191.   Yan GX, Antzelevitch C (1996) Cellular basis for the electrocardiographic J wave. Circulation 93:372-379 doi:10.1161/01.cir.93.2.372

192.   Yan GX, Shimizu, W., and Antzelevitch, C. (1998) Characteristics and distribution of m cells in arterially perfused canine left ventricular wedge preparations. Circulation 98:1921-1927 doi:10.1161/01.cir.98.18.1921

193.   Yang B, Papoian T (2018) Preclinical approaches to assess potential kinase inhibitor-induced cardiac toxicity: Past, present and future. J Appl Toxicol 38:790-800 doi:10.1002/jat.3584

194.   Yang C, Al-Aama J, Stojkovic M, Keavney B, Trafford A, Lako M, Armstrong L (2015) Concise review: Cardiac disease modeling using induced pluripotent stem cells. Stem Cells 33:2643-2651 doi:10.1002/stem.2070

195.   Yang Y, Bu P (2016) Progress on the cardiotoxicity of sunitinib: Prognostic significance, mechanism and protective therapies. Chem Biol Interact 257:125-131 doi:10.1016/j.cbi.2016.08.006

196.   Ye KY, Black LD, 3rd (2011) Strategies for tissue engineering cardiac constructs to affect functional repair following myocardial infarction. J Cardiovasc Transl Res 4:575-591 doi:10.1007/s12265-011-9303-1

197.   Yoshida S, Miyagawa S, Fukushima S, Kawamura T, Kashiyama N, Ohashi F, Toyofuku T, Toda K, Sawa Y (2018) Maturation of human induced pluripotent stem cell-derived

cardiomyocytes by soluble factors from human mesenchymal stem cells. Mol Ther 26:2681-2695 doi:10.1016/j.ymthe.2018.08.012

198. Zaccolo M (2009) cAMP signal transduction in the heart: Understanding spatial control for the development of novel therapeutic strategies. Br J Pharmacol 158:50-60 doi:10.1111/j.1476-5381.2009.00185.x

199. Zhang C, Chen B, Guo A, Zhu Y, Miller JD, Gao S, Yuan C, Kutschke W, Zimmerman K, Weiss RM, Wehrens XH, Hong J, Johnson FL, Santana LF, Anderson ME, Song LS (2014) Microtubule-mediated defects in junctophilin-2 trafficking contribute to myocyte transverse-tubule remodeling and Ca2+ handling dysfunction in heart failure. Circulation 129:1742-1750 doi:10.1161/CIRCULATIONAHA.113.008452

200. Zhang D, Shadrin IY, Lam J, Xian HQ, Snodgrass HR, Bursac N (2013) Tissue-engineered cardiac patch for advanced functional maturation of human ESC-derived cardiomyocytes. Biomaterials 34:5813-5820 doi:10.1016/j.biomaterials.2013.04.026

201. Zhang S, Liu X, Bawa-Khalfe T, Lu LS, Lyu YL, Liu LF, Yeh ET (2012) Identification of the molecular basis of doxorubicin-induced cardiotoxicity. Nat Med 18:1639-1642 doi:10.1038/nm.2919

202. Zhang SS, Shaw RM (2014) Trafficking highways to the intercalated disc: New insights unlocking the specificity of connexin 43 localization. Cell Commun Adhes 21:43-54 doi:10.3109/15419061.2013.876014

203. Zhang YS, Arneri A, Bersini S, Shin SR, Zhu K, Goli-Malekabadi Z, Aleman J, Colosi C, Busignani F, Dell'Erba V, Bishop C, Shupe T, Demarchi D, Moretti M, Rasponi M, Dokmeci MR, Atala A, Khademhosseini A (2016) Bioprinting 3D microfibrous scaffolds for engineering endothelialized myocardium and heart-on-a-chip. Biomaterials 110:45-59 doi:10.1016/j.biomaterials.2016.09.003

204. Zhao L, Zhang B (2017) Doxorubicin induces cardiotoxicity through upregulation of death receptors mediated apoptosis in cardiomyocytes. Sci Rep 7:44735 doi:10.1038/srep44735

205. Zhu Q, Deng Z, Zhu S, Zhao P, Wang M, Hu X (2017) Study on the clinical safe and effective methods of arsenic-containing compound-qinghuang powder in the treatment of myelodysplastic syndrome. Evid Based Complement Alternat Med 2017:2095682 doi:10.1155/2017/2095682

CURRICULUM VITAE

Jessica Miller

Louisville, KY, USA · Jessica.miller.3@louisville.edu

EDUCATION

UNIVERSITY OF LOUISVILLE   EXPECTED GRADUATION: 12/2022
PhD, Bioengineering

UNIVERSITY OF ALABAMA AT BIRMINGHAM   04/2019
BS, Biomedical Engineering

EXPERIENCE

2019 – CURRENT
DOCTORAL CANDIDATE, UNIVERSITY OF LOUISVILLE

- Processed porcine and donated human hearts for use in thin cardiac tissue slice cultures
- Conducted research that demonstrated that thin cardiac tissue slices are a more reliable screening platform for detecting clinical cardiotoxicities compared to hiPSC-CMs
- Designed a flow loop system to investigate cardiovascular disease induced tumorigenesis
- Identified essential humoral factors for maintaining human and porcine cardiac tissue slice integrity for extended culture
- Design, development, and implementation of a cardiac tissue culture model that stimulates human/pig tissue slices with physiological preload/afterload conditions
- Handled and transfected cardiac tissue slices with adenovirus
- Analyzed, interpreted, and organized data as well as wrote manuscripts for publication
- Conducted research and outlined experimental designs for fellowship grant applications
- Presented research findings at research conferences

- Oversaw undergraduate research volunteer, PhD, and post-doc instruction and integration into projects

2017 – 2019
UNDERGRADUATE RESEARCH VOLUNTEER, UNIVERSITY OF ALABAMA AT BIRMINGHAM

- Developed biomimetic cardiac tissue model designed to reproduce hemodynamic and pressure/volume changes associated with heart development to stimulate the maturation of hiPSC-CMs
- Investigated the role of nutlin-3a, an MDM2 inhibitor, in hiPSC-CM priming for cardiac regeneration techniques
- Interpreted research data and formatted manuscripts
- Presented research findings at 4 conferences and 1 seminar
- Recruited and integrated undergraduate research volunteers

Awards

2021 Best Doctoral Student Peer-Reviewed Journal Paper   04/2021

PUBLICATIONS

1. **Jessica M. Miller***, Moustafa H. Meki*, Ahmed Elnakib, Qinghui Ou, Riham R. E. Abouleisa, Xian-Liang Tang, Abou Bakr M. Salama, Ahmad Gebreil, Cindy Lin, Hisham Abdeltawab, Fahmi Khalifa, Bradford G. Hill, Najah Abi-Gerges, Roberto Bolli, Ayman S. El-Baz, Guruprasad A. Giridharan, Tamer M. A. Mohamed. Biomimetic cardiac tissue culture model (ctcm) to emulate cardiac physiology and pathophysiology ex vivo. Nature Communications Biology. 2022 5(1), 1-14.

2. Namrita Kaur, Andrea Ruiz-Velasco, Rida Raja, Gareth Howell, **Jessica M Miller**, Riham RE Abouleisa, Qinghui Ou, Kimberly Mace, Susanne S Hille,

Norbert Frey, Pablo Binder, Craig P Smith, Helene Fachim, Handrean Soran, Eileithyia Swanton, Tamer MA Mohamed, Oliver J Müller, Xin Wang, Jonathan Chernoff, Elizabeth J Cartwright, Wei Liu. Paracrine signal emanating from stressed cardiomyocytes aggravates inflammatory microenvironment in diabetic cardiomyopathy. IScience. 2022 25(3): e103973.

3. Hisham Abdeltawab, Fahmi Khalifa, Kamal Hammouda, **Jessica M Miller**, Moustafa M Meki, Qinghui Ou, Ayman El-Baz, Tamer Mohamed. Artificial intelligence based framework to quantify the cardiomyocyte structural integrity in heart slices. Cardiovascular Engineering and Technology. 2021: 1-11.

4. MH Meki*, **JM Miller***, T Mohamed. Heart slices to model cardiac physiology. FPhar. 2021 12, 23.

5. **Miller J M***, Meki M H*, Ou Q*, George S A*, Gams A, Abouleisa R R E, Tang X, Ahern B M, Giridharan G, El-Baz A, Hill B G, Satin J, Conklin D J, Moslehi J, Bolli R, Ribeiro A J S, Efimov I R, Mohamed T M A. Heart slice culture system reliably demonstrates clinical drug related cardiotoxicity. TAAP. 2020 406, 115213.

6. **Miller JM***, NM Mardhekar*, Rajasekaran V, Rajasekaran NS, Zhang J, and Kannappan R. DNA damage-free ips cells exhibit potential to yield competent cardiomyocytes. AJP Heart. 2020 318(4): H801-H815.

7. Qinghui Ou, Riham RE Abouleisa, Xian-Liang Tang, Hamzah R Juhardeen, Moustafa H Meki, **Jessica M Miller**, Guruprasad Giridharan, Ayman El-Baz, Roberto Bolli, Tamer MA Mohamed. SLICING AND CULTURING PIG HEARTS UNDER PHYSIOLOGICAL CONDITIONS. JoVE. 2020 157: e60913.

8. **Miller JM***, Mardhekar N*, Rajasekaran V, Zhang J, and Kannappan R. Assessing stem cell dna integrity for cardiac cell therapy. JoVE. 2019 143: e58971.

9. Kannappan R, Turner JF, **Miller JM**, Fan C, Rushdi A, Rajasekaran N, Zhang J. Functionally competent dna damage-free induced pluripotent stem cell-derived cardiomyocytes for myocardial repair. Circulation. 2019 140(6): 520-522.

10. Aaron J Rogers, **Jessica M Miller**, Ramaswamy Kannappan, Palaniappan Sethu. Cardiac tissue chips (ctcs) for modeling cardiovascular disease. IEEE Transactions on Biomedical Engineering. 2019 66(12): 3436-3443.

11. Aaron J Rogers, Ramaswamy Kannappan, Hadil Abukhalifeh, Mohammed Ghazal, **Jessica M Miller**, Ayman El-Baz, Vladimir G Fast, Palaniappan Sethu. Hemodynamic stimulation using the biomimetic cardiac tissue model (bctm) enhances maturation of human induced pluripotent stem cell-derived. Cardiomyocytes Cells Tissues Organs. 2018 206 (1-2): 82-94.

---

*Equally Contributed First Authors

Conference Abstracts

1. **Jessica M. Miller** et al. Biomimetic cardiac tissue culture model (ctcm) to emulate cardiac physiology and pathophysiology ex vivo. *American Heart Association*; Nov 2022; Chicago, IL.
2. **Jessica M. Miller** et al. Emulating cardiac physiology and pathophysiology ex vivo for drug testing using heart slices. *Safety Pharmacology Society conference*; Sept 2022; Montreal, Canada.
3. **Jessica M. Miller** et al. Emulating the cardiac mechanical and humoral cues to prolong human heart slice culture. *American Heart Association*; Nov 2021; Virtual. Circulation 144 (Suppl_1), A11204-A11204
4. **Jessica M. Miller** et al. Next generation of cardiac tissue slices for drug and therapeutic testing. *Research!Louisville*; Oct 2021; Louisville, KY.
5. **Jessica M. Miller** et al. Cardiac tissue slices: a potential platform for reliable clinical cardiotoxicity testing. *Genetic Toxicology Association 2021 Annual Meeting*; May 2021; virtual.

Conference Presentations

1. (Poster) **Jessica M. Miller**, Moustafa H. Meki, Ahmed Elnakib2, Qinghui Ou, Riham R. E. Abouleisa, Xian-Liang Tang, Abou Bakr M. Salama, Ahmad Gebreil, Cindy Lin, Hisham Abdeltawab, Fahmi Khalifa, Bradford G. Hill, Najah Abi-Gerges, Roberto Bolli, Ayman S. El-Baz, Guruprasad A. Giridharan, Tamer M. A. Mohamed. "Biomimetic Cardiac Tissue Culture Model (CTCM) to Emulate Cardiac Physiology and Pathophysiology ex vivo." American Heart Association, Chicago, IL, 2022.
2. (Poster) **Jessica M. Miller**, Moustafa H. Meki, Ahmed Elnakib2, Qinghui Ou, Riham R. E. Abouleisa, Xian-Liang Tang, Abou Bakr M. Salama, Ahmad Gebreil, Cindy Lin, Hisham Abdeltawab, Fahmi Khalifa, Bradford G. Hill, Najah Abi-Gerges, Roberto Bolli, Ayman S. El-Baz, Guruprasad A. Giridharan, Tamer M. A. Mohamed. "Emulating Cardiac Physiology and Pathophysiology ex vivo for drug testing using heart slices." Safety Pharmacology Society conference, Montreal, Canada, 2022.
3. (Oral presentation) **Jessica M. Miller**, Moustafa Meki, Qinghui Ou, Ahmad Gebreil, AbouBakr Salama, Xian-Liang Tang, Riham R A Abouleisa, Ayman S El-Baz, Guruprasad Giridharan, and Tamer M A Mohamed. "Emulating the Cardiac Mechanical and Humoral Cues to Prolong Human Heart Slice Culture." American Heart Association, virtual, 2021.
4. (Poster) **Jessica M. Miller**, Moustafa H. Meki, Qinghui Ou, Ahmed Gebriel, Abobakr -, Xian-Liang Tang, Riham R. E. Abouleisa, Guruprasad Giridharan, and Tamer M. A. Mohamed. "Next Generation of cardiac tissue slices for drug and therapeutic testing." Research!Louisville, Louisville, KY, 2021.

5. (Poster, virtual) **Jessica M. Miller**, Moustafa H. Meki, Qinghui Ou, Riham R. E. Abouleisa, Xian-Liang Tang, Ayman El-Baz, Guruprasad Giridharan, Roberto Bolli, and Tamer M. A. Mohamed. "Cardiac tissue slices: A potential platform for reliable clinical cardiotoxicity testing." Genetic Toxicology Association 2021 Annual Meeting, virtual, 2021